RAM ROBOTICS AND MECHATRONICS

EVALUATION OF RPAM ACTUATORS FOR USAGE IN HAPTIC TELEOPERATIONS

E.S. (Elias) Gudmundsson

MSC ASSIGNMENT

Committee:
dr. ir. M. Abayazid
M.S. Selim, MSc
dr. T.H.F. Hartman

October, 2023

054RaM2023
Robotics and Mechatronics
EEMCS
University of Twente
P.O. Box 217
7500 AE Enschede
The Netherlands

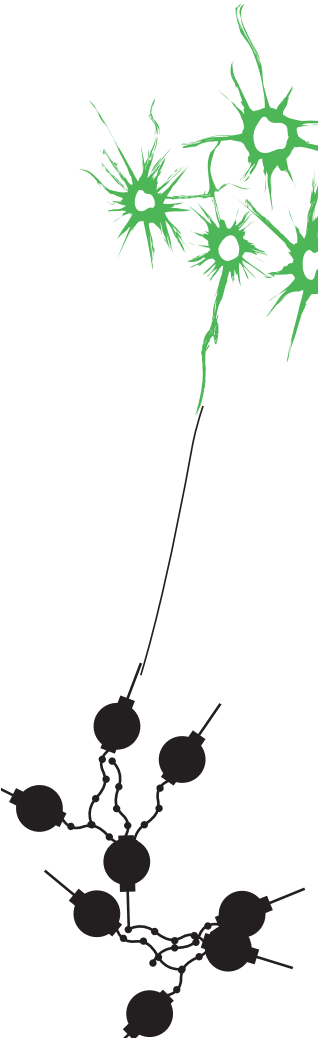

UNIVERSITY OF TWENTE. | TECHMED CENTRE UNIVERSITY OF TWENTE. | DIGITAL SOCIETY INSTITUTE

Summary

Minimally Invasive Surgery (MIS) has revolutionized the medical field over the past few decades, giving benefits such as decreased pain, reduced tissue damage and shorter recovery time. Due to the nature of the tools used, there are some challenges, such as limited sensory capabilities. Surgeon's must then rely solely on visual feedback. Research has therefore focused on developing robotic solutions that allows procedures to be conducted in - or near - imaging environments such as CT and MRI. Moreover, research has highlighted the need for sensory feedback, allowing the surgeon to feel forces perceived by the tool being operated. Incorporating haptic feedback (force feedback), to such devices has been shown to increase tissue characterization and reducing the maximum force applied, resulting in less tissue damage to the patient. This thesis aims to add to recent research by evaluating soft actuators called reverse Pneumatic Artificial Muscles (rPAM) for usage in remote MIS, specifically needle insertions, with haptic feedback.

In order to integrate haptic feedback to the system, developed by another student, some modifications had to be done. Friction was identified and minimized before integrating force sensors to the system, allowing for measurements of forces experienced by the user. Following that, a position controller is developed in order to mitigate the non-linear behavior of the actuators. The position controller adds a constant threshold pressure to the actuators which results in a near-linear increase of position with an increase in input pressure. The best fit line is calculated and fed-forward to the system, resulting in a smooth movement of the handle as well as the handle staying in place wherever it is placed. However, due to the small non-linearities of the actuators, the best fit line is reduced a small amount, increasing the user force required to move the handle. This results in a limitation where the measured user force is about 0.5 N to 1.5 N during an insertion without haptic feedback. A PID controller is used to control the user force. Safety features are added to the force controller as stability is crucial for these devices. The force controller is not activated until the setpoint force is greater than the user force, resulting in an enhanced feedback system rather than a fully haptic feedback system.

Evaluation of the actuators, for this specific purpose, is done by having 10 users control a 1 DoF needle insertion device with this haptic device. The users insert the needle through 3 phantoms, each with their own characteristics. The first phantom is stiff, but the depth of insertion is low. The second is also stiff but with a larger depth of insertion. The third phantom is half soft and half stiff. Users are instructed to insert 6 times into each phantom, where 3 insertions are without feedback and the other 3 with haptic feedback. Users are asked after each 6 insertions if they felt the feedback in the first 3 or the second 3 insertions. The results show that users felt the feedback for all 3 phantoms and felt a difference when entering the stiffer part of phantom 3, showing that tissue characterization is improved with haptic feedback. Moreover, the results show that the maximum force of the needle is decreased in phantoms 2 and 3 with haptic feedback compared to no feedback. Phantom 1 is shown to be very similar in the two cases due to the feedback starting very close to the end of the phantom. This is due to the limitation of the position controller.

While there is still some work needed for the haptic device before it can be considered for usage in MIS, the actuators efficacy for this usage has been shown through experiments. The actuators are able to provide the user with realistic feedback, which showed to be effective in lowering the interaction forces of the needle, in cases where the limitation of the position controller was not apparent.

Contents

1 Introduction

1.1 Context

1.1.1 Minimally Invasive Surgery (MIS)

Minimally Invasive Surgery (MIS), such as laparoscopic or endoscopic surgery, has revolutionized the medical field over the past few decades [1]. The use of long thin instruments through small incisions results in decreased pain, reduced tissue damage and shorter recovery time for the patient, compared to the traditional open surgeries [2, 3]. However, MIS presents its own set of challenges. Due to the nature of the tools used in MIS, some of the surgeons sensory capabilities are limited, such as hand-eye coordination and depth perception. The surgeon must then rely heavily on visual feedback, which may not provide the necessary information about tissue characteristics or the forces applied [2, 4]. Robotic systems have been developed to provide visual and sensory feedback to the surgeon to overcome these challenges. As these procedures often take place in imaging environments like Computed Tomography (CT) or Magnetic Resonance Imaging (MRI), the focus has been on creating robotic systems that are compatible with these environments, enabling the surgeon to operate the device remotely from a safe distance [5]. These types of procedures are known as Robotic-Assisted Surgeries (RAS).

1.1.2 Haptic Feedback

Haptic feedback enhances the user experience when interacting with a device, by providing them with physical sensations. There are two types of haptic feedback: tactile and kinesthetic. Tactile feedback focuses on sensing surface textures through skin perception, such as vibrations. Kinesthetic feedback, however, addresses the sense of movement and forces perceived by the muscles, tendons, and joints, allowing the user to perceive the forces and torques acting on the device. The advantages include improved user interaction, and enhanced safety in certain applications [6–8].

1.1.3 Haptic feedback in MIS

Haptic feedback has been shown to play a crucial role in enhancing safety in RAS [9]. Research has demonstrated that incorporating force feedback can improve tissue characterization accuracy by up to 20% for non-surgeons and 10% for surgeons when compared to relying solely on visual feedback [10]. A study using the surgical system FLEXMIN also revealed that the use of force feedback led to a significant decrease in applied forces, reducing the maximum applied force from 14.6 N without feedback to 10.23 N with feedback [11].

1.1.4 Pneumatic actuated devices

Pneumatic actuated devices use compressed air or gas to generate force and motion [12]. They have grown in popularity due to their fast response time, high force capabilities, and their ability to operate in hazardous environments [13–15]. Their low weight and ability to allow spacing between actuators make them ideal for use in soft wearable devices [16–18]. Additionally, their compatibility with CT and MRI imaging makes them a valuable component in RAS systems.

1.1.5 Pneumatic Artificial Muscles (PAM)

Pneumatic Artificial Muscles (PAM) [19] are a special type of actuators that generate force and motion using compressed air or gas. The idea was inspired from biological muscles, looking at how they contract in length and expand in diameter when activated [20]. The appeal of PAMs are the flexibility and light weight as well as the efficiency in force generation compared to their size. Moreover, they have a quick response time and have the added capability of operating

in various environments, including CT and MRI [19]. However, it does not come without its difficulties. The non-linear characteristics of PAMs can make modeling and precise control difficult [19, 21–23].

1.1.6 Reverse Pneumatic Artificial Muscles (rPAM)

Due to the limitations of traditional PAMs and other soft actuators, such as radial expansion, buckling issues and control difficulties, a new design was developed, called Reverse Pneumatic Artificial Muscle [24]. The design is largely based on the design of PAMs, with the main change being the reverse direction of the actuation when pressurised. A non-expanding thread is used to constrain the actuator from radial expansion, constraining it to axial expansion. Soft linear actuation is typically unsuitable for extension motion outputs because it tends to buckle when subjected to a payload, meaning that it cannot efficiently maintain structural integrity under the applied load [25]. However, rPAMs address this issue by ensuring that the actuators always encounter tensile stresses, which helps maintain their structural stability. This is achieved by pre-straining the actuators and then releasing the corresponding stresses through pressurization. When the actuators are pressurized, the internal pressure causes the fibers in the silicone material to relax and relieve the pre-existing tension. As a result, the actuators maintain a state of tensile stress throughout their operation, which helps maintain structural stability [24].

1.2 Objective of the thesis

The work in this thesis is built on the work of a previous student who developed a prototype of a rPAM actuated device. The primary goal of this thesis is to modify this device and incorporate force feedback. Given the limited haptic feedback available to surgeons in MIS procedures, the addition of force feedback to such a device has the potential to enhance surgical precision and improve patient outcomes. Therefore, the following objectives have been identified:

1. Modify the given device to reach the full potential of the workspace of the device. Specifically, reduce the friction and increase the actuator capabilities in order to maximize the device's controllability.
2. Integrate force sensors to accurately measure the user force.
3. Implement a control algorithm for the rPAM actuated device that accounts for the non-linear characteristics of the actuators and ensures precise force feedback and stability.
4. Evaluate the transparency and stability of the integrated force feedback system in the device.

By achieving these objectives, this thesis aims to contribute to the ongoing research in improving haptic feedback for MIS and usage of soft actuator technologies in surgical robotics.

1.2.1 Research question

The objectives of this research are formulated in the following research question:

1. What is the efficacy of reverse Pneumatic Artificial Muscles (rPAM) for usage in remote Minimally Invasive Surgeries with kinesthetic (force) feedback, especially for needle insertions in soft tissue; biopsies and ablations?

The following sub-questions were thought of to help answering the main research question:

1. How can the force experienced by the user be measured accurately while the device is operated?
2. How can the non-linear characteristics of the actuators be mitigated, to ensure a smooth insertion and accurate haptic feedback?
3. Which control architecture can provide the user with realistic haptic feedback, while ensuring a safe insertion?

1.3 Scope and limitations

This chapter outlines the scope of the research presented in this thesis, as well as the limitations associated with the study.

1.3.1 Scope

The scope of this thesis is primarily focused on the following areas:

1. reverse Pneumatic Artificial Muscle (rPAM) Technology: The research is centered on the exploration of different materials and their abilities. Other actuation technologies, such as traditional PAMs, are beyond the scope of this thesis.
2. Force Feedback Integration: The main objective of this research is to incorporate force feedback into a PAM actuated device and evaluate its effectiveness. Other aspects of haptic feedback, such as tactile feedback, are not the primary concern of this study.
3. Minimally Invasive Surgery (MIS): The rPAM actuated device with force feedback is specifically designed for MIS applications, such as needle insertions. Other types of surgical procedures, such as open surgeries or image-guided interventions, are beyond the scope of this thesis.
4. Insertions: While there are forces acting on a needle during both the insertion and extraction of the needle, the extraction is not considered for this project.

1.3.2 Limitations

While efforts are put into meeting the goals set in this thesis, there are still some limitations to our study:

1. Non-linear Characteristics of PAMs: The non-linear characteristics and complex dynamic behavior of PAMs can make precise control more challenging. While efforts will be made to develop and implement control algorithms that account for these factors, achieving very accurate control may not be possible.
2. Force Sensing: Accurate force sensing is crucial for the effective integration of force feedback in PAM actuated devices. However, the choice of force sensors and their placement might impact the overall performance and sensitivity of the system.
3. Force capabilities: The force that the actuators are able to exert to the user is dependent on many factors. While efforts will be made to maximize their capabilities, high force outputs might be difficult to achieve with the current hardware.

By acknowledging these limitations, the aim is to provide a realistic view of this research.

1.4 Structure of the thesis

This thesis starts by analysing current state of the art systems in a literature review, as well as pointing out the gaps and areas for improvement. Moreover, the current state of the system is analyzed. Subsequently, a materials and methods chapter explains the design of the system as well as the modelling and control. Following that, in the evaluation chapter, the experiments performed, as well as their results are laid out. Finally, a discussion chapter and a conclusion and future work chapter discuss the results and conclude the answer of the research question, before making recommendations for future development of the device.

2 Analysis

2.1 Literature Review

While haptic feedback has already been utilized in some medical devices [26, 27], this research focuses on devices that can be used during or in proximity to MRI imaging. Current teleoperated devices usually involve metallic motors that are incompatible with MRI imaging [28]. Surgeons must then rely on a video stream during surgery, which will have some small delay. By investigating soft actuation, this research proposes a solution that allows the surgeon to be present in the room while the patient is being imaged. The surgeon can then rely on his own vision while operating the device from a safe distance. A review of the literature on related technology is conducted, along with their methods for evaluating the efficacy of their devices, to aid in answering the research question "What is the efficacy of reverse Pneumatic Artificial Muscles (rPAM) for usage in remote Minimally Invasive Surgeries with haptic feedback, especially for needle insertions in soft tissue; biopsies and ablations?"

2.1.1 Haptic devices

Applications for haptic technology are diverse and can be seen in various industries, including virtual and augmented reality, gaming, automotive and the medical industry. Tactile feedback has been utilized in mobile devices due to their decreased size and weight requirements compared to kinesthetic devices. However, haptic devices can face limitations in delivering accurate and realistic sensations due to factors like latency, energy consumption, and hardware constraints.

Some applications of tactile feedback include regulating breathing patterns [29], enhancement of virtual reality experiences [30] and supporting in search and rescue operations [31]. Kinesthetic feedback is commonly used in teleoperated systems due to its ability to provide users with a physical sensation of the forces acting on the controlled device, making the experience more intuitive and natural. Some applications of kinesthetic feedback include space telerobotic missions [32], lanekeeping assistance (automotive) [33] and surgical robots [34].

Haptic feedback in surgical applications

The use of teleoperated robots has spread worldwide and has become an integral part of surgical training in most surgical subspecialties. However, despite the widespread use of robots, commercially available robots that relay haptic features to the operator is rare [35]. The only commercially available system that is FDA approved is the Da Vinci Robot [36], which does not include any haptic feedback [35].

Other surgical robots have been developed that are commercially available, but not used in common practice. The Senhance Surgical System is often considered the biggest competitor to the Da Vinci [37]. The system can provide kinesthetic feedback by transmitting the resistance felt by the robotic arms during surgery back to the surgeon's console [26]. Other strong competitors mentioned are Revo-I and Versius [37]. The Revo-I system provides the surgeon with tactile feedback by giving feedback when the robot is nearing a potential collision [37, 38]. On the other hand, the Versius system provides the surgeon with kinesthetic feedback, relaying both the force and its direction applied from the tips of the instruments [39].

Other surgical robots have been designed in recent years that are not currently commercially available yet. Researchers have also designed systems that is meant to advance this field.

FLEXMIN was developed in order to improve the ergonomics and workspace aspects of transanal surgery. They showed through experiments, where a point-and-touch task was tested, FLEXMIN's improved precision and larger workspace, compared to conventional sur-

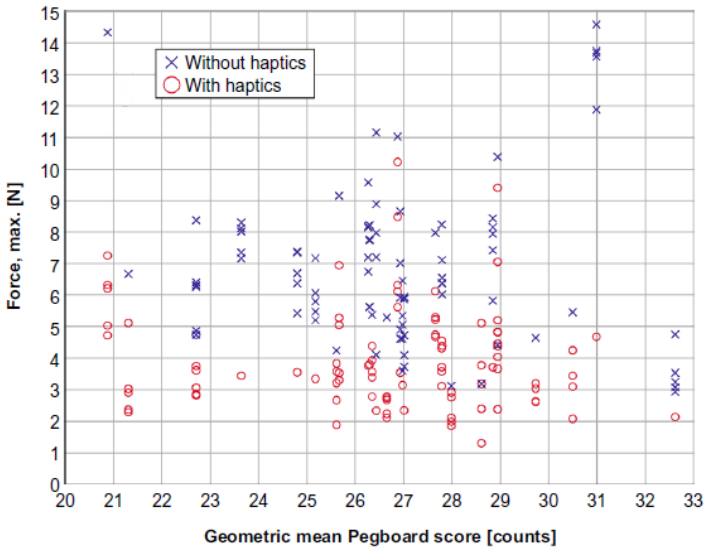

Figure 2.1: Haptic feedback evauluation of FLEXMIN [11]

gery instruments [40]. Haptic feedback was evaluated by comparing the maximum force applied with and without the feedback [11]. The results can be seen in table 2.1 and visually in Figure 2.1.

	Median	**Min**	**Max**	**IQR**
Without Haptic Feedback	6.43 N	2.94 N	14.58 N	2.964 N
With Haptic Feedback	3.57 N	1.30 N	10.23 N	1.936 N

Table 2.1: Comparison of maximum force with and without haptic feedback for the FLEXMIN system.

An endovascular catheterization robotic system (ECRS) was developed for the purpose of providing a safer and more efficient method for performing endovascular catheterization. The system provides kinesthetic feedback through a magnetically actuated mechanism. An evaluation was made for the force feedback by first establishing a mathematical model between haptic force and the magnetic field and then measuring the accuracy of the controller. Moreover, the maximum force was measured in the cases with and without haptic feedback and all of the six users showed decreased maximum force applied when haptic feedback was applied, compared to no haptic feedback. The results can be seen in Figure 2.2 [41].

A pneumatic haptic device was developed for usage in MRI-guided telesurgery. Specifically, percutaneous interventional procedures under continuous MRI guidance. The master device is mostly 3D printed while pneumatic actuation is used to provide haptic feedback. An aluminum load cell with integrated strain gauges measures the force feedback between the user and the 3D printed biopsy needle handle. They evaluated the system through a teleoperated needle insertion and rotation experiments performed to reach 10 targets in a soft tissue-mimicking phantom. The results showed that the slave robot follows the insertion motion of the haptic device while the haptic device displays the needle insertion force as measured by the FPI sensor [34]. The master device force tracking was evaluated in an earlier paper with the assumption that the needle insertion force is with limited acceleration. A simulated input force of a 20 N sine wave was applied while the master device's handle was held in place. The results showed a RMS error of 2.227 N [42].

A lightweight master device, using pneumatic bellows, was developed for a surgical robotic system. The bellows are designed to be smaller and lighter than electric motors, making the device

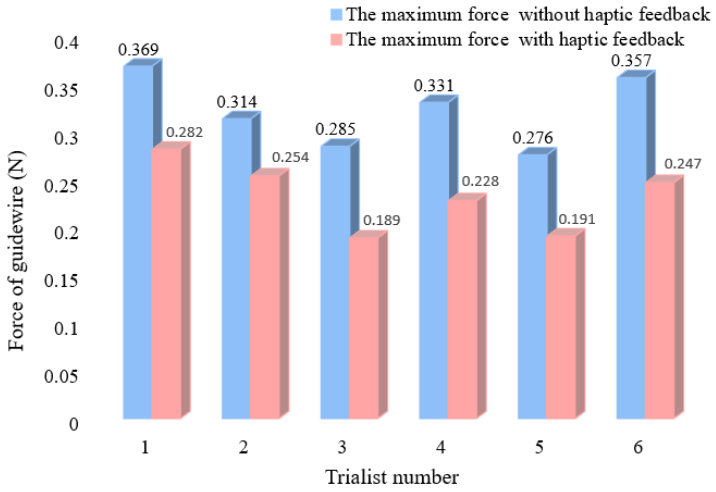

Figure 2.2: Haptic feedback evaluation of ECRS system [41]

more comfortable to operate. The small device is operated by compressing the bellows, which controls a slave gripping device using pneumatic actuation. The position of the hand operating the device is measured using a non-contact motion tracker while the Kinesthetic Feedback from the gripper is given by the pneumatic bellows. The evaluation of haptic feedback was done first by a step input force of 1 N or 15 N when the displacement becomes 3 mm. Next, a ramp input was given when the displacement becomes more than 3 mm. The ramp is defined as $f_{hu}^{ref}(t) = 0.5[t/3]\,[N]$. The results show a maximum error of about 0.3 N [43].

A novel haptic robot-assisted catheter operating system was designed to provide high-precision force feedback and detect catheter-vessel collision, thereby reducing the risk of damage to the blood vessel. A spring-based interface relays the force, felt by the catheter, to the master device. The accuracy of the haptic feedback was evaluated by inputting the force felt by the slave system to the master device. The forces range from 0 to 1.5 N and don't have any really rapid changes. The results show a mean error of 0.027 N [44].

Requirements for a haptic device in MIS

For a kinesthetic-focused haptic device, the most basic requirement is that it should be able to relay the ranges of forces to the user that can be expected during surgery. If we focus on the case of a liver insertion, the forces go up to about 3 N when inserting into bovine liver [45]. For an insertion into a human liver (healthy tissue), the forces are found to range up to 1.7 N for an insertion of 70 mm [46].

A few studies have outlined their requirements. In [47], they mention requirements such as low magnitude of friction forces, overall durability and compactness. Another study lists the desirable features of a haptic device [48]. These features include minimal backdrive friction, very little backlash in the transmission and capability for large force reflections. Moreover, they mention that human fingers can sense absolute and relative force variations of 0.5 N and ± 7%, respectively. Therefore, the force sensor on the slave side and the haptic interaction on the master side should have at least this precision.

For the human hand system, the just noticeable difference was evaluated [49]. The results for forces parallel to the hand (Table 2.2) show that the absolute force variation JND increases with an increase in the setpoint.

Reference [N]	JND%	JND [N]
-5.99	15.3	0.916
-3.28	16.3	0.535
-1.80	18.0	0.324
-0.87	18.1	0.157
-0.54	25.7	0.139
0.50	31.6	0.158
0.83	22.7	0.188
1.79	15.7	0.281
3.26	17.0	0.555
5.98	9.6	0.574

Table 2.2: Table showing the Reference force, JND% and the calculated JND in Newtons

2.1.2 Pneumatic Artificial Muscles (PAMs)

Designed in the 1950's, the PAM actuator has been used in biorobotic applications and in biomimetic robots due to the resemblance of the characteristics of actual skeletal muscles [19, 50]. Although there are multiple designs of PAMs, there are two designs that stand out as the most used. Those are Braided Muscles (Mckibben muscles) and Pleated Pneumatic Artificial Muscle [51]. Figure 2.3 shows a few different designs of PAMs.

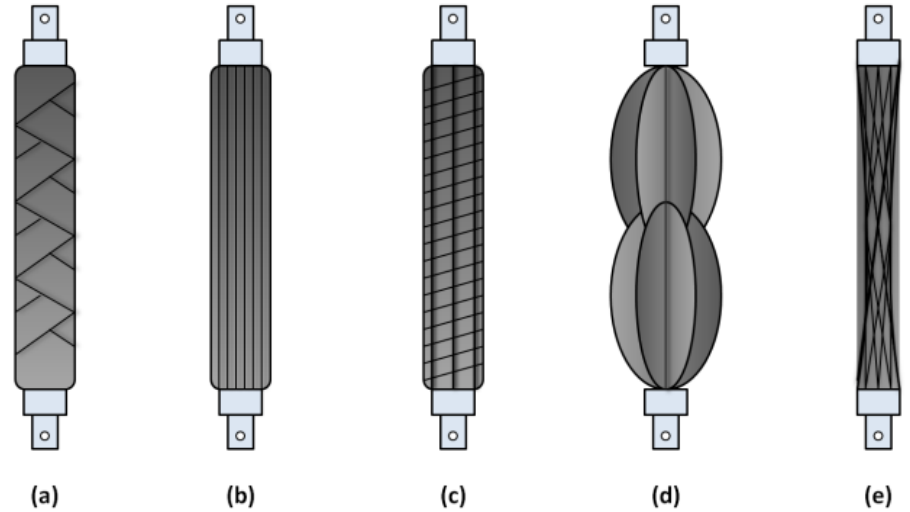

Figure 2.3: Different types of PAMs: (a) McKibben Muscle/Braided Muscle, (b) Pleated Muscle, (c) Yarlott Netted Muscle, (d) ROMAC Muscle and (e) Paynter Hyperboloid Muscle. [19]

Braided muscles

The braided pneumatic actuator, popularized by Mckibben was originally thought of as a tool to help movements of polio patients in the 1950's [52]. In recent years, it has become one of the most widely-used fluid-power actuators due to muscle-like properties such as high force to weight ratio, soft and flexible structure, minimal compressed-air consumption and low cost [22]. Applications range from Biorobotics, medical, aerospace and industrial [19].

The design consists of a inner tube made of rubber, surrounded by a braided mesh sleeve made of a strong material like Nylon. The braid fibers are helical and have a braid angle θ as shown in Figure 2.4. The braided sleeve and the inner tube are attached to a fitting at both ends of the muscle. When pressurised, the inner tube tries to expand. The braided sleeve mostly restricts this expansion because of its non-expanding nature. The restriction of the sleeve depends on

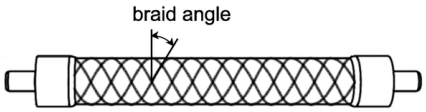

Figure 2.4: Braided muscle design, where the braid angle is shown [54].

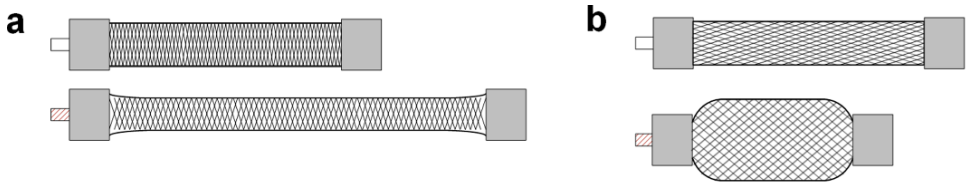

Figure 2.5: Different directions of actuation in PAMs: (a) Extensile: rPAM, (b) Contractile: Mckibben [57]

the braid angle. The braid angle is chosen depending on the application. A larger braid angle results in a less tight winding, which results in more contraction when pressurised, but with a reduced force exerted. A smaller braid angle then winds the sleeve more tight resulting in more force but a smaller contraction [51].

While braided muscles have some great benefits such as high power-to-weight ratio's, low cost and light weight, they also have several shortcomings. The inner tube needs a certain threshold pressure before it starts expanding, which can make accurate position control difficult to achieve. The dry friction between the sleeve and inner tube can cause a wear and tear in the muscle over time, resulting in a short life-expectancy [51]. However, by changing the fabrication process, one study showed an increase in the actuator life expectancy. By employing a swaging process to the fabrication, the number of fatigue cycles before damage occurs increased from a maximum of less than 18.000 cycles, as shown in previous research, up to more than 120.000.000 cycles with minimal wear and tear signs [53].

The expansion of the muscles can be problematic where space is limited and the non-linear characteristics of PAMs make them difficult to model and control [19, 21–24].

Pleated PAMs

Pleated PAMs were developed as an improvement of the braided muscle design. This new design solves the issue of material deformation by using stronger materials, like Kevlar which is most known for its use in bulletproof vests. Moreover, the stress distribution was greatly improved by designing the sleeve such that when the stress increases, it mostly increases in one direction. When this happens, the yarn that is along that direction straightens, but the yarns in parallel direction will resist it, which helps distribute the stress among the yarns [55]. Despite the non-linear force/displacement characteristics of the actuators, they can be effectively controlled using basic linear PI techniques [56].

reverse Pneumatic Artificial Muscles (rPAMs)

A different design, similar to traditional PAMs is the reverse PAM. The design, mostly differs in the direction of actuation. Instead of contracting when pressurised, rPAMs extend when pressurised. This is due to the fact that instead of a braided mesh design for the fibers, this design uses a simpler composition of helical fibers. Moreover, the actuators are pre-stretched which deforms the helix resulting in an outward force when pressurised [24]. The difference in direction can be seen visually in Figure 2.5.

Compared to traditional PAMs, rPAMs show advantages in certain areas. The design increases the stroke while also expanding only in the direction of actuation. Having the expansion only

in 1 DoF results in a linear force-extension relationship which in turn makes modelling the system easier. Moreover, the extensive design allows the actuator to be used where space is limited [24, 58, 59].

A soft robotic wearable wrist device was made using rPAM actuation [60]. The actuators provide the user with kinesthetic feedback with the aim of improving performance in a virtual path-following task. The forces applied to the user is related to the angle and velocity error. They evaluated their device by having users follow both a linear path and a sine-like path. The results show an improvement in the sine-like path, while no improvement were found in the linear path.

PAMs in surgical applications

PAMs have been used in rehabilitation devices due to their resemblance of organic muscles. However, in recent years, their usage in different aspects of the medical field has increased due to their flexibility, compliance, high power outputs compared to size and weight and their inherit safety when operating in a human environment [19].

A forceps' manipulator system was developed to improve haptic sensation during MIS. It utilizes two PAM of the Mckibben design for the gripper's pitch and yaw motions. The papers do not mention any experiments related to evaluating the haptic feedback [61, 62].

A soft-robotic end-effector was developed with the purpose of independently actuating endoscopic catheters. The end-effector uses Miniature Pneumatic Artificial Muscles (MPAMs) for positioning the catheter tip. The results show a region of 45 mm radius that the tip can be positioned at with an accuracy suitable for endoscopic surgeries [63].

Modelling of PAMs

A study comparing contractile and extensile PAMs found that current contractile force models were shown to be valid for extensile modeling [58]. Different models have been made to accurately model the complex behaviour of PAMs. Due to the non-linearities of PAMs, creating an accurate model is challenging. A review paper compiled different models from literature [50]. The paper mentions four classifications of the most common PAM models, defined by another paper [64], namely Geometrical-, Biomechanical-, Empirical- and Nonlinear models. The paper mentions the Chou and Hannaford model [21] as the simplest Geometrical model for a static performance.

$$F_g = \frac{Pb^2\left(\frac{3L^2}{b^2} - 1\right)}{4n^2\pi} \tag{2.1}$$

where

F_g = The simple geometric force of PAM [N]
P = The operating gauge pressure [Pa]
b = The thread length [m]
L = Length of the PAM [m]
n = Number of thread turns

Simple empirical models can be found by modeling the pulling force acting on PAMs as a mechanical spring with a variable stiffness [65]. The force is then given as:

$$F_{\text{elastic}} = K(P, L_s)L_s \tag{2.2}$$

where

$$F_{\text{elastic}} = \text{The elastic force generated by PAM [N]}$$
$$K = \text{Variable stiffness parameter [N/m]}$$
$$P = \text{The operating gauge pressure [Pa]}$$
$$L_s = \text{The stretched length of the PAM [m]}$$

The stiffness K has been considered as a second order polynomial of P and L_s which is given as:

$$K = q_1 + q_2 L_s^2 + q_3 P L_s + q_4 P^2 \tag{2.3}$$

where

$$q_1, q_2, q_3, q_4 = \text{Constant parameters determined from experimental data}$$

For a more in depth model, the non-linear model is needed. These models are more complex and require a better understanding of different factors. Determining accurate values for constants in these models often requires precise experimentation.

Modelling of rPAM

The inventors of the rPAM actuators described their methods of modelling rPAMs [24]. First, the authers describe an analytical model that predicts the extension of the actuator under a given internal pressure and load. The model consists of two components, the constraints- and the material model. The first is a geometrical model describing the geometrical relationships of the helical threads, while the second takes into account the material properties of the silicone. The following assumptions are made for simplicity:

1. There is no shift of or friction from the thread when actuated. This is ensured by the fact that the threads are slotted into grooves and then glued in place.
2. The actuator remains cylindrical.
3. The thread is inextensible.
4. The silicone rubber material is incompressible.
5. The analytical model will be quasi-static, describing the position of the actuator at steady state. All experimental data was taken at steady state as well.

The analytical model is based on the force balance equation:

$$F_{\text{ext}} = F_{\text{cons}} + F_{\text{int}} \tag{2.4}$$

where F_{ext} is the external axial load on the actuator in tension, F_{cons} is the helical constraint force, and F_{int} is the force due to internal material stresses calculated based on the Ogden model. The resulting equation for the constraint force is given as:

$$F_{\text{cons}} = -PA_{\text{in}} = -P\left(\frac{b^2 - 3L^2}{4\pi n^2} - \frac{A_0}{\lambda}\right) \tag{2.5}$$

where

P = The input pressure [Pa]
b = Total thread length [m]
L = Length of the soft actuator after deformation [m]
n = The number of helical turns of the thread
A_0 = The initial nominal cross-sectional area [m^2]
λ = The principal stretch

Using the Ogden model, the axial stress is given as:

$$\sigma = \sum_{i=1}^{3} \frac{2\mu_i}{\alpha_i} \left(\lambda_i^{-\alpha_i} - \lambda_i^{\alpha_i}\right) \tag{2.6}$$

where

σ = The axial stress within the material [Pa]
μ_i = Material constant for the i-th Ogden element
α_i = Material constant for the i-th Ogden element
λ_i = The principal stretch for the i-th Ogden element

The material force is then given as:

$$F_{\text{int}} = \sigma A = \sum_{i=1}^{3} \frac{2\mu_i A}{\alpha_i} \left(\lambda_i^{-\alpha_i} - \lambda_i^{\alpha_i}\right) \tag{2.7}$$

where

F_{int} = Force due to internal material deformation [N]
A = The nominal material cross-sectional area [m^2]

Using Equations (2.5) and (2.7) the force output of the actuator can be calculated for a given length.

The authors also show a Numerical model using Finite element analysis (FEA). The FEA outperforms the analytical model, but not by a lot. With no weight and low pressures, both models match closely with the experimental data. However, with higher pressures and weights added, the experiment showed more deformation of the actuators than the models predict. This is likely due to simplifications made for the models, showing a need for a more in depth modeling for an accurate solution.

Controlling PAM actuated devices

Controlling PAMs accurately requires an accurate mathematical model of their behavior. Researchers have developed different methods for this task. The position of a 1 DoF robotic lower limb system is controlled using a fuzzy sliding mode controller [66]. For comparison, a PID controller is used. The results show that the sliding mode controller performs much better than the PID. More researchers have also used a version of sliding mode controllers for position control of PAMs (and rPAMs) [24, 67]. The position of a forceps' manipulator is controlled

using an outer position feedback loop with a PD controller and a feed-forward block, and an inner pressure feedback loop with a PI controller [61].

For controlling the force, one research claims that the sole implementation of the classical feedback controllers (PID or lead-lag only, without feedforward and nonlinear passifying terms) had unacceptable tracking performance and often led to instability [68]. The paper proposes a method that guarantees stability and high tracking performance thanks to nonlinear passifying and feedforward terms. Other researchers went with a sliding mode controller which proved to be better than a traditional PID in tracking the force.

2.1.3 Force sensing

Accurately measuring force on the haptic device is a critical and challenging aspect of kinesthetic feedback, so picking the correct sensor is important. In [69], eight force and tactile sensing methods for usage in MIS were compared: displacement, current, pressure, resistive, capacitive, piezoelectric, vibration, and optical. The authors found that most electrical force sensors cannot be used in imaging environments, such as MRI, making optical fiber sensing one of the few practical options.

In [70], the authors argue that while resistive strain gauge sensing is also an option in environments such as MRI, it is less viable than fiber optic sensors due to susceptibility to electrical noise and the requirement that gauges must be placed a suitable distance away from the MR field.

While most studies go for the option of optical fiber sensors for devices that need to be inside an MRI (slave devices) [34, 70, 71], they are often heavy, expensive and not commercially available. However, a proposed solution that offers CT compatibility is a polymer force sensor [72]. The sensor was developed with the goal of complying with the requirements of needle insertion applications, in the context of interventional radiology.

2.1.4 Conclusion

The literature review has provided an overview of the state-of-the-art haptic devices as well as PAM devices, with a focus on applications in the medical field. It has been established that haptic feedback is missing in many of the surgical devices used today, despite the obvious correlation to improved safety when applied. Moreover, the review has shown how researchers evaluate their haptic devices, where the traditional method was found to be evaluating the transparency of the force feedback as well as comparing the maximum force applied with and without haptic feedback.

The review has also found that PAMs show good potential as safe actuators that have the possibility of being used in, or near to, environments such as MRI or CT. Although their usage in the medical field is not common, the review has shown that their high power-to-weight ratios and inherent safety when operating make them a promising alternative to traditional heavy metallic actuators. Pleated PAMs and rPAMs were found to be especially suitable, since they have improved the design of traditional PAMs in their own way. Pleated PAMs were found to be stronger and easier to control when compared to traditional PAMs, making them suitable for applications where the actuator needs to exert large forces as well as providing accurate position control. However, rPAMs were found to have an increased stroke length as well as having the quality of not expanding outwards, making them suitable in small devices where there is not a lot of space for expansion.

However, research into using rPAM actuation in order to apply force feedback to the user is limited. One wearable device was made using rPAMs with the aim of improving path accuracy. Moreover, a forceps' manipulator was designed using the Mckibben design but the force feedback was not evaluated. While rPAMs were found to be suitable for the wearable device, the use

case for that device is not specific for MIS. Moreover, the efficacy of the kinesthetic feedback was not evaluated in that case, only the path following accuracy with and without the feedback was evaluated. More research is needed to highlight their efficacy as actuators in stationary master devices used specifically for MIS.

In conclusion, while significant improvements have been made in surgical devices, there is still a need for research to improve accuracy and safety during operations. Haptic feedback, both tactile and kinesthetic feedback, has shown to improve both accuracy and safety when applied and PAMs have been found to be promising as actuators to apply kinesthetic feedback to the user.

2.2 Current state of the system

In this section, the state of the device developed by a Bachelor's student is described [73]. The device is designed with the purpose of evaluating the feasibility of rPAM actuators as a haptic device. The design was thought of as a joystick controller. Two rPAM actuators are placed such that they provide force in opposite directions on the same axis. In between, there is a joystick that the user should control. This can be seen visually in Figure 2.6.

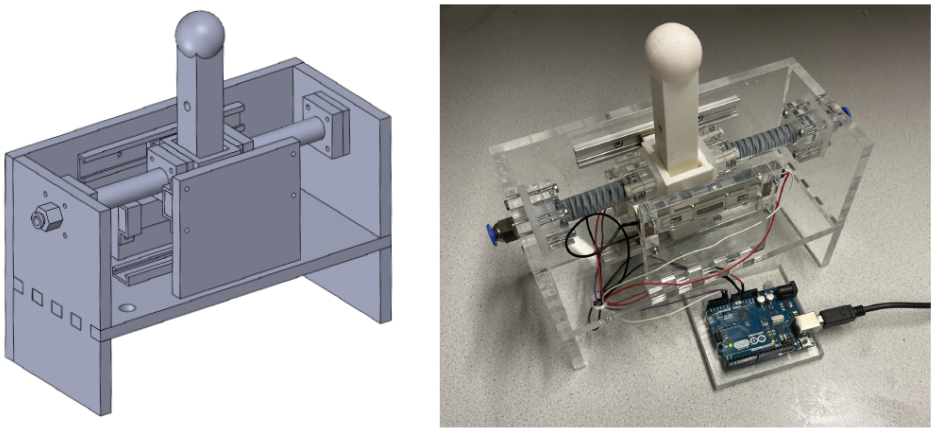

(a) CAD model (b) Realized model

Figure 2.6: The CAD model and realized model of the given device [73].

The device has two linear guide rails, one at the bottom of the joystick and the other at the rectangle connector, called the ring. The ring is also connected to a slide potentiometer on the other side. A second slide potentiometer is connected to the side of the joystick handle.

All these parts, including the sliders and rails, are held together within perspex glass. The joystick and ring are made from 3d printed materials. The reason for the material choice is to show that with minimal modifications, this device can be fully - or almost fully - MRI/CT compatible. Due to some laser cut tolerance, there is an offset present in the plates. That means that the back plate, that holds the linear guide rail and the second potentiometer, is not completely parallel to the detachable plate on the other side of the device, which holds the first potentiometer.

2.2.1 Hardware

An Arduino Uno is used to give air pressure commands, while measuring the position and force using a potentiometer and a force sensor.

Two potentiometers are used to measure the position of the joystick. Each potentiometer is a slider potentiometer, with one connected directly to the joystick and the other to the ring.

The air pressure is controlled using two regulator valves with an input of 400 kPa and two outputs of maximum 200 kPa. A pneumatic shield is mounted on an Arduino Uno where the air pressure commands are given. An Arduino is programmed to drive the 24V regulator valves through the shield.

To test this device, a ATI40 mini FT-sensor was mounted to the joystick to measure the user force during movements. The setup for the sensor and the regulator valves, as well as the potentiometers used, can be seen in Appendix A.1.1.

2.2.2 Actuator

The actuators are designed, mostly in the same way as presented by the original paper [74]. The paper presents their design of the actuator in the following way:

1. Insert a carbon fiber or metallic rod of appropriate diameter into the center of the body mold to create the hollow cylindrical core inside the actuator. Introduce silicone rubber into the body mold.
2. After silicone rubber has cured, remove the rod inside the body mold, then remove the silicone from the body mold. Tie two symmetrical helices of thread around the cylindrical silicone rubber body guided by the grooves. Apply an outer layer of uncured silicone rubber around the threads to permanently bond the thread to the actuator.
3. Sandwich each of the ends of the actuator between two layers of acrylic with an integrated vent screw to serve as pneumatic fitting and tighten to form the end caps.

This can be seen visually in Figure 2.7. The design of the current actuator mostly differs in the end caps. Instead of sandwiching the ends between two layers of acrylic, the mold is designed to include end fittings. These fittings include holes for screws that can be used to mount the actuator to the constraining plates. However, due to no threading being present there, a small glass plate (see Figure 2.8) was added the the outside of the actuators, constraining them from ballooning.

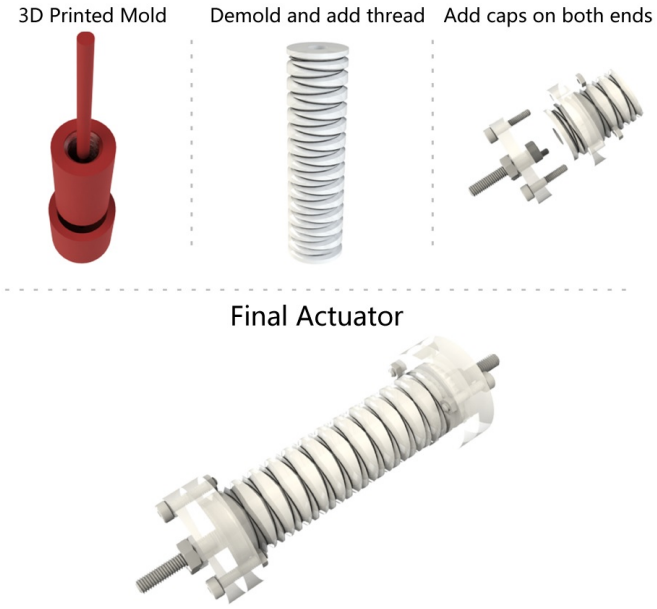

Figure 2.7: The fabrication of the original rPAM [74]

The fabrication process of the current actuators can be seen in Figure 2.9.

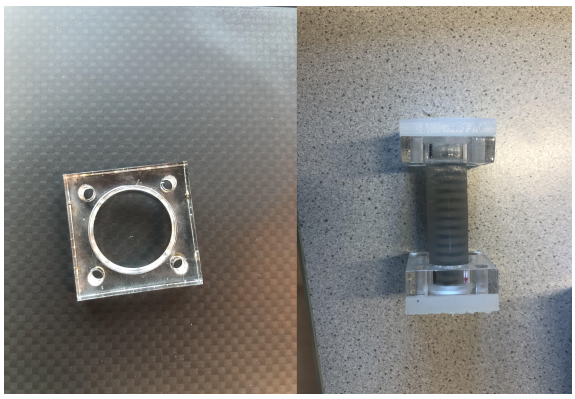

Figure 2.8: The small glass construction plate that constrains the ends of the actuators from ballooning.

Figure 2.9: The fabrication of the given device's actuators

2.2.3 Software

Arduino's integrated development environment (IDE) is used to communicate with the hardware and visualize the output data.

2.2.4 Dimensions

The dimensions of the main parts of the given device can be seen in Table 2.3, where the actuator length and width are the length and width of the end fittings and not the middle part of the actuators. Moreover, the height is given in the case of the actuators standing freely and not connected sideways to the device.

Item	**Length [mm]**	**Width [mm]**	**Height [mm]**
Glass container	218	98	138
Joystick	20	20	140
Ring	40	32	30
Actuators	30	30	60

Table 2.3: Specifications of Items

2.2.5 Recommendations

In the conclusion chapter of the BSc thesis [73], the student defined some recommendations for further development of the device. This list of possible improvements was considered for the design of the device, explained in section 3.1 in the following chapter.

- The friction created by potentiometers and sliders could be decreased.
- The design of the actuator could be optimised by increasing the threaded area to avoid structural failures.
- Moulds can be more precise to avoid moulding errors.
- A user study should be conducted to get inside the perception felt by the user from the haptic feedback.

3 Materials and Methods

3.1 Design and Implementation

In this section, the process of modifying the device in order to control it is laid out. First, the mechanical modifications performed in order to minimize friction in the device is explained. Following that, the changes made to the actuator design are given. Finally, the integration of force sensors to the device is explained.

3.1.1 Design goals

The given device had some obvious issues, some of which were defined already by the student that made the device [73]. For the purpose of modifying the device such that it could be used as a haptic device in medical applications, the following design goals for thought of:

1. Friction should be so low that a typical user can not recognise it.
2. Moving the handle should require the same force throughout the workspace.
3. The workspace should be maximized, such that the only limiting factor is the actuator capabilities.
4. The user should be able to feel at least 3 N as a feedback force throughout the workspace.
5. The actuators should have the same intrinsic characteristics over an extended period of time. They should not lose any functionality or break after a short time.
6. When the user releases the handle, there should be negligible backlash.

3.1.2 Mechanical modifications

In order to control the device, friction must be minimized. Each part that was thought to be causing friction was changed or modified. These changes were done iteratively until the device was easy to move. The steps taken will be explained in the order they were done.

1. The bottom linear rail connected to the joystick was removed. The joystick is operated at the top and with a single bearing at the bottom, causing torque instead of a linear force. This caused friction on the rail guide since the bearing was now tilted and not moving freely. Figure 3.1 shows this relation.
2. The second potentiometer, connected to the ring, was removed. The joystick and ring move together so as long as the potentiometer has repeatability and good accuracy, there is no need to measure the position of both.
3. The design of the handle was changed to be more similar to a computer mouse than a joystick. This was done since moving a joystick in 1 DoF is not intuitive, while for a 3 DoF system it would be. Moving a computer mouse however, is intuitive to move in 1 DoF. The new handle, and the resulting force from the user, can be seen in Figure 3.2.
4. The linear guide rail and potentiometer are then found to be the leading cause of friction. For the handle to move freely in the 1 DoF, the linear rail and potentiometer must be completely parallel. Otherwise, the two bearings will be moving slightly differently from each other, which causes unwanted friction. After a few failed attempts to make them completely parallel, a different solution was thought of. Instead of a slide potentiometer, a strip potentiometer was integrated to the system. The strip simply needs a contact point and it will tell you the position. The contact point was chosen to be at the ring, where a small hole was added to the design of the ring allowing a small disk-like object to be placed as the contact point. This can be seen in Figure 3.3. In order to ensure that the non-parallel glass plate structure would not effect the readings or cause friction in the device, a spring made from a flexible sheet of metal was placed inside the hole. This ensures that the contact disk retracts inward when pressure is applied.

5. After the slide potentiometer is removed, there is nothing holding the ring in place on one side. This can cause unwanted movements which in turn causes friction. To solve this, a steel cylinder is mounted to the ring. This cylinder rolls on top of the glass structure, holding the handle and ring stable. This can be seen in Figure 3.3.

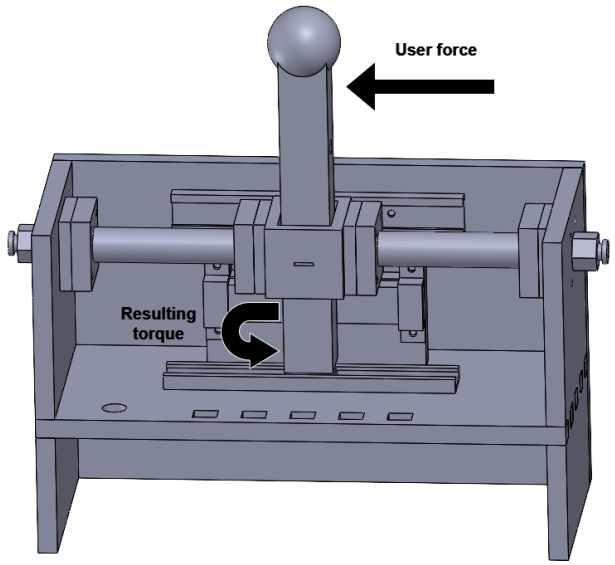

Figure 3.1: This image shows the torque created when a user pushes the joystick handle forward

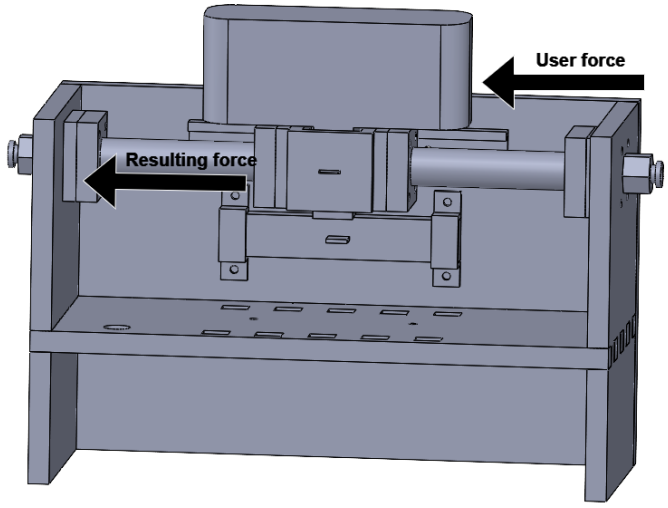

Figure 3.2: The new handle and the force created when a user pushes the handle forward

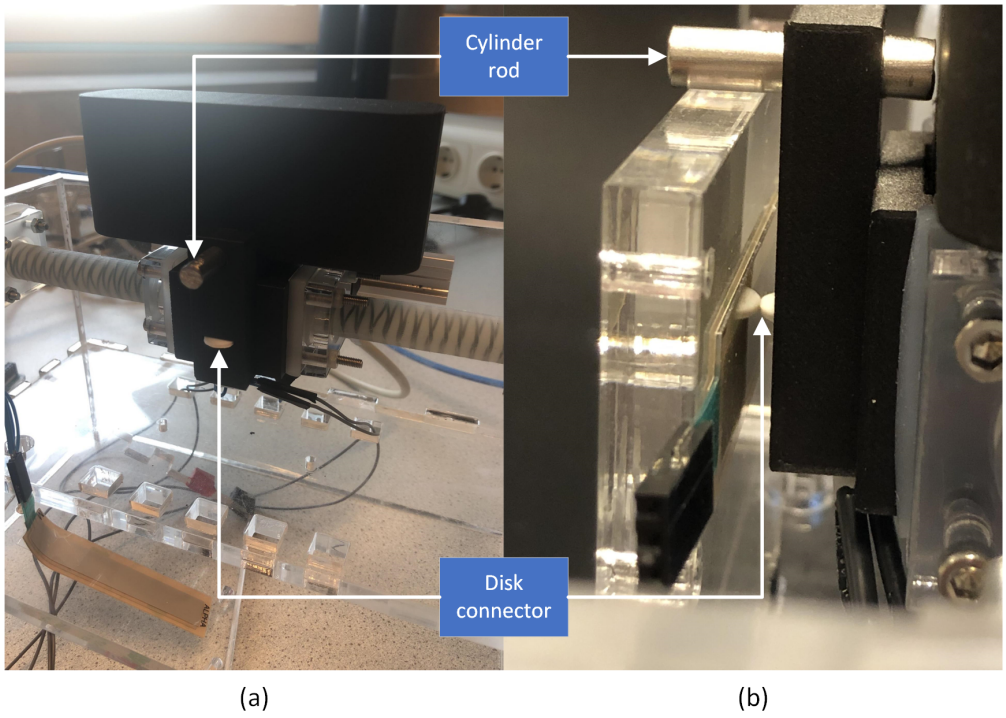

Figure 3.3: The disk contact point to the strip potentiometer. (a): Front view with potentiometer unconnected. (b): Side view with potentiometer connected. Cylinder rod is shown on the top sliding on the perpex glass.

3.1.3 Actuator design modifications

Some structure fails were found during use of the device, including ballooning of the actuator where no threading is constraining the actuator. Figure 3.4 shows this effect.

Figure 3.4: Ballooning of the actuator where threading is not constraining the actuator from radial expansion.

In order to solve this, the mold was modified to increase the threading area as much as possible. With the new design, one glass structure is enough to hold the ends of the actuators in place as well as constraining them from ballooning, while two were needed before. The difference in design and the resulting actuators from each design can be seen in Figure 3.5.

During the literature review conducted by the BSc student [73], Dragonskin 10 was found to be the ideal choice. However, access to Dragonskin proved to be difficult so the student opted to use a less strong Ecoflex 00-30 instead. The numbers represent the stiffness of the material, while Ecoflex is in the shore 00 category and Dragonskin is in shore A. There are three shore

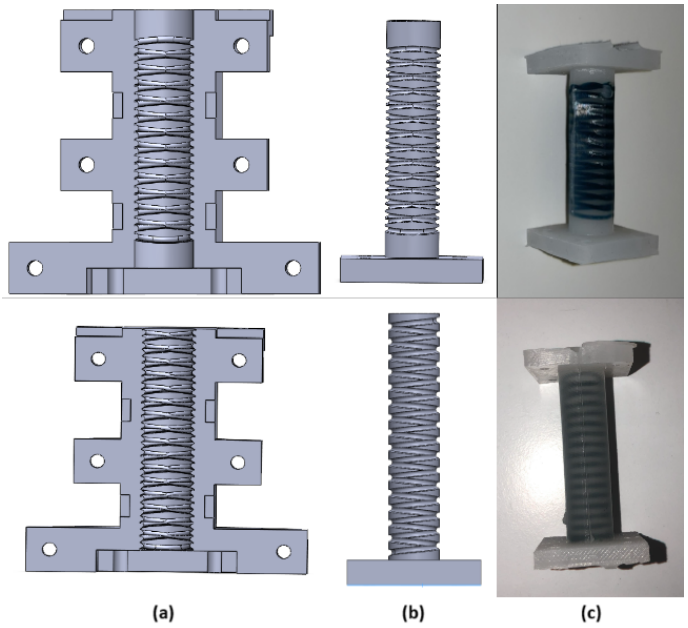

Figure 3.5: The difference in actuator threading. The old design (above) has less threading than the new design (below). (a): CAD model of the mold. (b): CAD model of the resulting actuator. (c): Resulting actuator

scales, all ranging from 0 to 100. Shore 00 is the softest, A next and D the hardest. Shore 00 is typically used for soft and flexible materials, A for flexible mold rubber materials and D for hard and semi-rigid plastics and rubbers [75]. Each shore then increases in stiffness when going up from 0 to 100. The difference in shore hardness can be seen in Figure 3.6.

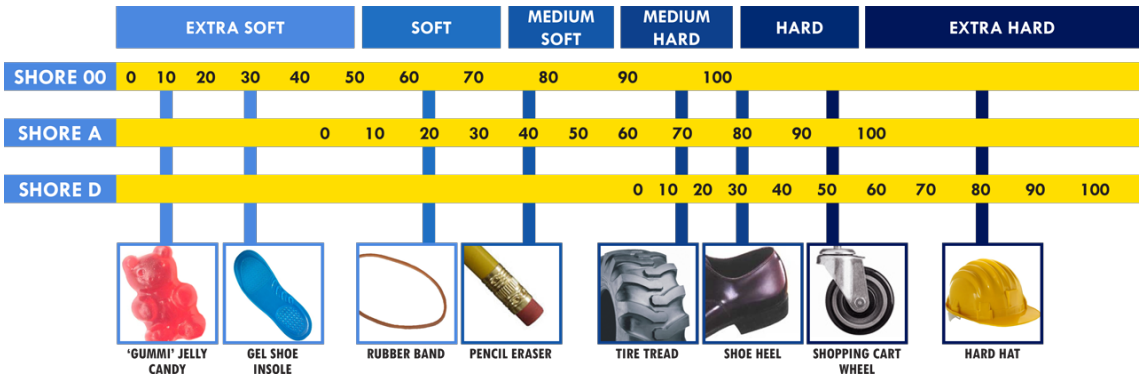

Figure 3.6: A scale showing the different hardness's of rubbers [76]

To increase the workspace of the device, different materials were tested. The original Ecoflex 00-30 was compared to Ecoflex 00-50 and Dragonskin 10 NV. Each increase in the hardness of the materials results in a stronger and stiffer actuator, resulting in a need for higher pressures to move. Ecoflex 00-50 was chosen for this application since Dragonskin needed higher pressures to move around the workspace, than the hardware supported.

3.1.4 Integration of force sensors

In order to measure the feedback force provided by the pneumatic actuators to the user, force sensors need to be mounted to the device. This subsection tries to answer the sub-research question: "How can the force experienced by the user be measured accurately while the device is operated?".

As this device's main advantages are the light weight, inexpensive material, high power output and possible MRI/CT compatibility, the force sensors were chosen with that in mind. Through literature review, fiber optic sensors were found to be the best fit for MRI compatibility. However, they were found to be expensive, heavy and not really commercially available. Resistive strain gauges were also found to be semi-compatible to MRI environments, while a safe distance is still needed when they are used. However, a polymer force sensor was found to be CT compatible. For this reason, a flexible pressure sensor [77] made using the latest advances in piezoresistive polymer composite processing and printing-based micromachining technology was chosen. However, the materials used in this specific sensor is not known. The only visible metallic part is the end connectors. Due to the qualities of the sensors, such as its light weight, low cost and high accuracy, this sensor was chosen. Therefore, until the effect of these sensors is tested near MRI or CT imaging, it is assumed that they are okay to operate near the imaging. Figure 3.7 shows the lightweight sensor.

Figure 3.7: The pressure sensor used to measure the user force [77]

The sensors are placed on each side of ring, such that the user force can be measured when the handle moves in either direction. The sensors are hot-glued to the ring to keep them in place, without applying any pressure on them as that would result in a rise in force measurements. The connected sensors with soldered wires can be seen in Figure 3.8.

Contact point

The force sensors are integrated to each side of the ring, such that when the handle moves, it would touch one of the sensors. This is done by decreasing the size of the handle input, that is placed in the ring. Four cylinder sleeves are integrated to the handle where a rod can be inserted. The sleeves are printed on a Bambu Lab X1C [78] from a material called Iglide [79], which shows minimal friction when a metal object slides on it. Figures 3.9 and 3.10 show the design and how bolts are used to connect the handle to the ring. These bolts have a large smooth area where there is no threading. Figure 3.9 also shows a small disk in the center of the handle connector. This connector disk is printed on both sides, such that the contact point to both sensors is always the same, allowing for user force detection in both directions. Since the friction is so low that it doesn't keep the handle stuck after moving, as well as the decreased size of the handle connector compared to the ring, the force sensors always show 0 N when the user releases the handle. The handle was printed using a micro carbon fiber called Onyx [80] using the Markforged Mark Two printer [81] in order to have the print as precise as possible. If the print did have some precision issues, it is likely that it would introduce some friction when sliding the handle on the bolts, as the holes would not be perfectly parallel.

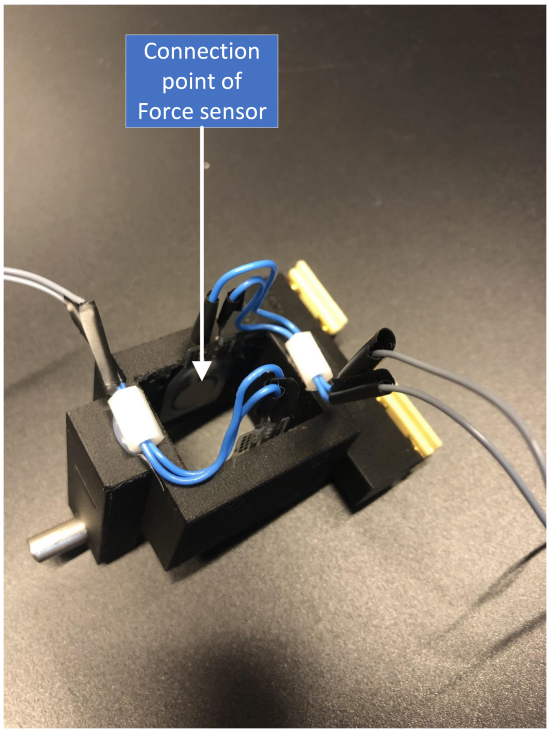

Figure 3.8: Upside down view of the ring. The force sensors are placed on each side of the ring, in order to measure the user force in both directions.

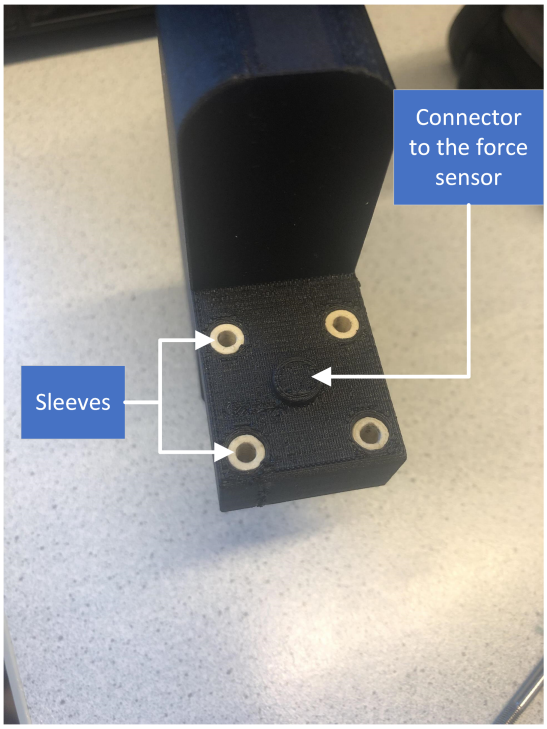

Figure 3.9: The designed handle connector where four cylinder sleeves are in place for the rod, which connects the handle to the ring. The handle can then slide on the rod with minimal friction. A small disk is printed in the center as a contact point to each force sensor.

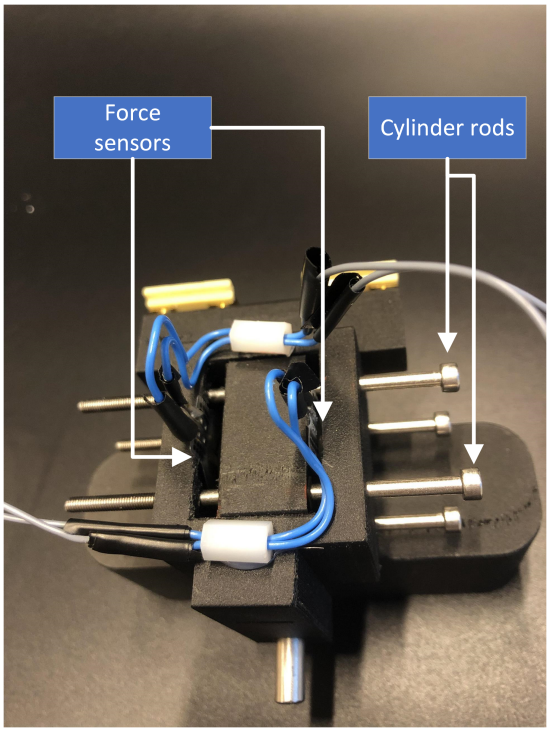

Figure 3.10: Upside down view of the handle connected to the ring. Long bolts with a large smooth area, keep the handle stable and connected to the ring. The bolts slide on sleeves, made from Iglide that adds insignificant friction when metals slide on it.

Measurement circuit

In the datasheet of the force sensor [77], there are two methods to measure the sensor. The first method uses an operational amplifier (OP-AMP) in an inverting configuration to obtain a voltage output that varies linearly with respect to force input. The second method uses a fixed resistor in a voltage divider configuration, resulting in a logarithmic relation between voltage output and force input. Appendix A.3.1 shows the schematics for each configuration.

Method one was chosen for its obvious advantages of a linear increase of voltage proportional to the force. The datasheet gives instructions for connecting the sensor in an inverting OP-AMP configuration, as can be seen in Figure A.13.

In the datasheet of the OP-AMP chosen [82], a typical application circuit is given. There, voltages of -2.5 V and +2.5V are fed to the OP-AMP as the power-supply. However, the Datasheet of the pressure sensors show an example connection of where the negative power supply should be ground. Therefore, +5 V was chosen as the positive power supply (+Vr). That results in V1 (Figure A.13), which is given as -Vr, being -5 V. For simplicity, one Arduino should power the circuit. However, since the Arduino does not provide negative voltages, a DC-DC converter is implemented to the circuit. The converter, takes in 5 V and gives outputs of +5 V and -5 V. However, when the -5 V output was measured, the measurements were not stable, rather the voltage ranged from -4.8 V to -5.2 V. Therefore, a -5 V regulator was added to the circuit.

The resulting circuit can be seen in Figure 3.11.

Calibration

As Figure A.13 shows, the output voltage V2, is dependent on the internal resistance of the sensor. The reason for that is that the resistance changes when the sensors are touched, which is why they work as force sensors. Most likely, there are small differences in the manufactur-

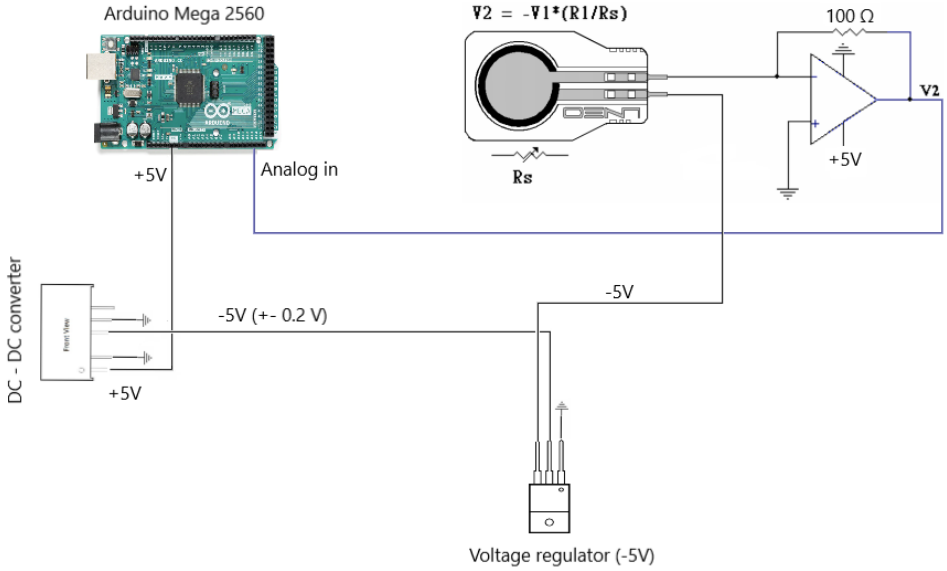

Figure 3.11: The resulting circuit connecting the force sensor to the Arduino

ing of each sensor, causing each sensor to have different characteristics. In order to calibrate the sensors and find the linear relationship between Force and output voltage, the handle is clamped in place such that one sensor is touching the connector part of the handle. A small stand was made, that fits in between the bolts holding the handle in place with the ring. Next, a box is placed on the stand and weights are added to the box. Each weight weighs around 11 g, so a few are collected together until the total weight is ~ 100 g. This is then added to the box and repeated. The stand as well as the box with all the weights can be seen in Figure 3.12.

The resulting plots show a linear relationship between Force and output Voltage. There is a small difference in slope. The resulting equation also shows a non-zero intercept, due to the weight of the material in the ring. Since 0 N should show 0 V, this intercept is removed in the measurement conversion, as shown in Figure 3.13.

3.1.5 Dimensions

The dimensions for the new and modified parts is given in table 3.1, where the handle connector is the part of the handle that connects to the ring.

Item	Length [mm]	Width [mm]	Height [mm]
Handle	100	30	40
Handle connector	15	29.5	35
Force sensors	16	0.2	27
Potentiometer	69	0.6	16

Table 3.1: Specifications of Items

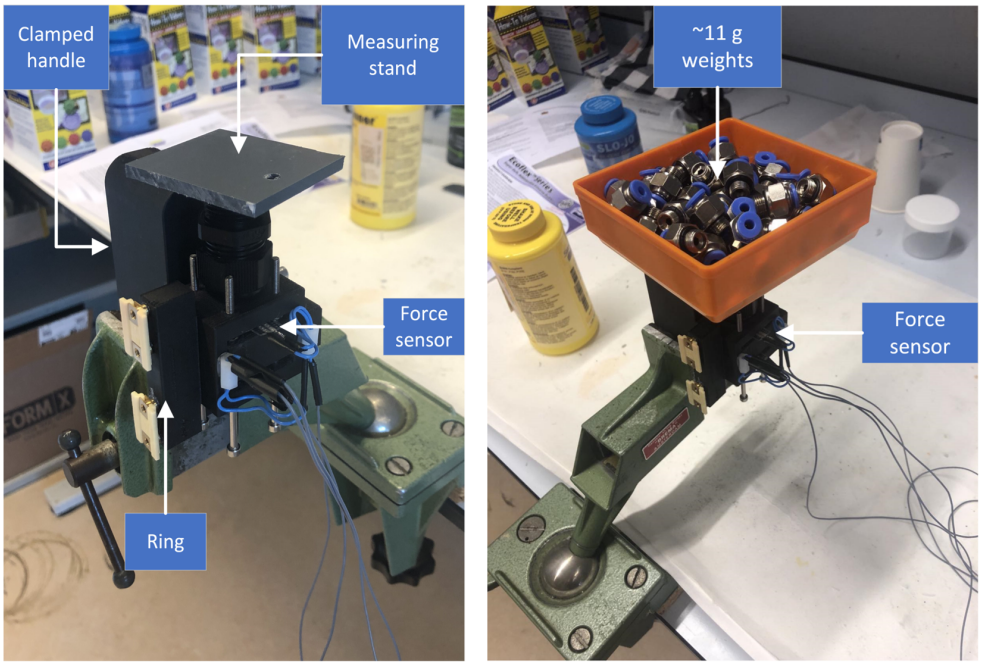

Figure 3.12: (a): The stand used for calibrating the sensors. The handle is kept sideways in place using a clamp and the stand is placed such that it pressurizes one sensor. (b): The setup used for calibrating the sensors. The weights inside the box are added in intervals with each addition weighing at ~ 100 g.

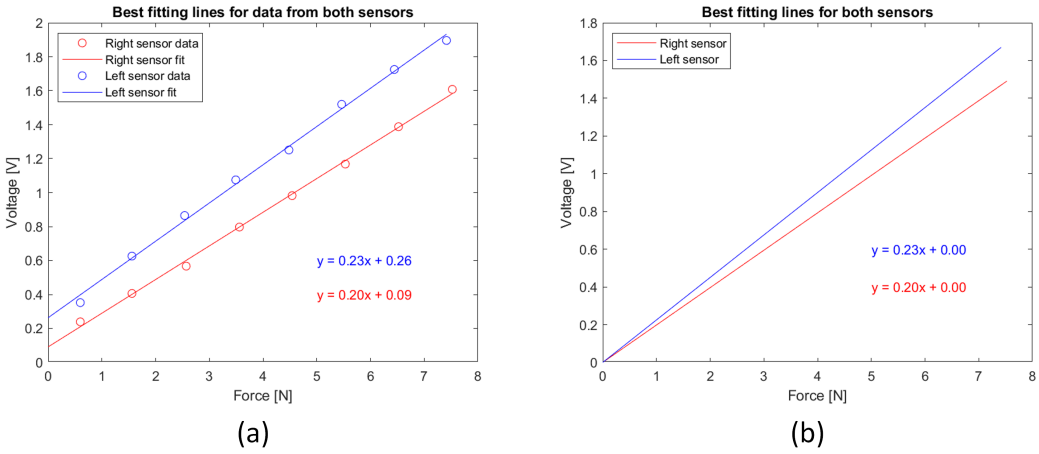

Figure 3.13: (a): Best fitting lines for collected data. (b): Resulting lines after removing intercept.

3.2 Modelling and control

In this section, the characterization of the actuators is explained as well as the control architecture and the integration of haptic feedback. Finally, the slave system used for testing is described, as well as the control architecture needed to control it with the haptic device.

3.2.1 Position control

In order to control the device such that the handle can move easily throughout the workspace as well as minimizing backlash when the user releases the handle, position control was integrated. This section aims to answer the sub-research question: "How can the non-linear characteristics of the actuators be mitigated when moving the handle, to ensure a smooth insertion and accurate haptic feedback?"

Requirements

The objective of the position controller is to keep the position constant when the handle is released. Moreover, the position controller should remove the nonlinear characteristics of the actuators which make the handle more difficult to move in certain places of the workspace. However, the controller must also make sure that safety is ensured during insertion and that no unwanted movement of the handle happens. Therefore, the requirements of the position controller are found to be:

1. The controller should ensure that when the handle is released, the position is kept stable.
2. The controller should be designed in a way that when the same user force is applied, it always results in the same movement of the handle independent on position in the workspace.
3. The controller should avoid sudden unintended movements of the handle, meaning that if a user is performing an insertion, the controller's output should never be high enough to push the handle forward more than the user intends.

Modelling

According to the literature review, rPAMs have the unique near linear relationship between air pressure and position [83]. For this reason, complicated modelling is not needed in order to control the position. Instead, a linear estimation of pressure vs position is sufficient for this task. In order to calculate the equation of the linear relationship between pressure and position, a sine wave input pressure was fed into the system for 100 seconds with an amplitude of 110 kPa while the pressure and the position were measured. The long duration of the input is picked to check the repeatability of the relationship, while the amplitude is picked as the maximum the actuators can handle before buckling. The resulting plot showed a linear relationship for air pressures in a certain range but for pressures closer to 0, there is no change in position for a change in pressure. As discussed in the literature review, PAM actuators need a certain threshold pressure before they start expanding in the axial direction. In order to linearize the system, 39 kPa is fed to both actuators at all times. This keeps the actuators at constant stress, such that any increase in pressure will result in axial force. This resulted in a near linear relationship between pressure and position. The non-linear plot and the corrected linear plot can be seen in Figure 3.14. The Figures show both actuators, and the direction of actuation is indicated by the sign of pressure. Adding positive pressure (P1) results in an increase in position whereas adding negative pressure (P2) results in a decrease in position. This relation can be seen visually in Figure 3.15.

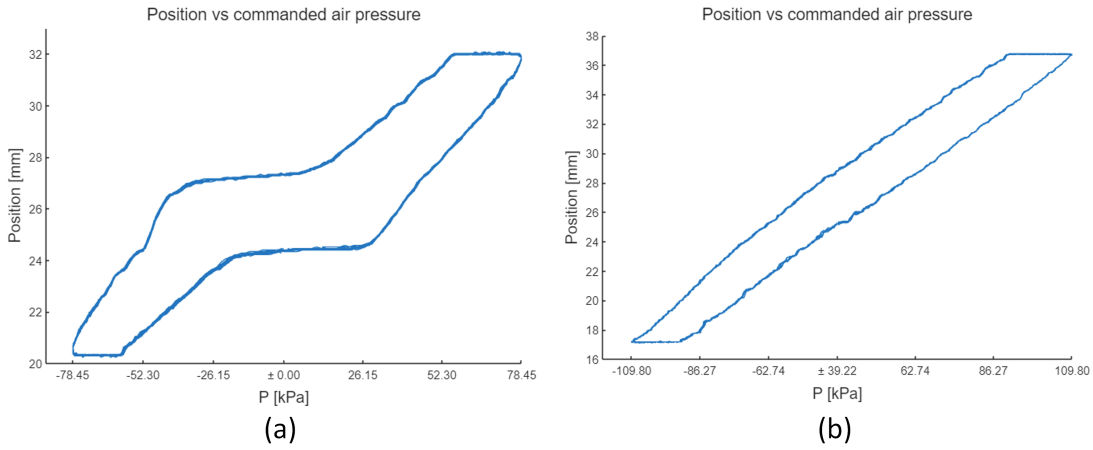

Figure 3.14: (a): Position vs input pressure for the whole range of air pressures. (b): Position vs input pressure with the threshold pressure of about 0.39 bars added to each actuator at all times.

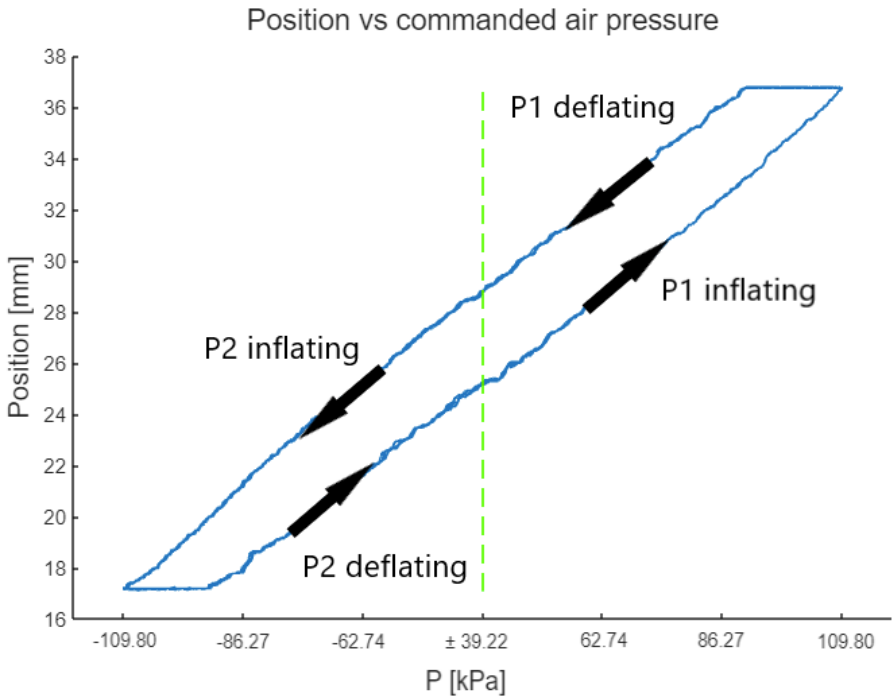

Figure 3.15: Directional plot of the position vs pressure relation. Negative pressure relates to the direction of the actuator.

The plots show two approximately linear regions, one for P2 deflating and P1 inflating and the other for P1 deflating and P2 inflating. They have very similar slopes, but different intercepts. In order to find the equation for each line, where each line represents a direction of movement, the edges of the skewed rectangle are found. A simple method is developed for this purpose, which is explained in Appendix A.2.3. It should be noted that the x-axis in Figures 3.16 and 3.17 is the relative pressure to the threshold pressure and not the absolute pressure. That means that 0 in those plots is actually 39.22 [kPa], or a 0 increased pressure from the constant threshold pressure.

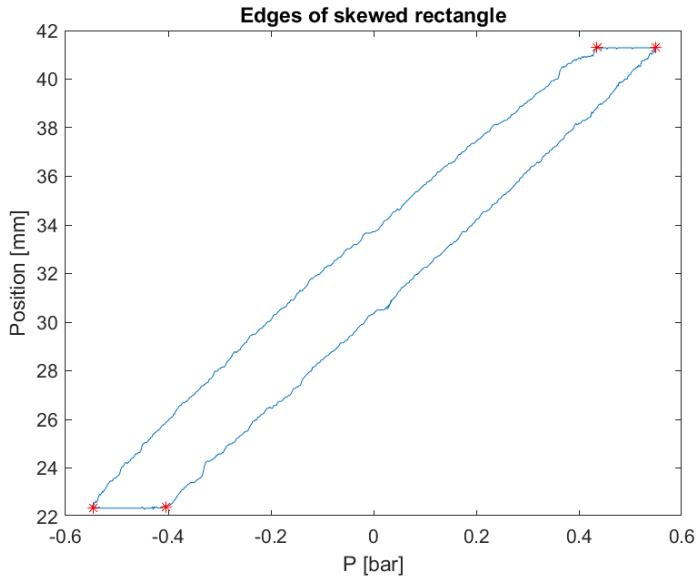

Figure 3.16: The edges of the rectangle are found by taking minimums and maximums of x- and y-. The corners are then the closest point to: Top left = $[x_{min}, y_{max}]$, Top right = $[x_{max}, y_{max}]$, Bottom left = $[x_{min}, y_{min}]$, Bottom right = $[x_{max}, y_{min}]$

Once the edges have been identified, the points between the slopes are taken and the best fitting line is found using the Matlab function polyfit. The resulting equation for the slope is

$$y = 16.55x + 29.13 \tag{3.1}$$

where

x = Input pressure (addition to the threshold pressure) [bar]
y = Position [mm]

The resulting slope if near-linear, but does have a very small curve. For this reason it is not a good idea to blindly feed-forward this equation to the system. In that case, at some points in the workspace the feed-forward would apply too much pressure, causing the handle to move further forward than commanded. This would result in the operated needle, moving further than wanted. For this reason, the best fit line is moved a small amount by changing the intercept. Figure 3.17 shows the best fit line and the modified line. In the new line, there is a small decrease in the fed forward pressure where P2 is inflating (negative pressure region) and a small increase in pressure where P1 is deflating (positive pressure region). This results in a bit stiffer system where the user has to input more force to the handle in order to move it. Moreover, this results in an increase in safety during usage where the handle is operating another device. The slope that is then fed-forward is:

$$y = 16.55x + 28.0 \tag{3.2}$$

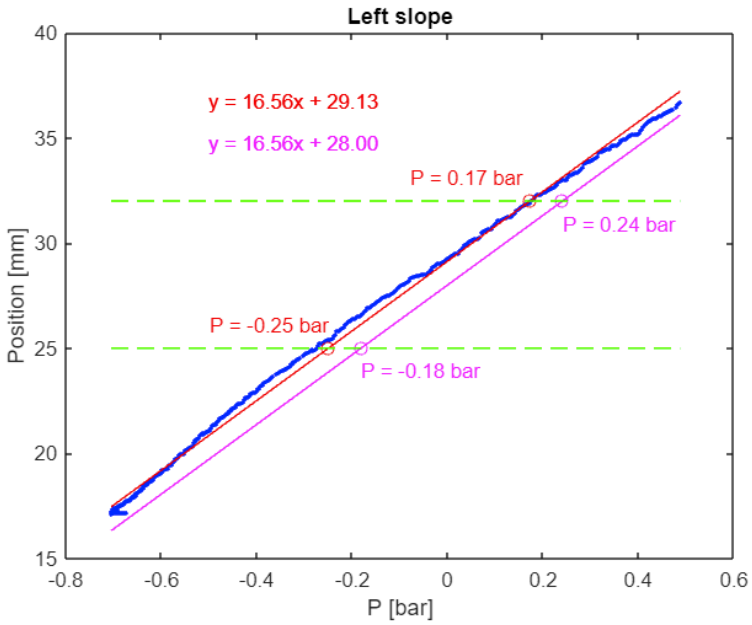

Figure 3.17: The best fit line (red) is modified to ensure safety (pink). When P2 is inflating (negative P), the feed-forward pressure is 0.18 bars instead of 0.25 bars. Similarly, when P1 is deflating (positive P), the feed-forward pressure is 0.24 bars instead of 0.17 bars (more pressure in the deflating stage results in slower movement.

Modifying Equation 3.2 for x, results in the equation:

$$\begin{aligned} y &= 16.55x + 28.0 \\ y - 28.0 &= 16.55x \\ 16.55x &= y - 28.0 \\ x &= \frac{y - 28.0}{16.55} \end{aligned} \tag{3.3}$$

In the same way, the equation for the right slope is:

$$x = \frac{y - 27.0}{16.85} \tag{3.4}$$

The reason for the rectangle shape of the plot (Figure 3.15) is known as the Hysteresis effect [84–86]. This effect is often modelled in order to reduce unwanted effects, such as when switching directions. However, due to time constraints this is not done for this project.

Since there are two force sensors integrated on each side of the handle, the direction can be determined by simply checking if either sensor is showing values greater than 0. Determining which slope to feed-forward to the system, is therefore easily done using the force sensors as input.

Control

The equations found are used by reading the values of the potentiometer and solving the equation to determine what input pressure maintains that position (according to the linear relation). The mathematical representation for this controller is then:

$$
\begin{aligned}
P_1 &= \frac{d_{\text{handle}} - 28.0}{16.55} && \text{when } F_R > 0 \;\&\; d_{\text{handle}} > d_{\text{equilibrium}} \\
P_1 &= \frac{d_{\text{handle}} - 27.0}{16.85} && \text{when } F_L > 0 \;\&\; d_{\text{handle}} > d_{\text{equilibrium}} \\
P_2 &= \frac{d_{\text{handle}} - 28.0}{16.55} && \text{when } F_R > 0 \;\&\; d_{\text{handle}} < d_{\text{equilibrium}} \\
P_2 &= \frac{d_{\text{handle}} - 27.0}{16.85} && \text{when } F_L > 0 \;\&\; d_{\text{handle}} < d_{\text{equilibrium}} \\
P_1 &= P_1^{\text{prev}} && \text{when } F_L = 0 \;\&\; F_R = 0 \\
P_2 &= P_2^{\text{prev}} && \text{when } F_L = 0 \;\&\; F_R = 0
\end{aligned}
\tag{3.5}
$$

where

$$
\begin{aligned}
d_{\text{handle}} &= \text{position of the handle [mm]} \\
d_{\text{equilibrium}} &= \text{position of the equilibrium point [mm]} \\
P_1 &= \text{input pressure of actuator 1 [bar]} \\
P_2 &= \text{input pressure of actuator 2 [bar]} \\
F_R &= \text{force measurement of the sensor to the right of the handle [N]} \\
F_L &= \text{force measurement of the sensor to the left of the handle [N]} \\
P_1^{\text{prev}} &= \text{previous pressure value of actuator 1[bar]} \\
P_2^{\text{prev}} &= \text{previous pressure value of actuator 2[bar]}
\end{aligned}
$$

This feed-forward system was developed in Matlab's Simulink using the support package for Arduino hardware. The support package includes blocks that help you easily connect to certain pins on the Arduino. Once the Simulink is ready, the corresponding code is generated and executed on the Arduino. The Simulink model for the feed-forward position controller can be seen in the Appendix A.2.1.

In Simulink, the equilibrium point is not used to see which actuator to use. Rather, a check is performed to see if the desired pressure is positive or negative. Positive pressure results in pressure being fed to actuator 1 and negative pressure to actuator 2, as Figure 3.15 shows. Moreover, the resulting equation only fits when both actuators are pressurized with the threshold pressure at all times.

3.2.2 Force control

In order for the force of the needle to be fed back to the device, a force controller is integrated to the system. Due to time constraints, a classical PID is used instead of more complex controllers recommended in literature. Moreover, a PID is shown in literature to work as a force controller for PAM actuated devices, however without great accuracy and possible instability. This section aims to answer the sub-research question: "Which control architecture can provide the user with realistic haptic feedback, while ensuring a safe insertion?"

Requirements

The objective of the force controller is to relay the forces experienced by the needle back to the user. The user force usually has some noise and can change very quickly. Controllers might then try to react quickly and have unstable behaviours for a short time before reaching the desired force. For this type of system, stability is more important than transparency. The reason for that is that any instability can cause the user to move the handle forwards or backwards in a motion that he is not comfortable with. This can result in an unsafe insertion. While you want the forces to be as accurate as possible, it is not crucial that they are exactly the same as the needle experiences. It is more important that the user force follows the needle force, such that an increase in the forces experienced by the needle is felt as an increase in forces felt by the user. Therefore, the requirements of the force controller are found to be:

1. The controller should be able to relay the forces experienced by the needle back to the user with an accuracy of at least 0.3 N RMSE.
2. The controller should avoid unstable behaviors, even if it means sacrificing some level of accuracy, therefore prioritizing stability over transparency.

Modelling

Buckling of PAMs, especially for extensile PAMs, is a common problem which needs to be analysed and avoided to ensure a safe operation [58, 59]. In order to avoid buckling, the pressure where buckling starts at different positions, or different stretches of the actuator, is measured. Table 3.2 shows the points of buckling based on the position in the workspace.

Initial Stretch	Maximum Force	Pressure where bending starts
150%	1.89 N	105 kPa
144.63%	1.89 N	100 kPa
141.13%	2.13 N	95 kPa
137.32%	2.43 N	105 kPa
133.36%	2.42 N	75 kPa
129.85%	1.78 N	85 kPa
125.51%	1.76 N	80 kPa
122.81%	1.33 N	70 kPa
120.15%	0.92 N	60 kPa
117.69%	1.64 N	65 kPa

Table 3.2: Table showing maximum force and points of buckling for different positions in the workspace.

This information is added to the controller structure as saturation based on position. When the handle is moved forward, towards insertion, the maximum pressure that the controller can apply decreases. This in turn, decreases the maximum force the actuators can provide. Once the actuators start to buckle, any increase in pressure results in more buckling, resulting in a decrease of axial force. Modelling of the same behaviour for actuators made from Dragonskin 10 was completed, showing a large increase in Forces throughout the workspace. This can be seen in Appendix A.4.1.

Theory

A PID is a controller that takes in a setpoint value, subtracts the measured value of the force and feeds that error to the controller. The P component of the PID controller, is the Proportional term. The proportional part of the controller multiplies the error with a constant K_p, giving the equation $\mathbf{P}_{out} = K_p \times \mathbf{e}(t)$. Increasing the K_p, decreases the rise time, possibly increases the overshoot and usually leaves a steady state error. The I component corresponds to the integral part of the controller. The integral component accumulates the past errors, meaning that

if an error has been present for some time, it will accumulate and the controller will respond. This takes care of the steady state error, but might also have the effect of slowing the rise time a bit and might also increase the overshoot. This is also dependent on a constant K_i with the equation $\mathbf{I}_{out} = K_i \int \mathbf{e}(t)\,dt$. The D component is the Derivative term of the PID controller. It provides a prediction of future error, based on its rate of change. It helps in reducing the magnitude of the overshoot produced by the integral component. The derivative part is dependent on a constant K_d with the equation $\mathbf{D}_{out} = K_d \frac{d\mathbf{e}(t)}{dt}$. The resulting equation for the PID controller is then the combined equations:

$$\mathbf{u}(t) = K_p \times \mathbf{e}(t) + K_i \int \mathbf{e}(t)\,dt + K_d \frac{d\mathbf{e}(t)}{dt} \tag{3.6}$$

where

$\mathbf{u}(t)$ = the controller output [bar]
$\mathbf{e}(t) = F_{\text{desired}} - F_{\text{user}}$ = the error (controller input) [N]
K_p = constant for the proportional part of the PID controller
K_i = constant for the integral part of the PID controller
K_d = constant for the derivative part of the PID controller

Control

The input to the PID is the difference between the needle force and the user force (error). This error is used by the PID to calculate the desired air pressure. This can be seen visually in Figure 3.18.

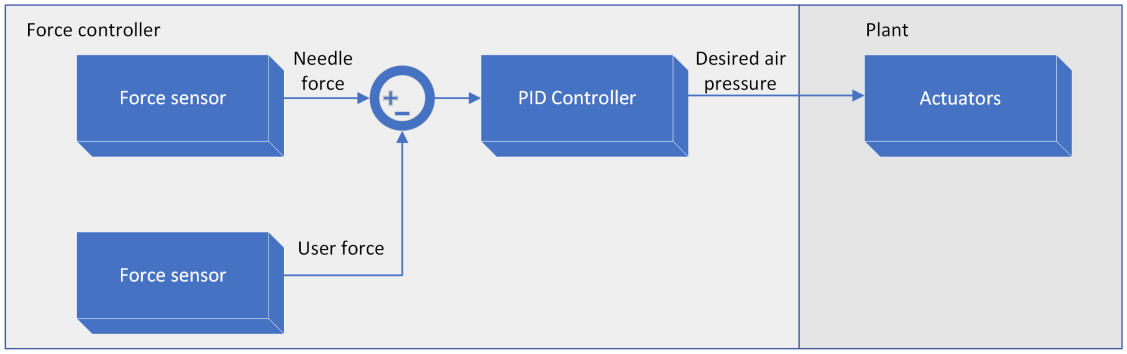

Figure 3.18: Block diagram showing the workings of the force controller.

However, it is not desirable to have the force controller always active. There is some criteria that needs to be met before the force controller activates. Firstly, the user must be moving in the direction of insertion, since we only care about insertion for this thesis. If both force sensors on the haptic device measure 0 N, the force controller should not react. If it would, the actuator would increase the pressure until its saturation point, trying to increase the user force. Another criteria is that the needle force should be greater than the user force. If this is not a criteria, and during an insertion the user force is greater, the controller tries to react by increasing the pressure in the direction of insertion until the forces are equal. This would lead to an unsafe insertion as the handle moves quicker than intended by the user.

Another safety layer is added to the output of the controller, where a rate limiter is added. For an increase in pressure, it is very uncomfortable for the user if the increase is too fast. A limit of 40 kPa per second is added for the increase. For a decrease in pressure, a quick decrease results in the handle jumping forward. This can result in an unsafe insertion. Therefore, a stronger limit of 2.35 kPa per second is added.

Tuning

Tuning the PID was done by providing a sinusoidal setpoint (desired force) that starts at 0 N and increases to 1.6 N with a frequency of 0.25 rad/s (See Equation 3.7). The handle is kept still, using a weight, while the PID controls the pressure to try to follow the input. Figure 3.19 shows the tuned controller, with K_p, K_i and K_d as 25, 10 and 1, respectively. The Figure shows the user force following the setpoint without ever becoming unstable. The RMSE was found to be 0.3353 N.

$$y(t) = 0.8\sin(0.25t - 90°) + 0.8\,[\text{N}] \tag{3.7}$$

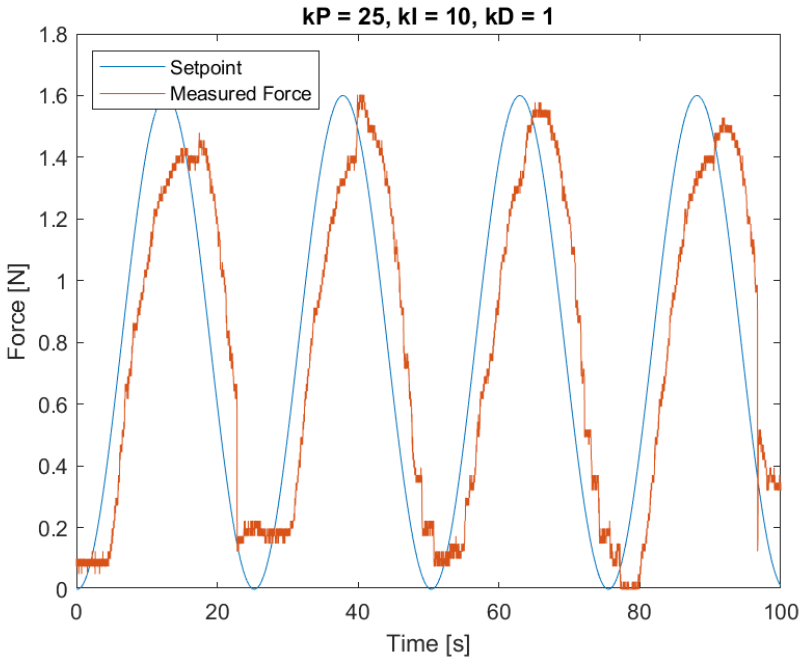

Figure 3.19: Tuning of the PID was performed using a sine input.

3.2.3 Hybrid control

The combined control consists of simultaneous position and force control. The control frequency is set as 100 Hz. The feed-forward controller keeps the current position, while the force controller feeds back the needle force to the user. The potentiometer gives the current position of the handle, controlled by the user. The feed-forward controller takes this position and calculates the needed air pressure to hold the current position, and feeds this into the actuators. The force controller takes in the difference between the force that the needle experiences and the user force on the handle, and increases the air pressure until both forces are equal. Figure 3.20 shows a block diagram of the combined control system.

To keep the force controller from reacting when the user is not actively holding the handle, a check is performed to see if either force sensor on the handle is experiencing force. If not, the force controller is kept inactive and the feed-forward controller is the only input to the actuators. However, if user force is detected, another check is performed to see which direction the user is moving the handle. For backward direction, the force controller should not react, as for this project we are only interested in haptic feedback during insertion. If however, the handle is moving forward, the force controller is activated. Another check is performed to see if the needle is experiencing more force than the user is applying. If not, the force controller should not react, as it would then decrease the actuator pressure, resulting in the handle moving further forward than expected by the user. Once the needle experiences a greater force than the

user is applying, then the force controller activates and increases the air pressure until the same force is experienced by the user. This can be seen visually in a flowchart in Figure 3.21.

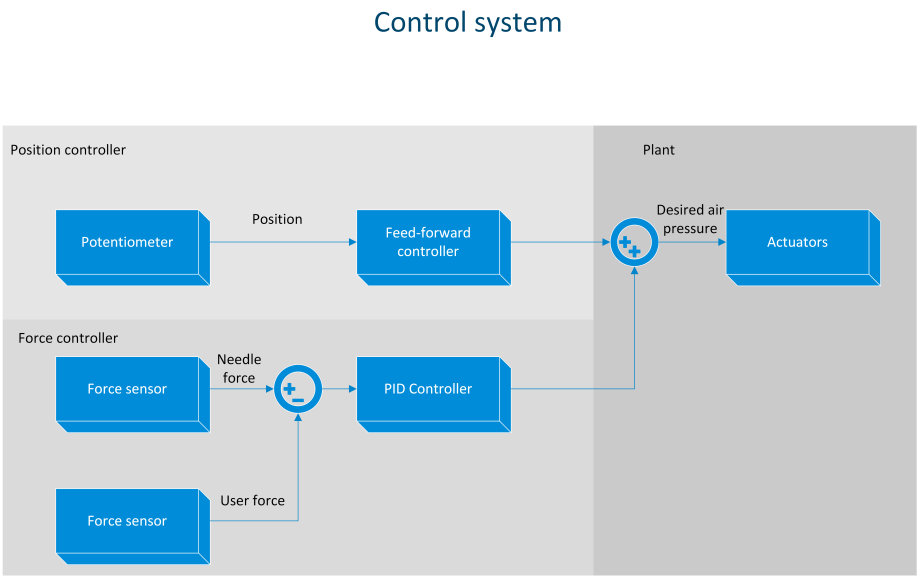

Figure 3.20: A block diagram showing the combined control system

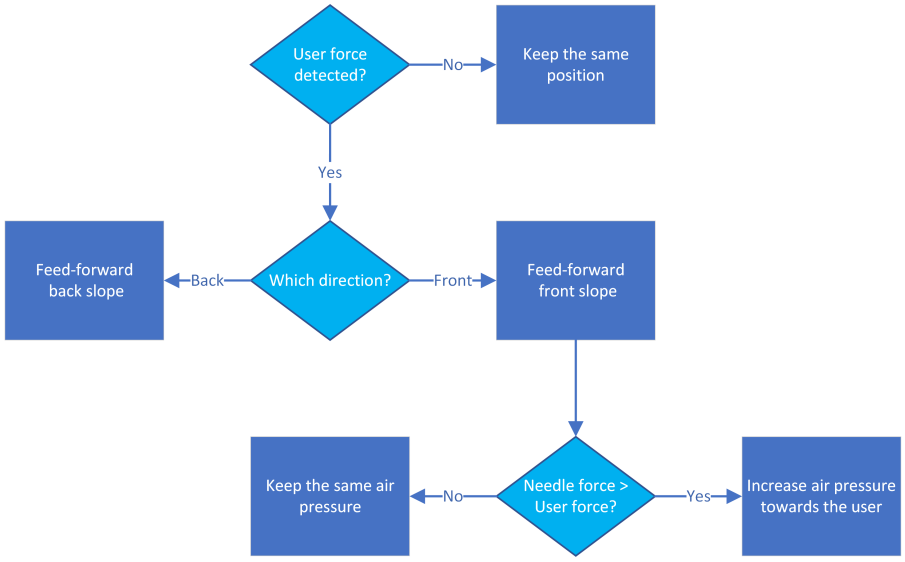

Figure 3.21: A flowchart showing the combined control system

The mathematical representation for the combined position and force control is found to be:

$$
\begin{aligned}
P_1 &= \frac{d_{\text{handle}} - 28.0}{16.55} + K_p \times \mathbf{e}(t) + K_i \int \mathbf{e}(t)\,dt && \text{when } F_R > 0 \;\&\; d_{\text{handle}} > d_{\text{equilibrium}} \;\&\; F_R < F_{needle} \\
P_1 &= K_p \times \mathbf{e}(t) + K_i \int \mathbf{e}(t)\,dt && \text{when } F_R > 0 \;\&\; d_{\text{handle}} < d_{\text{equilibrium}} \;\&\; F_R < F_{needle} \\
P_1 &= \frac{d_{\text{handle}} - 28.0}{16.55} && \text{when } F_R > 0 \;\&\; d_{\text{handle}} > d_{\text{equilibrium}} \;\&\; F_R >= F_{needle} \\
P_1 &= \frac{d_{\text{handle}} - 27.0}{16.85} && \text{when } F_L > 0 \;\&\; d_{\text{handle}} > d_{\text{equilibrium}} \\
P_2 &= \frac{d_{\text{handle}} - 28.0}{16.55} && \text{when } F_R > 0 \;\&\; d_{\text{handle}} < d_{\text{equilibrium}} \\
P_2 &= \frac{d_{\text{handle}} - 27.0}{16.85} && \text{when } F_L > 0 \;\&\; d_{\text{handle}} < d_{\text{equilibrium}} \\
P_1 &= P_1^{\text{prev}} && \text{when } F_L = 0 \;\&\; F_R = 0 \\
P_2 &= P_2^{\text{prev}} && \text{when } F_L = 0 \;\&\; F_R = 0
\end{aligned}
\tag{3.8}
$$

where

d_{handle} = position of the handle [mm]
$d_{\text{equilibrium}}$ = position of the equilibrium point [mm]
P_1 = input pressure of actuator 1 [bar]
P_2 = input pressure of actuator 2 [bar]
F_R = force measurement of the sensor to the right of the handle [N]
F_L = force measurement of the sensor to the left of the handle [N]
P_1^{prev} = previous pressure value of actuator 1 [bar]
P_2^{prev} = previous pressure value of actuator 2 [bar]
$\mathbf{e}(t) = F_{\text{desired}} - F_{\text{user}}$ = the error (controller input) [N]
K_p = constant for the proportional part of the PID controller
K_i = constant for the integral part of the PID controller
K_d = constant for the derivative part of the PID controller

In order to keep the actuators from breaking when both controllers are active, a saturation is applied to the actuators input. This saturation is the maximum pressure the actuators can handle before they start buckling (at any position). The saturation in the force controller based on empirical modelling of the buckling makes sure the actuators don't buckle at specified positions during an insertion.

The complete Simulink model can be seen in Appendix A.2.1, where the "Needle movement" block takes care of moving the stepper motor connected to the needle insertion device, when the handle moves. The haptic device can therefore, with this model, control the position of the needle, while also comparing giving the haptic feedback to the master device when the needle experiences more force than the user is applying.

3.2.4 Slave system

In order to test the system, a slave system made by another student is borrowed [87]. This device consists of a needle, a stepper motor, a force sensor and 3D printed housing. The stepper motor moves the needle forward and the force sensor moves with it. The force sensor only moves with the stepper motor, so when a force is acting on the tip of the needle, it is measured by the force sensor, placed at the base of the needle. Figure 3.22 shows this 1 DoF needle insertion device.

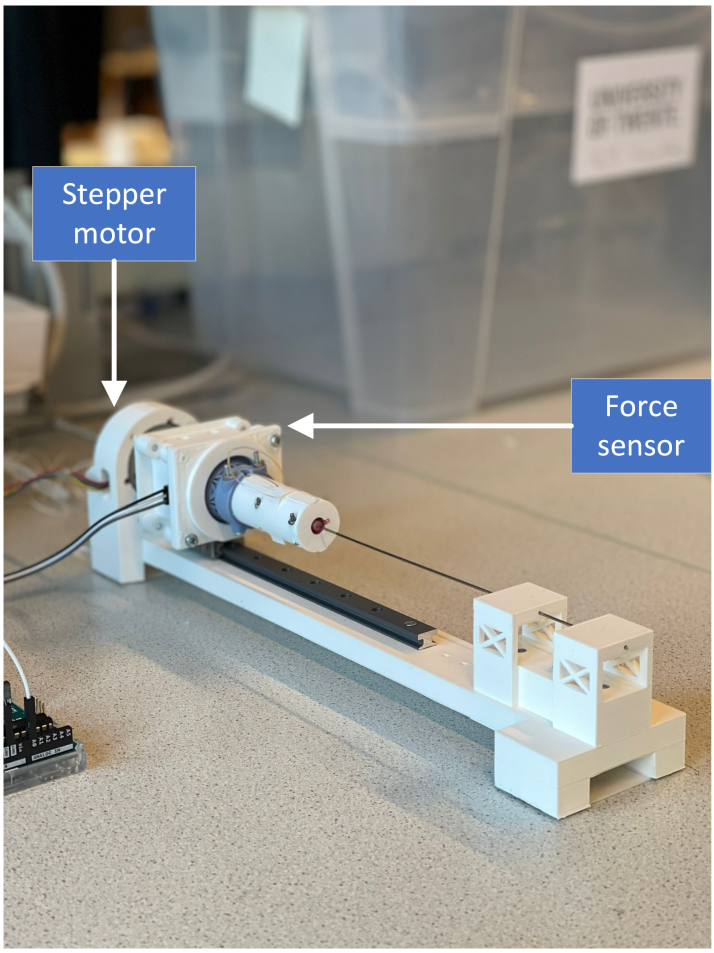

Figure 3.22: A needle insertion device borrowed for testing the haptic device.

Control

In order to control this slave device with the haptic device, some control algorithm is needed. This is done by measuring the position of the handle in [mm], calculating how many steps are needed by the stepper motor in order to achieve that distance and moving the stepper motor until that distance is reached. The steps already moved are counted and subtracted from the steps originally needed to move to the desired position. A counter is used as input to the stepper motor. The counter goes from 0 to 3 and then resets. This makes sure that the input to the stepper motors is always 0, 1, 2 or 3. These are the 4 steps that the stepper motor has for one revolution.

4 Evaluation

In this chapter the system is evaluated to help answer the research question "What is the efficacy of reverse Pneumatic Artificial Muscles (rPAM) for usage in remote Minimally Invasive Surgeries with kinesthetic (haptic) feedback, especially for needle insertions in soft tissue; biopsies and ablations?". Sub-questions were thought of to help answer this research question. Each evaluation is performed to help in answering these questions.

4.1 Position controller

4.1.1 Goal

To evaluate the position controller, the sub-question "How can the non-linear characteristics of the actuators be mitigated when moving the handle, to ensure a smooth insertion and accurate haptic feedback?" is considered. The goal is to see if the position controller is able to mitigate the non-linear characteristics, resulting in a smooth insertion. If the force-position relationship is linear with negligible slope, then the efficacy of the position controller has been shown.

4.1.2 Experimental protocol

The force is measured while moving the handle from equilibrium point to the end of the workspace, in the case of no controller and position controller. The

4.1.3 Results and Discussion

Figure 4.1 shows that with no controller, the force required to move the handle rises quickly. However, with the position controller, applying 0.5 N of force is enough to move the handle to the end. There is however, a small increase in the force which could be improved on. This is due to the minor non-linearities in the pressure - position relation. The non-linear characteristics have been mitigated, which shows the efficacy of the controller. However, the small increase in forces is unwanted. Since the force increase is so small, it is not considered as a problem for now and the controller is deemed sufficient. The reason for the different starting point in Figure 4.1 is that there is a region around the equilibrium point where the overall stress is not enough to pull the handle to the equilibrium point. Therefore, in the case of no controller, the handle's equilibrium point is the equilibrium point at pressurized state ± some threshold.

Figure 4.1: Plot showing the force required to move the handle to the end of the workspace, starting from the equilibrium point. The equilibrium point changes when the position controller is active due to the threshold pressure.

4.2 Force control

To evaluate the force controller, the sub-question "Which control architecture can provide the user with realistic haptic feedback, while ensuring a safe insertion?" is considered.

4.2.1 Goal

The goal of this experiment is to evaluate if the controller is able to provide realistic feedback while keeping stability. The RMSE should be low in order to keep the feedback realistic, while instability, such as vibrations during movement, should be negligible.

4.2.2 Experimental protocol

In order to simulate a realistic insertion, the desired force is made as a ramp, where an increase in position increases the desired force. This is similar to an insertion, where the interaction force on the needle increases linearly with an increase in insertion depth.

4.2.3 Results and Discussion

Figure 4.2 shows the user force following the setpoint force while keeping stability the entire time. The RMSE is found to be 0.43 N, which is 0.13 N higher than the requirement for this controller. It would be good to improve the RMSE to make the feedback more accurate and realistic. However, due to time constraints and the prioritization of stability over transparency, this is deemed sufficient for this project.

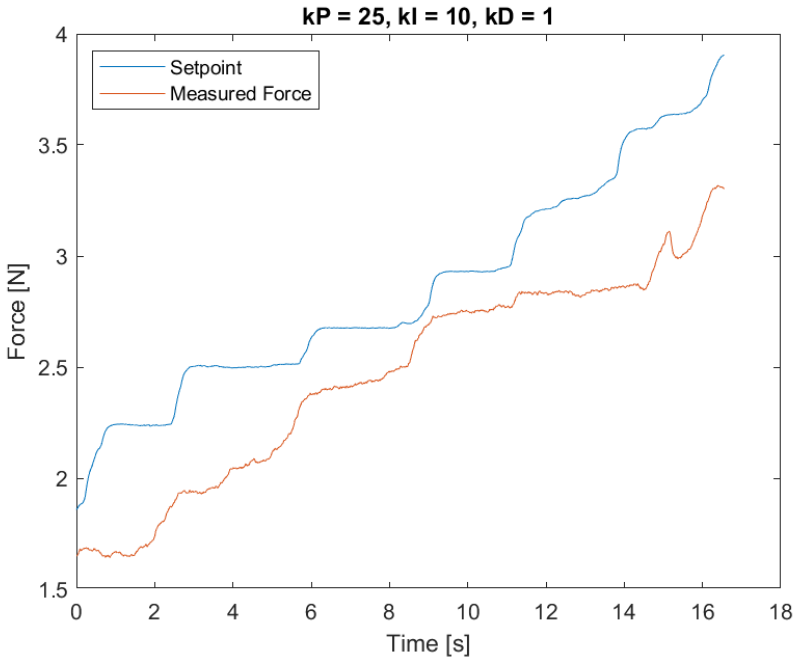

Figure 4.2: Evaluation of the force controller is performed using a ramp input, where the setpoint increases proportional to the change in position of the handle. This resembles forces in an actual insertion. The reason for the y-axis starting at 1.5 N is to show only the area after the controller kicks in and before the actuators buckle. The RMSE is found to be 0.43 N.

4.3 Haptic device

To evaluate the whole system, user experiments are conducted. Parts of the sub-questions mentioned above are considered for this, as a validation, as well as the main research question.

4.3.1 Goal

The goal of this study is to evaluate the actuators efficacy for usage in needle insertions with haptic feedback. The smoothness of insertion is validated through a questionnaire while the force controllers efficacy to ensure a safe insertion is validated through a comparison of interaction forces on the needle. The hypothesis is that haptic feedback lowers the interaction forces, resulting in less tissue damage in the patient. Moreover, the actuators ability to provide users with a realistic feeling while inserting is evaluated through a questionnaire.

4.3.2 Experimental protocol

A testing rig was made by 3D printing a rectangle shaped block that has a cavity that allows phantoms to be placed into and held in place, while allowing the needle to exit on the other side. This can be seen visually in Figure 4.4. Three phantoms are created from the silicone materials, DragonSkin 10 NV and Ecoflex 00-50. It has been shown that Ecoflex 00-30 is a good representation of porcine and bovine liver tissue [88]. For simulating a tumor, one study used a Silicone Rubber with thickness 3 mm and shore hardness of 70A (Figure 3.6 shows the hardness scale) [89]. Due to limitations of available silicones, Dragonskin 10 (shore stiffness 10A) is chosen as the stiffer material and Ecoflex 00-50 as the softer material. Table 4.1 shows the materials and depths of each phantom, while Figure 4.3 shows the full test setup.

Ten users are instructed to do an insertion in one motion through a phantom. The reason they are instructed to go all the way through the phantom, is to make sure that in all tests, the depth of insertion is the same. Three phantoms are made, each with their specific qualities. Each

Phantom	Material/s	Height
Phantom 1	Dragonskin 10 NV	9 mm
Phantom 2	Dragonskin 10 NV	14 mm
Phantom 3	Ecoflex 00-50 + Dragonskin 10 NV	13 mm

Table 4.1: Table showing phantom materials and their heights.

phantom is inserted through, both with and without force feedback, three times per user. The position controller is always active, while the force feedback is only active in 3/6 insertions. All users are first shown how to operate the master device and how the slave device reacts. Following that, they are first allowed to play around with the device for a bit, in order to get familiar with the system. They are instructed to insert the needle into a phantom, both with- and without haptic feedback, a few times for each phantom. All users are instructed to move the handle with two fingers and to insert the needle at a velocity that they feel is safe for an insertion into a human subject.

Once the users are familiar with the system, they are instructed to insert the needle through phantom 1 without haptic feedback. Once the needle is all the way through the phantom, the user is instructed to release the handle and the needle is positioned again close to the insertion point. This is done three times before switching to haptic feedback. After three insertions with haptic feedback, the phantom is switched and the user is asked which three insertions were with feedback. Based on the confidence and correctness of the answer, the question related to the effect of feedback for that phantom is answered. Once both questions specific to phantom 1 have been answered, the second phantom is inserted into. The insertion protocol is reversed for this phantom, starting with 3 insertions with haptic feedback following 3 insertions without feedback. Finally, for phantom 3, the same order as phantom 1 is used. Phantom 3 has one extra question related to the difference in feedback when entering a stiffer material. Once the questions related to phantom 3 have been answered, the user is asked to answer the general questions.

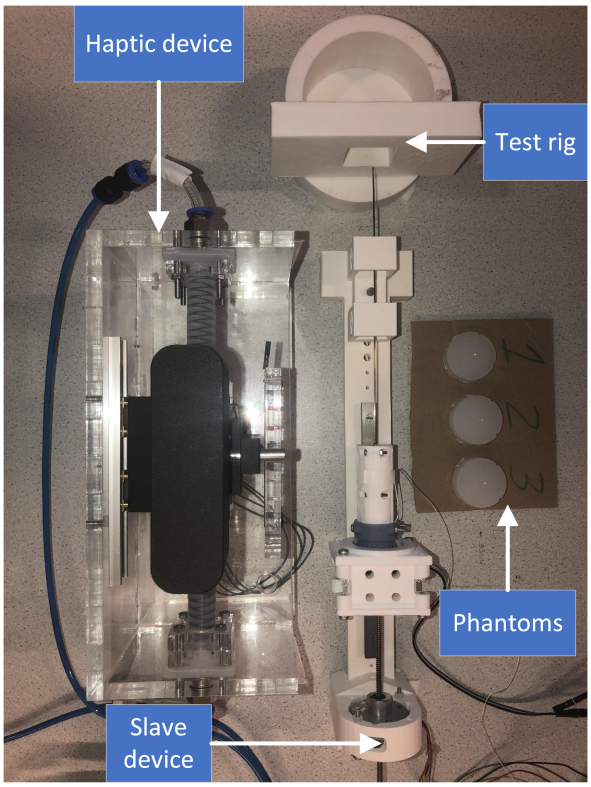

Figure 4.3: The testing setup for testing the haptic feedback

Figure 4.4: The needle is shown when inserted into the phantom. The test rig holds the phantom in place, while allowing the needle to go through on the other side.

4.3.3 Results

Phantom 1

Looking at the average forces experienced by the needle (Figure 4.5), in three cases the forces decrease when haptic feedback is given. However, in the other 7 cases, the results show a slight increase in forces in the case of haptic feedback.

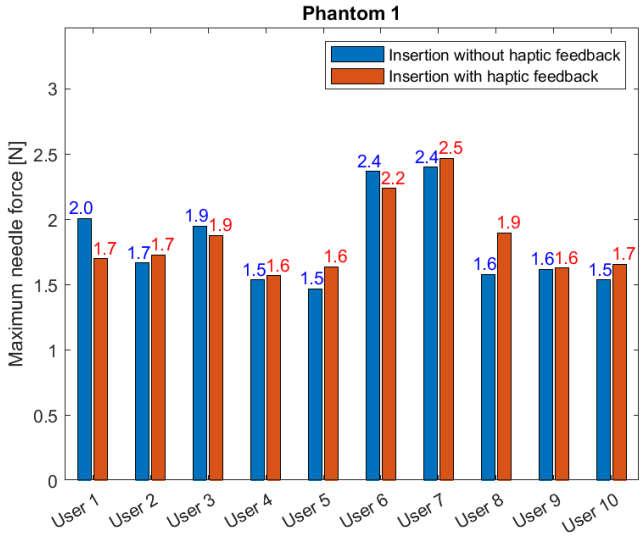

Figure 4.5: Average of the three insertions into phantom 1.

Phantom 2

For Phantom 2, the average of each three insertions (Figure 4.6), shows that eight out of ten users showed a decrease in forces in the case of haptic feedback. The two users that had higher forces in the case of haptic feedback, were found to use excessive force in one or two insertions, out of the three.

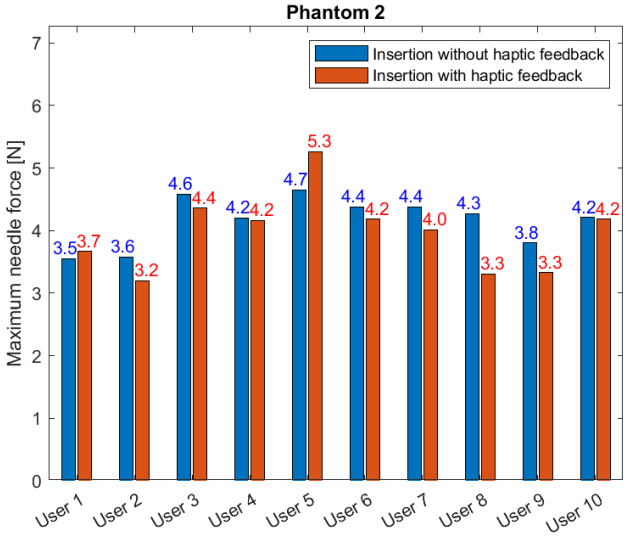

Figure 4.6: Average of the three insertions into phantom 2.

Phantom 3

When looking at the average (Figure 4.7), 4 out of 5 users show a decrease in interaction forces in the case of haptic feedback, while one user showed negligible difference.

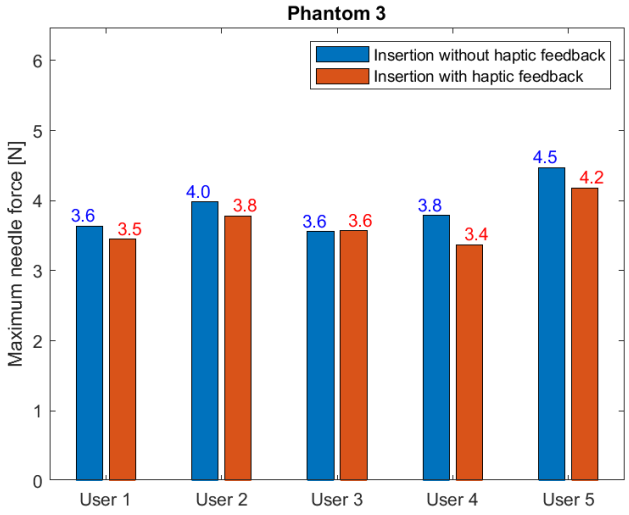

Figure 4.7: Average of the second two insertions into phantom 3. The first insertion is removed due to a problem with the phantom that caused high outliers in the case without haptic feedback.

Overall summary

Figure 4.8 shows a boxplot of the 3 phantoms. The shape of the boxplot shows how the data is distributed. The center line, inside each box, represents the median value. The top and bottom part of the box represent the first and third quartiles, while the top and bottom line show the maximum and minimum, neglecting outliers. Outliers are shown with a small circle.

The results show that for the first phantom, there is a small increase in the median value, but a lower range of forces in the case of haptic feedback. For the second and third phantom, there is a decrease in the median value, in the case of haptic feedback, while the range of forces increase.

Comparing the average values of all users (Figure 4.9) we see a small increase for phantom 1, while phantom 2 and 3 show similar decrease in the case of haptic feedback. Each insertion can be seen in a scatter plot in Appendix A.5.

The results from the questionnaire (Table 4.2) show that users felt comfortable using the device, both with and without haptic feedback. Users also answered that they did feel the effect of force feedback, with a perfect score in the second two phantoms. Moreover, all users stated that they felt a difference when entering the second half of phantom 3, showing that tissue characterization is possible. However, users did not agree on the friction being the same throughout the workspace.

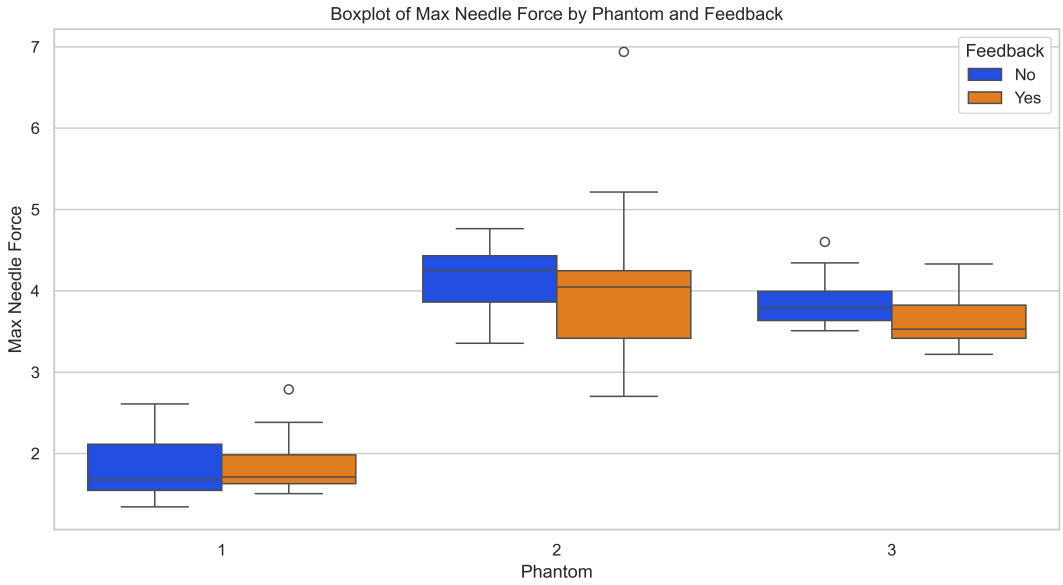

Figure 4.8: A box plot comparing the results without and with feedback, for each phantom.

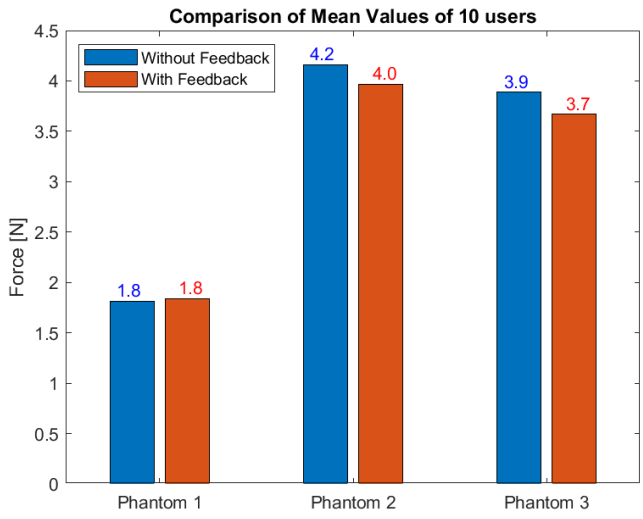

Figure 4.9: The average needle force of all users comparing no feedback to haptic feedback

Questions		Statement	Mean	σ
General questions	Q1	The system was intuitive to use	4.4	0.516
	Q2	I didn't feel any disturbance from sound during the experiments	3.9	0.994
	Q3	Most people would quickly learn how to use the system.	4.7	0.483
	Q4	I felt confident using the system.	4.3	0.675
	Q5	I felt the same friction throughout the workspace (when moving without haptic feedback)	3.1	1.663
Specific to phantom 1	Q6	I felt the effect of the force feedback	4.2	1.229
	Q7	The device felt comfortable to use during the insertion	4.1	0.568
Specific to phantom 2	Q8	I felt the effect of the force feedback	5	0
	Q9	The device felt comfortable to use during the insertion	4.2	0.632
Specific to phantom 3	Q10	I felt the effect of the force feedback	5	0
	Q11	The device felt comfortable to use during the insertion	4.3	0.675
	Q12	I felt a difference when entering the second half of the phantom	4.6	0.548

Table 4.2: Subjects' experience evaluation while doing an insertion with the haptic device. Participants rated these statements using a 5-point Likert scale (1 = strongly disagree, 5 = strongly agree).

4.3.4 Discussion

Phantom 1

Phantom 1 showed a small increase in both the average and median value, in the case of haptic feedback. This can be explained by looking at the range of forces during the insertion compared to the range of user forces needed to move the handle. The forces the needle experiences in the case of no feedback, ranges from 1.5 N to 2.4 N, while the user forces range from 0.5 N to 1.5 N. Therefore, for this phantom, the haptic feedback starts very late in the insertion, or not at all. For the case of force feedback starting late in the insertion, it results in the same movement throughout the phantom, until it slows the user down close to the end. The needle will then have the same velocity during most of the insertion, but slow down in the end. According to literature, a higher velocity during insertion results in higher friction forces and lower puncturing forces [90]. Therefore, if the velocity stays the same for most of the insertion, but slows down just before puncturing, the friction forces will be the same but the puncturing force will be higher. Consequently, this results in a higher overall force.

Phantom 2

For phantom 2, the forces experienced by the needle are greater than for phantom 1. The feedback starts earlier here and is more apparent throughout the insertion. The average and median value decrease, agreeing with the hypothesis, while the ranges of forces increase. This can be explained by looking at the maximum velocity of each user. In the cases where the forces are greater with haptic feedback applied, the maximum velocity of the handle is also greater. Therefore, it can be concluded that due to the high push-back from the actuators, some users exerted too much force to counter it, resulting in a quick motion forward. An increased training time would solve this issue. This explains some of the higher forces measured, while the lower forces measured are expected with haptic feedback.

Phantom 3

For phantom 3, the first half of the phantom is softer than the second half. The reason for that is to test if users can feel a difference when entering a stiffer material. The median value and average decreased in the case of haptic feedback, while the ranges of forces increase. This is consistent with the results of phantom 2. Due to a problem with the phantom, results from users 6-10 were deemed unusable, as the issue caused inconsistencies and inaccuracies in the data, making it unreliable for analysis and interpretation. Moreover, the first insertion was removed due to a different issue with the phantom. This is explained in detail in Appendix A.6.

Overall summary

Comparing the average values of all users (Figure 4.9), the results show that for beginner level users, the difference between haptic feedback and no feedback is negligible for penetrating phantom 1. However, a deeper insertion, with forces ranging up to 3.5 - 4.5 N, results in a safer insertion in the case of haptic feedback. The questionnaire show the efficacy of the actuators to provide haptic feedback to the user. Moreover, it highlights a need for a more in depth model for the position control, increasing the smoothness of insertion.

5 Discussion

5.1 Design

5.1.1 Mechanical design

While steps were taken to minimize friction in the device, the whole mechanical design of the device was not considered for this project. The design should be re-designed to be more modular, as replacing one actuator results in a complete disassembly of the device. The glass plates are glued together which means that if one part breaks, the entire structure must be replaced. Moreover, precision errors in the glass cutting resulted in two opposing plates being non-parallel. Therefore, a spring system was integrated to the system where the potentiometer is connected to the ring. However, replacing the spring is a tedious task. Moreover, users often got distracted when operating the device due to the actuators extending or compressing. It might be better to have a plate on the top that covers the actuators from the eyes of users.

5.1.2 Actuator design

While the actuators almost never got worn out or torn in the center area, they often tore up at the ends (see Figure 5.1). This is where the current design differs from the design of the original rPAM actuators [24]. This tearing happened frequently enough to cause concern over the efficacy of these actuators. The design should be changed to something more similar to the original design and that design should be evaluated for longevity in order to evaluate the efficacy of these actuators. Moreover, employing a swaging process to the fabrication should be looked into, as literature showed great improvement of longevity with that addition.

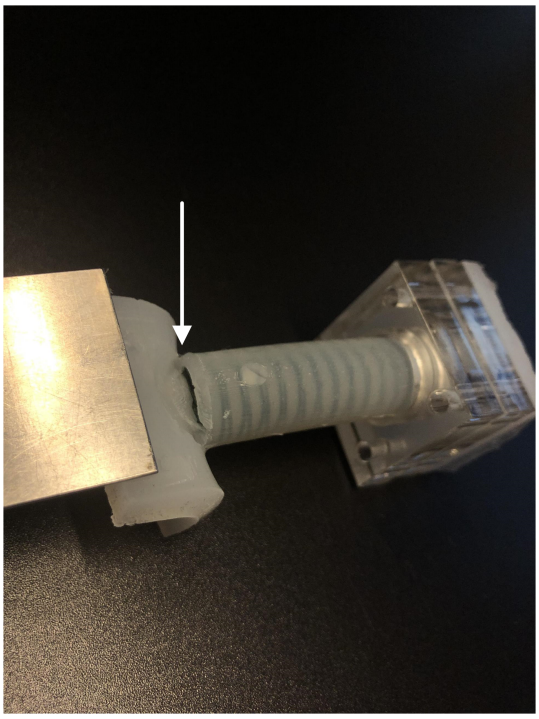

Figure 5.1: A tear in the actuator.

5.1.3 Handle design

The handle was designed to mimic the forward and backwards movement in 1 DoF naturally. However, it was found that a more natural way to move the handle, while keeping a stable movement with haptic feedback, was to hold it with two fingers and not the whole hand. This realization questions the effectiveness of the current design. Other ideas should be considered, where the insertion feels more intuitive. Alternatively, an actual needle could be integrated to the design, imitating an actual biopsy. Moreover, the handle connector, which connects the handle to the ring, should be optimized. Currently, there is a bit of clearance between the handle connector and the ring. This was done to make sure that neither force sensor would be touching the handle if the user is not touching the handle. However, clearance can be minimized in order to have a more natural feel when operating the device. In order to keep the handle away from the force sensors when the user is not touching the handle, springs can be integrated to system. Placing springs on the rods that the handle slides on, would make sure the handle is pushed to its center position when no outside force is applied. This would allow the clearance to be minimized so the user feels that it is connected to the ring, moving as one object.

5.1.4 Workspace limitation

The current design of the device has some workspace limitations, which in turn limits the depth of insertion for one motion of the handle. One way to resolve this, is by constraining the slave device to only move in one direction at a time, declutching the master from the slave. The user can then pick which direction he wants (insertion or extraction) and when the end of the workspace is reached, the handle can be moved all the way back to the beginning of the workspace without the slave device reacting. This way, a deeper insertion can be performed by this device with a few motions of insertion and extraction, respectively. This option was implemented and tested in Simulink, showing good results. Another option is to change the system to control the velocity of the needle, rather than the position. The user can then move the handle forward, increasing the velocity, while the haptic feedback pushes back, lowering the velocity. However, this option might not be as intuitive for users when compared to a position controlled system.

5.2 Hardware

5.2.1 Microcontroller

The current microcontroller board (Arduino Mega 2560) is not powerful enough to run the current software with the specifications picked for frequency of the controller, frequency of the sampling of sensors etc. When you run the Simulink model with the current hardware, it tries to accomplish all the processing within the given timeframe. However, when Simulink is not able to run at the wanted speed due to hardware constraints, the simulation time is slower than real-time. Meaning, if you tell the program to run for 10 seconds, it might run for 20 seconds while the simulation time is 10 seconds. Therefore, it can be seen that the current hardware is not able to run at the wanted frequency. This limits the reaction time of the controller, which in turn leads to less transparency and accuracy of the system. A more powerful microcontroller should be considered in order to improve the control frequency as well as giving the option for a more complex system. However, it should be considered that the current pneumatic regulator is a shield made for mounting an Arduino. Therefore, a new shield might be necessary in order to change the microcontroller.

5.2.2 Force sensors

Since the device is a master device, it can be operated from a safe distance from the MRI or CT imaging. However, if this device is to be used near MRI or CT imaging, in the same room, more research needs to be done to evaluate their ability to operate near the imaging. Even though a similar sensor was shown to be sufficient for devices operated near CT imaging, no research was found related to MR imaging. Moreover, this specific sensor has no public data on materials used. The only visible metallic part is the connector part to the electronics. However, in the case that the sensors are not able to be used near MR or CT imaging, changing the force sensors is a relatively easy task as long as they are small and light-weight.

5.3 Modelling and Control

5.3.1 Position control

Due to the minor non-linearity of the relationship between input pressure and position, the position controller is limited to provide a bit less pressure than the best fit equation finds. This is done due to the prioritization of safety and stability over transparency. However, this adds a limiting factor to the device. Since the position controller, in most cases, provides less pressure than needed to move the device freely, the user must use some force to move the handle. This force is found to range from 0.5 to 1.5 N for most users. Since this force is not consistent between users, it can not be easily neglected in the force controller when comparing the user force to the needle force. Therefore, if a user moves the device with 1.5 N of force, the force controller doesn't react until the needle is experiencing more than 1.5 N. This limits the device when the needle experiences low forces during an insertion, resulting in an enhanced feedback system rather than a fully transparent haptic system. Since the relationship between input pressure and position is not completely linear, a more in-depth model should be found and added to the feed-forward system. A second order equation was tested for this purpose, but due to the hardware limitation of the Arduino, it was not able to run. Due to the high repeatability of rPAMs, a complete model of this behaviour is sufficient to minimize this effect, resulting in a smooth movement of the handle with minimal forces. This would allow the user to feel the haptic feedback for lower forces during the insertion.

Requirements

The following requirements were thought of before designing the controller.

1. The controller should ensure that when the handle is released, the position is kept stable.
2. The controller should be designed in a way that when the same user force is applied, it always results in the same movement of the handle independent on position in the workspace.
3. The controller should avoid sudden unintended movements of the handle. Meaning, if a user is doing an insertion, the controller's output should never be high enough to push the handle forward more than the user intends to.

Through observation, requirement 1 has been fulfilled. The second requirement is mostly fulfilled, but a small improvement should be made to really satisfy the requirement. The third requirement is also fulfilled as the best fit line is lowered in order to ensure no unintended movements during an insertion.

5.3.2 Force control

While the PID was able to provide the user with sufficient forces during an insertion, the accuracy should be improved. The value for the desired RMSE was picked based on the just noticeable difference (JND) that the human hand can feel, in the direction similar to this project. While the lower forces showed a JND of 0.14 N, the requirement was set at 0.3 N for the RMSE. This was picked as the user force measured during an insertion without feedback was in the

range [0.5, 1.5] N and 0.3 N JND corresponds to about 1.5 N reference force. When the user force required to move the device has been lowered to around 0 N, the requirement should be changed to 0.14 N RMSE. Tuning the PID might result in better results. However, a more complex controller is needed to ensure stability and improve the transparency greatly. In literature, most researchers use a form of sliding mode controller to control PAM actuators. Therefore, it should be considered as an improved controller. Other controllers can also be considered as long as stability is guaranteed and the accuracy is increased.

Requirements

The following requirements were thought of before designing the controller.

1. The controller should be able to relay the forces experienced by the needle back to the user with an accuracy of at least 0.3 N RMSE.
2. The controller should avoid unstable behaviors, even if it means sacrificing some level of accuracy, therefore prioritizing stability over transparency.

The first requirement is not met. The user force does follow the setpoint with decent accuracy, but it should still be improved on. Due to time constraints, this result was deemed sufficient for this project. The second requirement is fulfilled, as the controller has safety features for this purpose.

5.3.3 Actuator buckling

Through testing of the actuators limits, both with Ecoflex 00-50 and Dragonskin 10 (see Appendix A.4.1), it was found that buckling of the actuators is a limiting factor. At lower stretches of the actuators, they start buckling at lower pressures and can therefore not provide the same axial force as they can at different stretches. This limits both the workspace of the device as well as the forces that can be provided throughout the workspace. The reason for that, is that when the actuators start bending during haptic feedback, it makes any extra force bend the actuators more. Therefore, if either the haptic feedback increases or the user applies more force to the handle, it results in the actuator bending more. When the actuator bends more, it looses its ability to constrain the user movement which can result in an unsafe insertion. This limitation must be thought of and put as a limitation to the controller. While an empirical model was found, comprehensive and accurate mathematical modelling of the actuators, that takes into account material properties and dimensions, is essential to improve the efficacy of the actuators.

5.3.4 Slave system

Controlling the slave system was found to be smooth during an insertion. However, there is an added complexity when the user releases the handle before the desired distance is met. It is not a good idea to keep moving the needle, even though the user has released the handle, as that would mean an increased insertion than intended by the user. Therefore, the steps needed is reset when a user releases the handle. When the movement should continue, the stepper motor should start from step 0, then 1 and so forth (forward direction). For this reason, the counter is reset when movement starts again. However, it has been noticed that sometimes there is a slip, meaning that sometimes the motor moves one step backwards before moving forward. This is likely due to some modelling issues in Simulink where the reset signal does not reach in time before a signal is sent to the stepper motor to start, resulting in the counter starting at a random value before resetting to 0. This needs to be fixed to ensure a safe insertion, as in the case of stopping before retracting the needle could result in one step forward (deeper insertion) before the retraction starts.

5.4 Haptic requirements

The following design goals were thought of such that it could be used as a haptic device in medical applications. While these goals are important for the continuation of this project, they are not necessarily thought of as requirements for this thesis.

1. Friction should be so low that a typical user can not recognise it.
2. Moving the handle should require the same force throughout the workspace.
3. The workspace should be maximized, such that the only limiting factor is the actuator capabilities.
4. The user should be able to feel at least 3 N as a feedback force throughout the workspace.
5. The actuators should have the same intrinsic characteristics over an extended period of time. They should not lose any functionality or break after a short time.
6. When the user releases the handle, there should be negligible backlash.

The first requirement has been fulfilled. This was noticed during the user trial. Discussion with some users that answered that they didn't feel the same friction throughout the workspace, resulted in the conclusion that the friction they feel is due to the position controller.

Through testing of forces exerted when moving the handle to the end of the workspace, showed a very minimal increase in forces with an increase in position. Therefore, it can be said that the 2nd requirement is fulfilled.

After the friction was minimized, the actuators were able to move the handle to each end of the workspace with no user input. However, the ends can only be reached with some buckling of the actuators. Therefore, the complete workspace is not used due to a limitation of the actuators. Therefore, the 3rd requirement is fulfilled.

During modelling of the actuator's capabilities, for usage in the force controller, it is found that the maximum force the actuators can provide, with no movement from the user, is 2.42 N. However, at the end of the workspace where the actuator stretch is low, they can only provide around 1 N of axial force. The reason for this, as mentioned before, is the buckling of the actuators. Changing the material to Dragonskin 10 however, resulted in a minimum of 7.5 N throughout the workspace. Therefore, the 4th requirement is fulfilled as long as Dragonskin 10 is used.

The 5th requirement is not fulfilled as the actuators are found to change characteristics over time. During the user trial for example, the position controller had to be re-calibrated for the 10th user. Moreover, the actuators often break at the ends, as discussed before. Most likely, they are related to the same issue. If the ends are slowly breaking, the actuators characteristics will change before eventually breaking.

The final requirement states that there should be negligible backlash. From experiments (Appendix A.4.4), it was shown that the backlash has been greatly improved. However, it is still noticeable. Therefore, a more in depth position controller should be implemented, ensuring safety when operating the device.

6 Conclusion and Recommendations

6.1 Conclusion

This study set out to investigate the efficacy of rPAM actuators for usage in remote MIS with force feedback. Steps were taken in order to minimize friction and increase the actuators capabilities, in order to make control of the device achievable. Force sensors have been integrated to the haptic system to accurately measure the user force during usage of the device. Precise 3d printing made sure that negligible friction was present when moving the handle, allowing for accurate measurements. Empirical modelling was performed in order to control the position and to limit the force controller, keeping the system stable. Stability of the controllers was prioritized over transparency due to the possible damage that instability can cause during insertions.

Through experiments where ten users were instructed to insert a needle into 3 phantoms, the haptic system was evaluated. The results showed that the system performed similarly as haptic devices found in literature, lowering interaction forces and increasing tissue characterization. However, due to a limitation of the position controller, phantom 1 showed different results than hypothesised. Therefore, the range of forces needed for the current state of the device to perform as expected has been shown through experiments.

Each sub-question was answered during the study, which helped in answering the main research question: "What is the efficacy of reverse Pneumatic Artificial Muscles (rPAM) for usage in remote Minimally Invasive Surgeries with kinesthetic (force) feedback, especially for needle insertions in soft tissue; biopsies and ablations?". While not all requirements have been met for a haptic device, the actuators efficacy has been shown through experiments. From the results, it can be concluded that the actuators are able to provide the user with realistic haptic feedback, which showed to be effective in lowering the interaction forces of the needle, in cases where forces are greater than the base user force. Therefore, it can be concluded that the efficacy of the actuators has been shown through experiments.

6.2 Recommendations for future work

The following recommendations have been thought of based on the discussion:

1. Make the fabrication process of the actuators more stable. Design new molds with end-fittings similar to the original design. Look into swaging process, as it has shown a great improvement in life expectancy in PAMs.
2. Change the material of the actuator to Dragonskin. It has been shown to increase the range of forces while also handling higher stress before breaking.
3. Modify the handle design to be more intuitive to use for needle insertions. Adding an actual needle, or something similar in diameter, might be a good way to make it more natural to move. Moreover, the handle connector should be modified to remove clearance. Adding a spring system could be useful to remove any clearance while still having both sensors read 0 N, when no user is touching the handle.
4. Modify the mechanical design to be more modular and remove need for a spring system where the disk connects to the potentiometer.
5. Integrate a more in depth force control system, such as sliding mode control.
6. Develop a precise mathematical model of the actuators in order to control the position.
7. Change the microcontroller to a more powerful one, such as STM32.

A Appendix

A.1 Current state of the system

A.1.1 Hardware

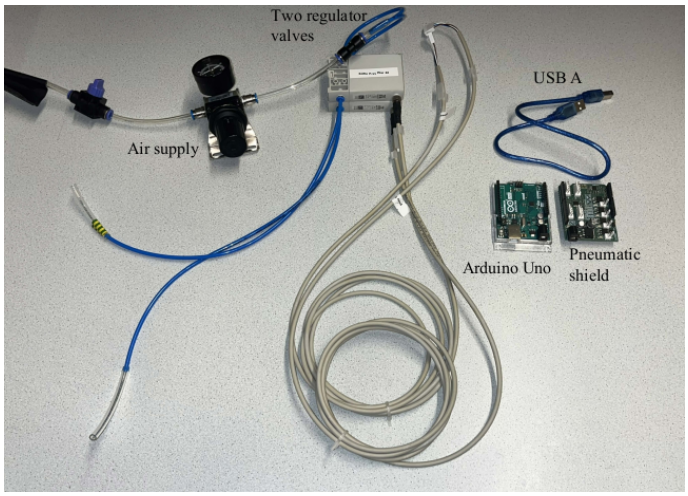

Figure A.1: The control system of the air pressure.

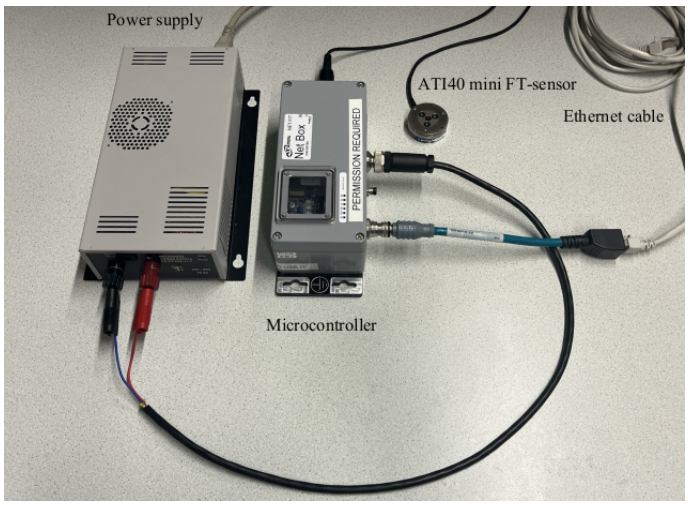

Figure A.2: The setup of the force sensor ATI40 [91].

A.1.2 Capabilities

Three tests were conducted in order to evaluate the capabilities of the device for usage as a haptic device. The first test measured the force needed to move the joystick from starting position to 0.5, 1.0, 1.5, 2.0 and 2.5 cm respectively with air pressure applied in the opposite direction of the movement ranging from 0 to 50 kPa for each movement. For this test, only one slider and one potentiometer is connected. The results can be seen in table A.1.

The discrepancies happen at high displacements and at pressures close to the actuator limits, since there the actuator starts bending. When the actuator bends, an increase in pressure is not guaranteed to cause an increase in axial force. On the contrary, the increase in pressure will usually just cause more bending of the actuator. This effect can be seen in Figure A.5.

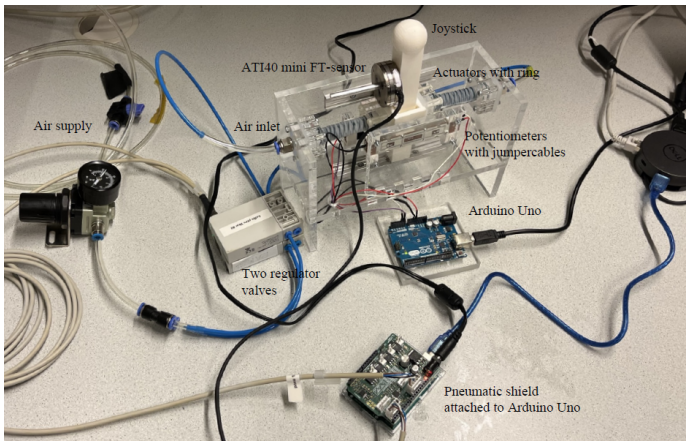

Figure A.3: The full setup of the device with the force sensor mounted on the joystick.

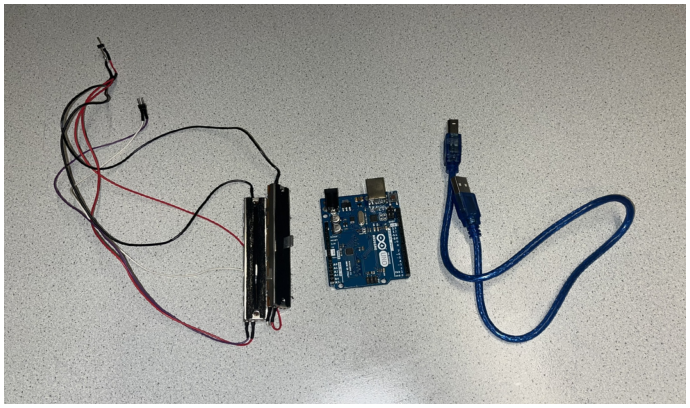

Figure A.4: The sliding potentiometer previously used.

Air Pressure / Displacement	0 kPa	10 kPa	20 kPa	30 kPa	40 kPa	50 kPa
0.5 cm	7.0 N	10 N	12.5 N	15.5 N	22.5 N	16.5 N
1.0 cm	8.5 N	13 N	17.5 N	25 N	27.5 N	23.5 N
1.5 cm	11.0 N	16.5 N	20.0 N	26.5 N	31.0 N	27.5 N
2.0 cm	14.5 N	17.0 N	35.0 N	28.5 N	27.0 N	33.0 N
2.5 cm	21.5 N	24.5 N	32.0 N	37.5 N	38.5 N	38.5 N

Table A.1: Maximum force seen during movement of joystick to different displacements with different air pressures restricting the movement

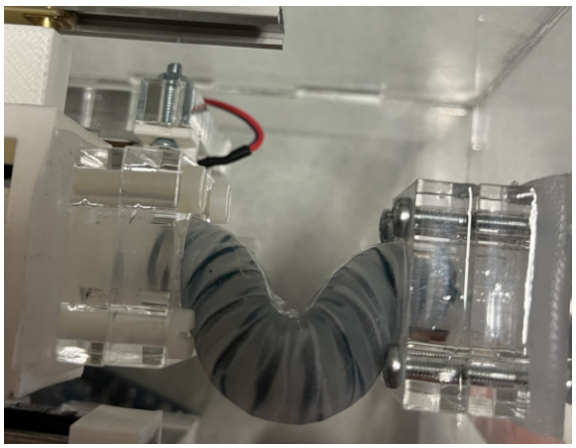

Figure A.5: The actuator bending at high displacement and/or high pressures.

The second test measured the movements capabilities of the actuators. In order to test this, only one potentiometer is connected to the ring and the joystick and sliders are not used. This is done to minimize the friction in the device, showing the pure actuator possibilities. The results can be seen in table A.2.

Air Pressure	Displacement
10 kPa	0 mm
20 kPa	4 mm
30 kPa	8.2 mm
40 kPa	12.8 mm
50 kPa	16.1 mm

Table A.2: Displacement capabilities of the actuators when minimal friction is considered

For the final test, the backlash from releasing the handle is measured by dragging the joystick to different displacements (5, 10, 15, 20 and 25 mm) and then releasing it. Different air pressures are applied, pushing in the same direction as the backlash. This was done in order to find safe air pressures to operate such that if the handle is released while force feedback is being applied, the handle doesn't backlash aggressively. If there were no friction in the device, the joystick should move back to the equilibrium point even without any air pressure. However, due to the friction present in the device, the results show that for distances 5, 10 and 15 mm, the joystick doesn't move at all, even with 10 kPa of pressure trying to push it towards the equilibrium point. For 30 kPa pressure, the actuators were able to push the joystick back towards the equilibrium point for all distances. With an air pressure of 40 and 50 kPa, the actuators were able to push the joystick over the equilibrium point, with the maximum being almost 10 mm over the equilibrium. For this test, only one potentiometer is used and it is not explained whether the linear rails are used.

A.2 Modelling and Control

A.2.1 Simulink models

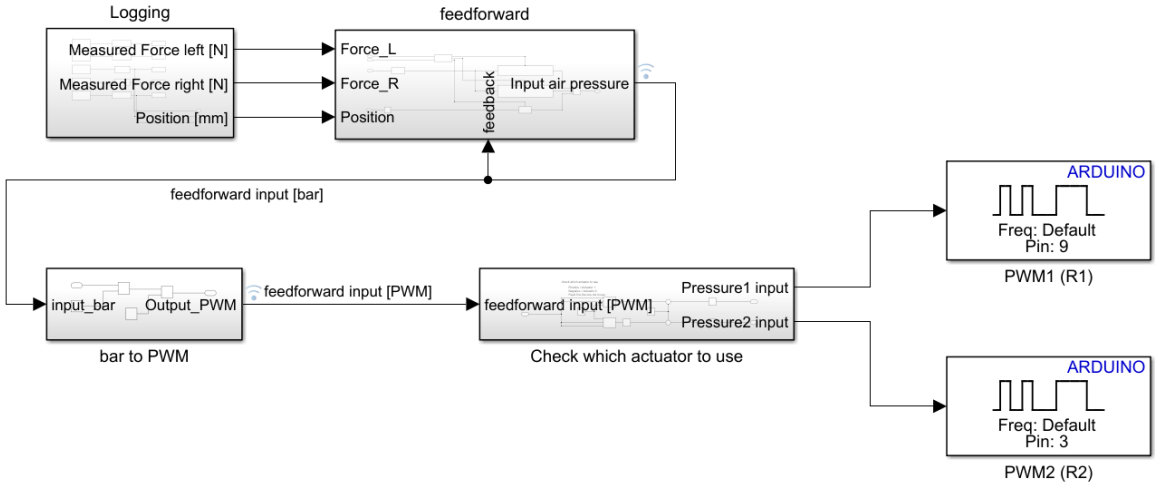

Figure A.6: The simulink model for the feed-forward system.

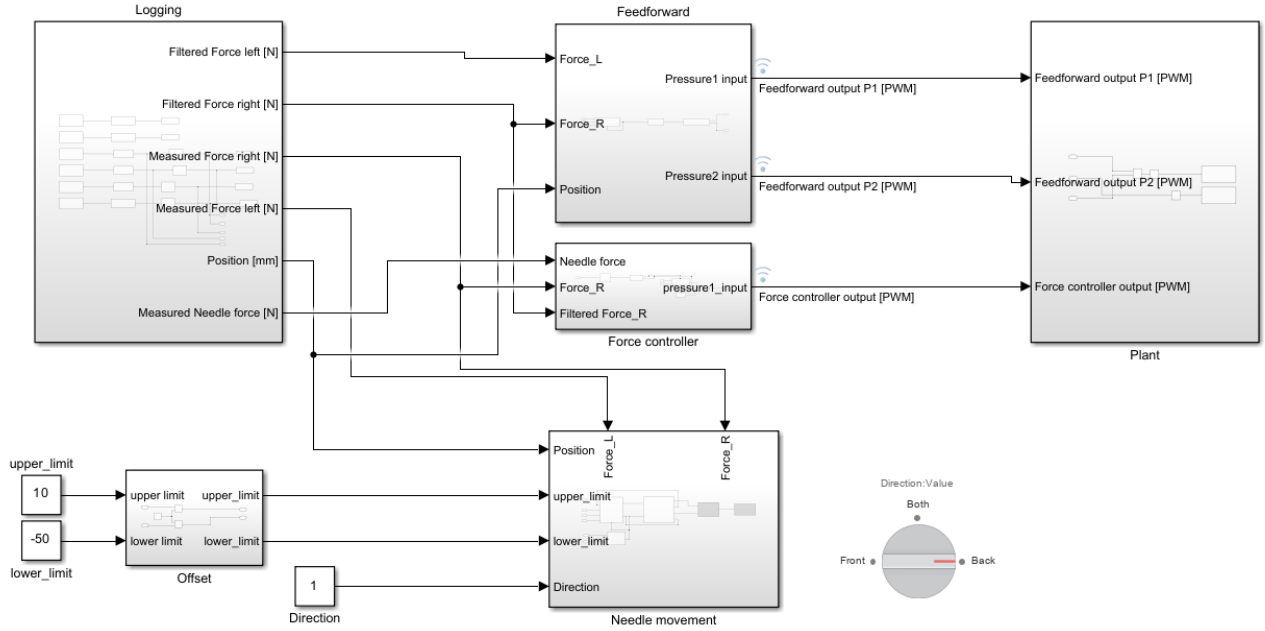

Figure A.7: The simulink model with the combined control system as well as controlling the needle position.

A.2.2 Right slope

In the same way as the left slope if found, the right slope is found. However, the modified line is now a bit above the best fit line, instead of below. This is due to a reverse in where the deflating zone is and where the inflating zone is.

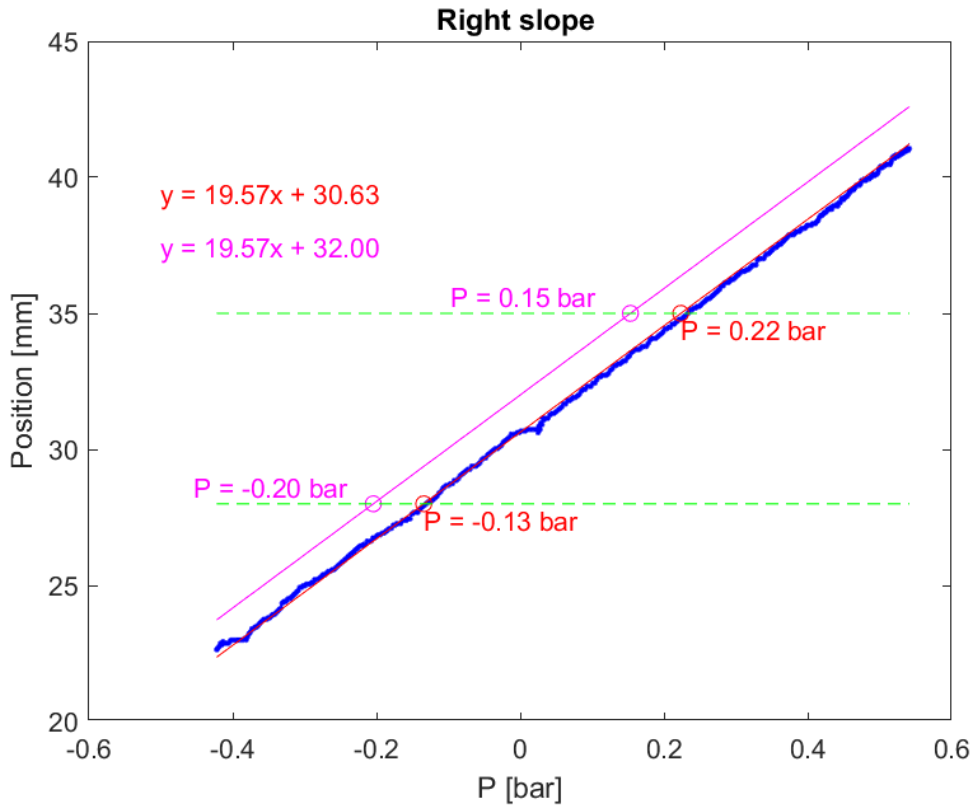

Figure A.8: The best fit line and modified line for the right slope.

A.2.3 Method for finding edges

For this method to work, the x-axis needs to be in a measurement where the range of the x-axis is lower than the range of the y-axis. For this reason, the measurement unit of bars is chosen (see Figure 3.16) instead of the SI unit kPa. The top left corner is found by calculating the closest value in distance to an imaginary point that has the values of the minimum pressure and maximum position. Similarly, the top right corner corresponds to the point closest to the maximum of both pressure and position. The bottom left corner corresponds to the point closest to the minimum of both and the bottom right corner to the maximum pressure and minimum position. Note that this only works for this relation and not all skewed rectangles. The reason it works for this relation is that the whole x-axis is less than 1.6 bars, while the y-axis is about 20 mm. That means that when the point closest to the minimum pressure (~ -0.7 bars) and maximum position (~ 37 mm), it will be top left and not bottom left. Using equation A.1 to calculate the distance between the two points, the distance to top left is 1.2 and the distance to bottom left is 20.

$$d = \sqrt{(x_2 - x_1)^2 + (y_2 - y_1)^2} \tag{A.1}$$

$$d_{TL} = \sqrt{(0.5 - (-0.7))^2 + (37 - 37)^2} = 1.2 \text{ [mm]}$$

$$d_{BL} = \sqrt{((-0.7) - (-0.7))^2 + (17 - 37)^2} = 20 \text{ [bar]}$$

where

d = Distance to point [mm]

d_{TL} = Distance from imaginary point to top left corner of the rectangle [mm]

d_{BL} = Distance from imaginary point to bottom left corner of the rectangle [mm]

$(-0.7, 37)$ = Imaginary point using the minimum pressure and maximum position ([bar, mm])

$(0.5, 37)$ = Point of top left corner ([bar, mm])

$(-0.7, 17)$ = Point of bottom left corner ([bar, mm])

A.2.4 Best fit line Pseudo code

Algorithm 1 Main Algorithm

LOAD DATA
CALCULATE $P_{\text{one\_cycle}}$:
    $P_{\text{one\_cycle}} = P1_{\text{input}} - P2_{\text{input}}$ ▷ $P2_{\text{input}}$ is represented as negative pressures
    $P_{\text{one\_cycle}}$ = Select elements from one cycle
FIND CORNERS: corners = findCorners($P_{\text{one\_cycle}}$, pos)
ASSIGN POINTS:
    A = First row in corners
    B = Second row in corners
    C = Third row in corners
    D = Fourth row in corners
SET DEGREE: degree = 1
FIND BEST FIT LINES:
    Call findBestFitLines function with A, B, C, D, $P_{\text{one\_cycle}}$, position and degree as parameters
    Returns: line1, line2, coeffsAC, coeffsBD, pointsAC, pointsBD
SET X RANGES:
    $xRange_l$ = minimum and maximum x-values among A, B, C, D
    $xRange_r$ = minimum and maximum x-values among A, B, C, D
SET THRESHOLD: threshold = x
LEFT SLOPE:
    pointsAC = filter_points function with pointsAC, line1 and threshold_left as parameters
    Calculate equation and yfit using polyfit and polynomial values using the calculated equation
RIGHT SLOPE:
    pointsBD = filter_points function with pointsBD, line2 and threshold_right as parameters
    Calculate equation and yfit using polyfit and polynomial values using the calculated equation

Algorithm 2 Function: findCorners

```
function FINDCORNERS(pressure, position)
    Check input validity:
    if length(pressure) ≠ length(position) then
        error('Pressure and position must have the same length.')
    end if
    Remove duplicate points:
    uniqueData = unique rows in combined pressure and position data
    Find min and max values:
    minPressure = minimum pressure in uniqueData
    maxPressure = maximum pressure in uniqueData
    minPosition = minimum position in uniqueData
    maxPosition = maximum position in uniqueData
    Find corners:
    topLeft = findClosestPoint function with uniqueData, minPressure, and maxPosition as parameters
    topRight = findClosestPoint function with uniqueData, maxPressure, and maxPosition as parameters
    bottomLeft = findClosestPoint function with uniqueData, minPressure, and minPosition as parameters
    bottomRight = findClosestPoint function with uniqueData, maxPressure, and minPosition as parameters
    Combine the corners into a matrix:
    corners = matrix combining topLeft, topRight, bottomLeft, bottomRight
    return corners
end function
```

Algorithm 3 Function: findBestFitLines

```
function FINDBESTFITLINES(A, B, C, D, pressure, position, degree)
    - Validate degree
    - Find points between A and C and B and D
    - Perform RANSAC to find best fit lines or curves
    - Return line functions and coefficients
end function
```

Algorithm 4 Function: filter_points

```
function FILTER_POINTS(data, line_func, threshold)
    - Iterate over each data point
    - Compute distance from point to line
    - If distance ≤ threshold, keep the point
    - Return filtered points
end function
```

A.3 Materials and Methods

A.3.1 Components

DC-DC converter

Figure A.9: The DC-DC converter used to convert 5 V to -5 V. The converters part number is MPA0505S-1W [92].

Voltage regulator

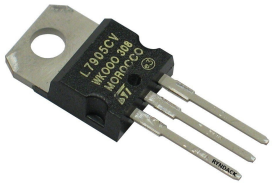

Figure A.10: The voltage regulator used to regulate the -5 V. The regulators part number is LM7905 [93].

Op-amp

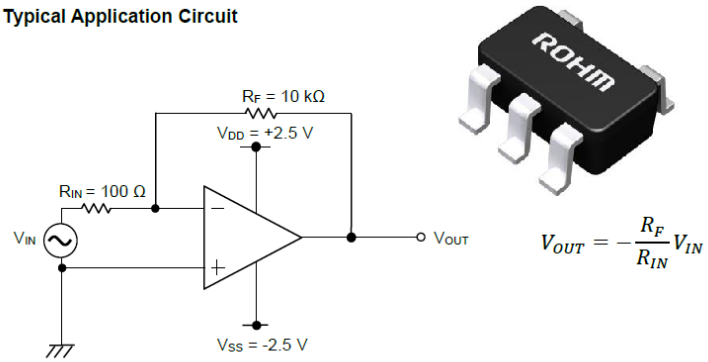

Figure A.11: The op-amp used to amplify the change in resistance in the force sensors on the haptic device, as well as a typical circuit. The op-amps part number is BD7281YG-C [82].

Force sensor on the haptic device

While the accuracy of the sensor is not given, the linearity is given as 99% and the repeatability error as maximum ± 2 % error. The range of forces are 0 to 20 N. The datasheet mentions two methods to measure the sensor:

Figure A.12: The force sensor used on the haptic device. Its part number is GD10-20N [77].

1 Using an operational amplifier (OP-AMP) in an inverting configuration to obtain a voltage output that varies linearly with respect to force input.

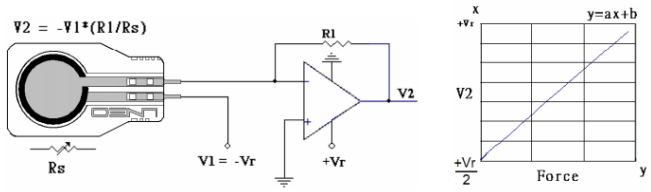

Figure A.13: Measurement circuit that results in a linear relationship between force and voltage [77].

2 Using a fixed resistor R1 in a voltage divider configuration for an output V2 that increases logarithmically with respect to added force.

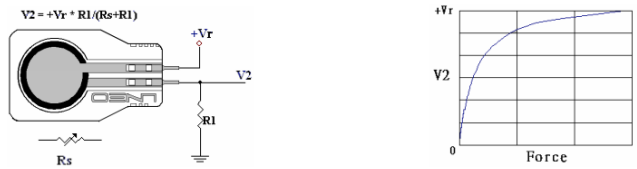

Figure A.14: Measurement circuit that results in a logarithmic relationship between force and voltage [77].

Force sensor on the slave side

The accuracy is given as ± 3 % for the Full Scale Span (FSS). The range is from 0 to 10 N.

Figure A.15: The force sensor used on the slave device. Its part number is 32311096 [94].

A.4 Experiements

A.4.1 Actuator capabilities

To effectively see the difference in the actuator capabilities based on its internal material, the Ecoflex 00-50 was compared to the Dragonskin. Since the hardware can not apply the air pressure needed for the Dragonskin, the air pressure is manually modified in that case. For each material, two actuators are made, integrated to the system and tested. The objective is to see if there is a difference in the maximum range for the workspace or the maximum force the actuators can provide to the user throughout the workspace. The results can be seen in Tables A.3 to A.5, where Table A.3 and A.4 show the capabilities of the different actuators at different places in the workspace. Table A.5 then summarizes the main capabilities of each actuator, showing the workspace and maximum force it can produce.

Ecoflex 00-50

Initial Stretch	Maximum Force	Pressure where bending starts
150%	1.89 N	105 kPa
144.63%	1.89 N	100 kPa
141.13%	2.13 N	95 kPa
137.32%	2.43 N	105 kPa
133.36%	2.42 N	75 kPa
129.85%	1.78 N	85 kPa
125.51%	1.76 N	80 kPa
122.81%	1.33 N	70 kPa
120.15%	0.92 N	60 kPa
117.69%	1.64 N	65 kPa

Table A.3: Table of Initial Stretch, Maximum Force, and Pressure for Ecoflex 00-50.

Dragonskin 10

Initial Stretch	Maximum Force	Pressure where bending starts
159.8%	13.25 N	210 kPa
149.6%	14.45 N	200 kPa
138.2%	12.67 N	170 kPa
131.0%	7.52 N	150 kPa

Table A.4: Table of Initial Stretch, Maximum Force, and Pressure for Dragonskin 10.

Material	Maximum Force	Maximum pressure	Workspace with current hardware
Ecoflex 00-50	2.43 N	130 kPa	21.1 mm
Dragonskin 10	14.45 N	400 kPa	17.8 mm

Table A.5: Table comparing main attributes of Ecoflex 00-50 and Dragonskin 10. Current hardware only supports 200 kPa output which limits the workspace of the Dragonskin actuators.

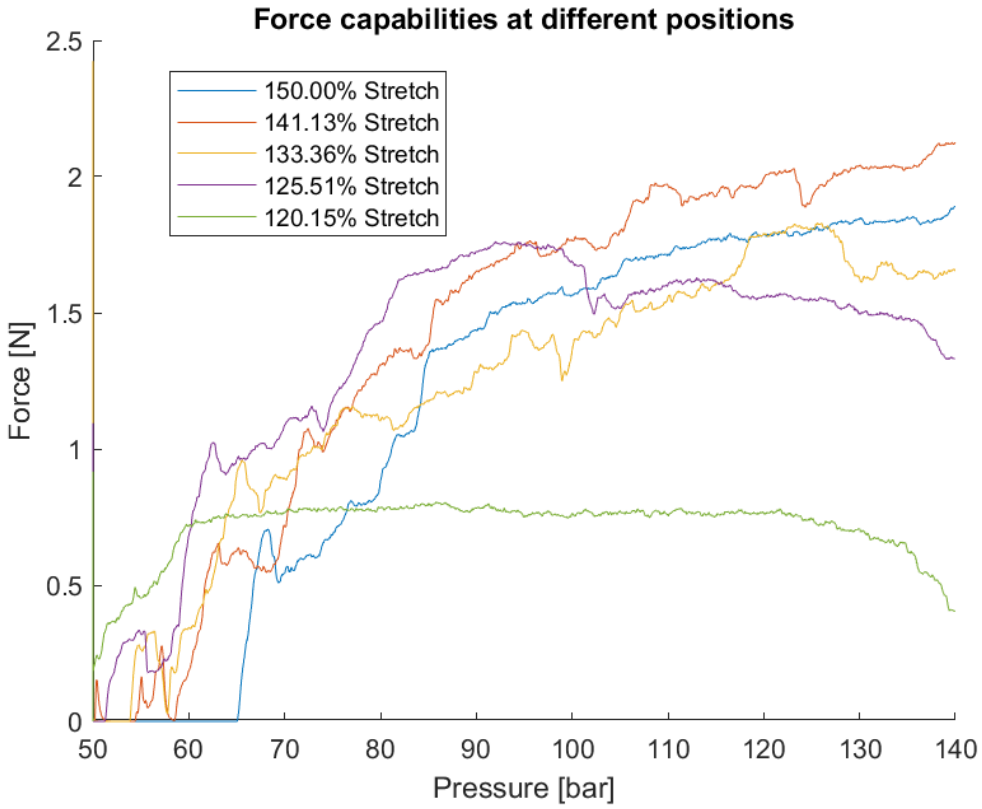

Figure A.16: The forces experienced by the user while the handle is kept still at different starting position and the pressure increased to its maximum. The equilibrium point (center of the workspace) is at 150 % stretch for each actuator.

A.4.2 Actuator capabilities after user trial

In order to see the actuators durability and their characteristics, the capabilities are tested again after the user trial. Table A.6 shows the results. The reason for the higher forces here compared to the first test, is that for this test the handle is held in place by hand, while the other test used a weight. A small issue with the weight was noticed that it caused the handle to turn a bit, causing some of the force to be absorbed by the handle and the rods connecting the handle to the ring. Therefore, this is a more accurate representation of the forces the actuators are able to provide.

Ecoflex 00-50

Initial Stretch	Maximum Force	Pressure where bending starts
150%	3.30 N	130 kPa
146.24%	3.13 N	110 kPa
143.63%	2.88 N	100 kPa
139.14%	2.73 N	80 kPa
135.02%	2.87 N	80 kPa
133.44%	2.06 N	75 kPa
130.35%	1.82 N	70 kPa
128.30%	1.54 N	65 kPa
127.51%	1.38 N	65 kPa

Table A.6: Table of Initial Stretch, Maximum Force, and Pressure for Ecoflex 00-50. Repeated after user trial to check repeatability.

A.4.3 Force required to move handle

The force required to move the handle without any position controller is checked in order to see the maximum forces the user can feel while inserting. The handle is moved from the equilibrium point, and 2.6 mm forward. The reason for the small distance is the buckling of the actuators at higher pressures.

Pressure [kPa]	Force required (N)
0	1.6
10	2.1
20	2.6
30	3.8
40	4.2
50	4.7
60	5.4
70	7.1
80	7.5

Table A.7: Force required to move a handle against the actuator's pressure

A.4.4 Backlash

In order to check the backlash of the system, a pressure of 100 kPa is applied to one actuator. First, no system is added to the system. The only input is 100 kPa and the handle is moved to certain positions before releasing. The amount of mm the handle moves after it is released is measured. Next, the feedforward system (position controller) is added. Finally, a check for user input is added, stopping the handle in the case of no user input. The difference between the 3 systems can be seen in Figure A.17. The results show that if the handle is pushed all the way to the equilibrium point, the first system ("No system") results in 14.75 mm backlash. However, with the full system it only results in 7.55 mm backlash.

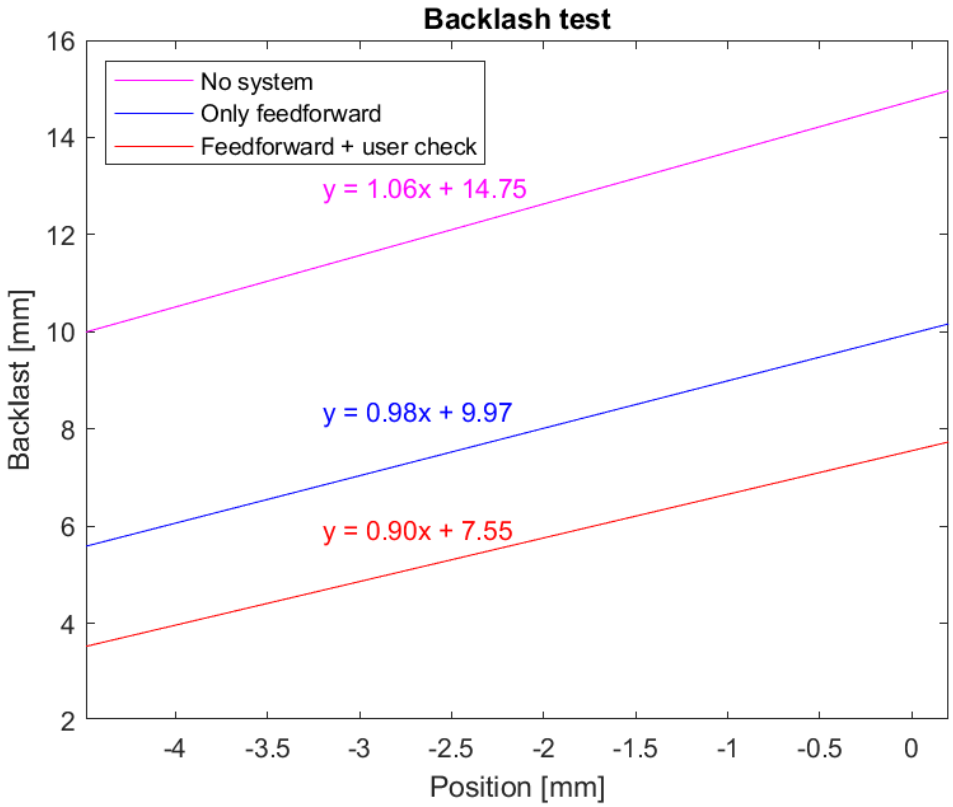

Figure A.17: The backlash is tested with different capabilities. Each addition minimizes the backlash. The x-axis is the position from the equilibrium point (with no input). The 100 kPa pushes the handle a few mm to the back. Therefore, the closer to 0, the more backlash is measured.

A.5 User trial results scattered

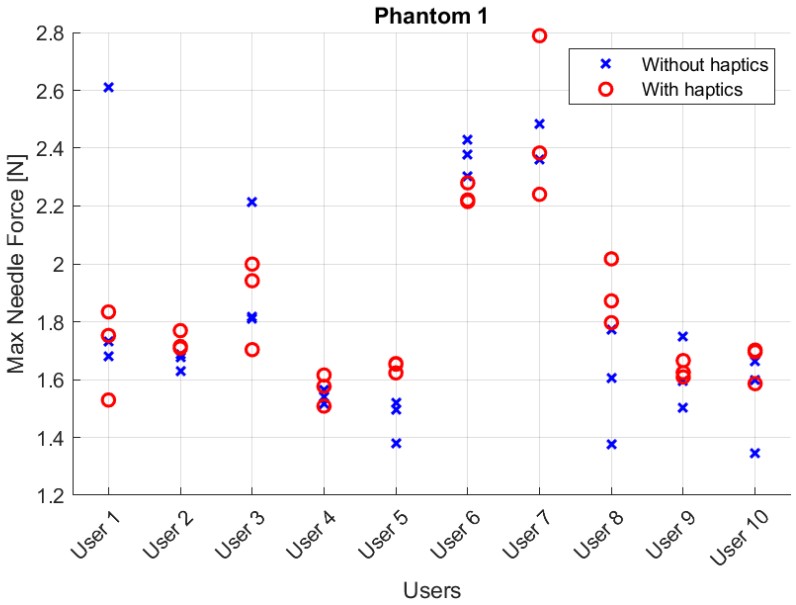

Figure A.18: Each insertion into Phantom 1 showed on a scatter plot for each user.

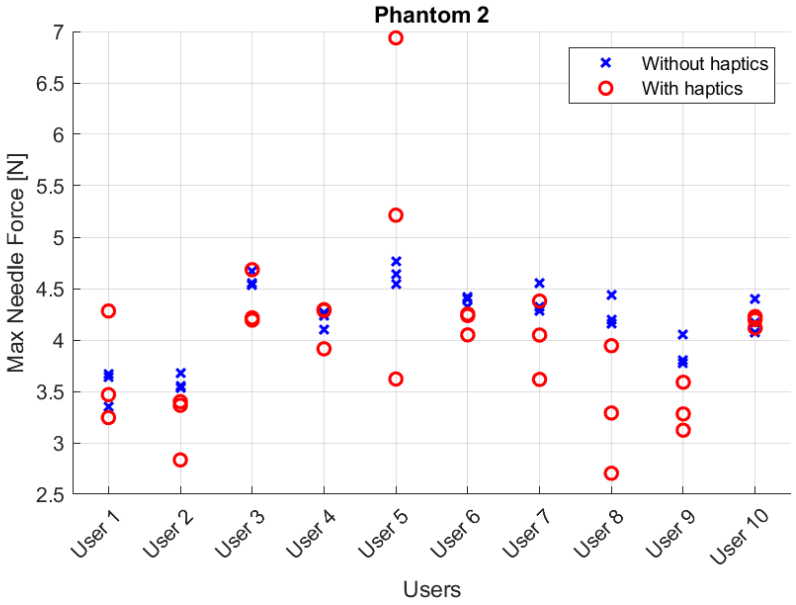

Figure A.19: Each insertion into Phantom 2 showed on a scatter plot for each user.

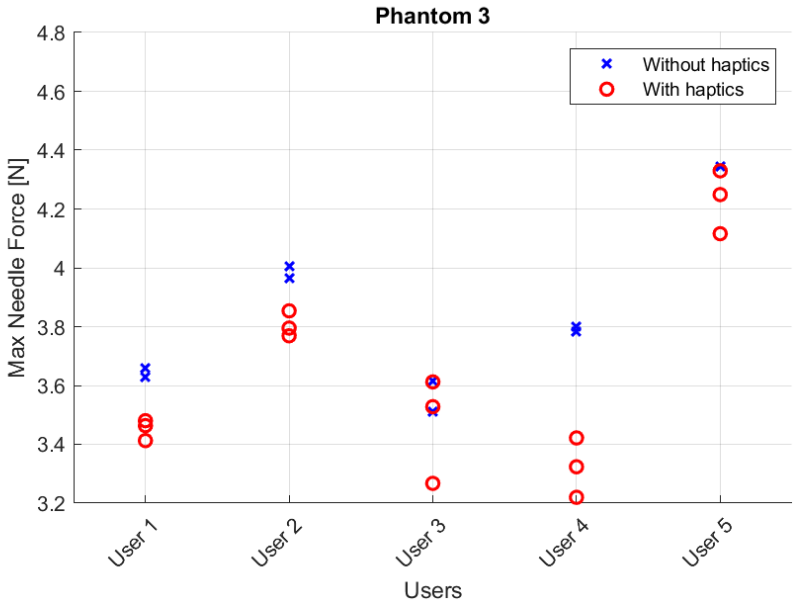

Figure A.20: Each insertion into Phantom 3 showed on a scatter plot for each user.

A.6 Data correction

The results from phantom 3 showed a clear difference from the first 5 users to the second 5 users. The peak forces decreased rapidly and the results showed an increase in the average forces in the case of haptic feedback. Nothing in the data showed a clear difference from user 1-5 compared to users 6-10. The data considered was maximum speed of handle, average speed of handle, total insertion time and maximum user force. The average of all 10 users can be seen in Figure A.21.

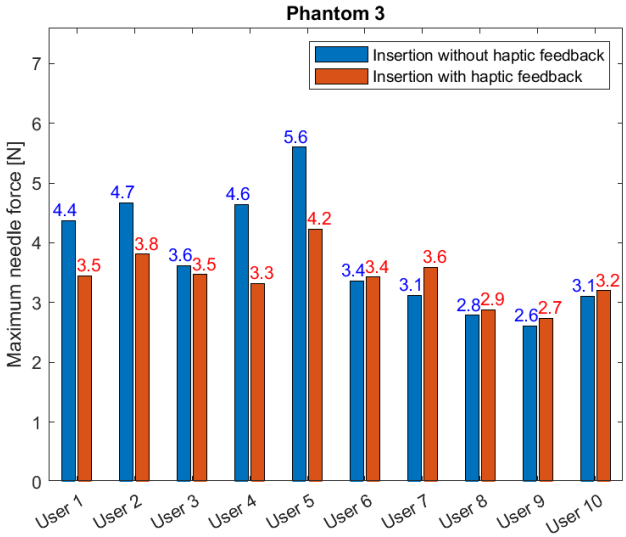

Figure A.21: The average of peak interaction forces during insertion into phantom 3 before data correction.

Since nothing in the data showed a clear difference between the two groups, some tests were conducted to figure out why there was a change after user 5. First, I performed the test in the same order as the 10 users. Table A.8 shows the average of each insertion into each phantom, in the case of haptic feedback, for my test and the 10 users from the user trial. The results are

very similar for the first two phantoms, but a lot lower for phantom 3. This led to a hypothesis that the Ecoflex material in phantom 3 had lost its abilities and is now not giving the same forces. Since this was not found in phantoms 1 and 2, the Dragonskin is thought to be safe for insertions into the same point multiple times.

Phantom	Average of 10 users [N]	My average [N]
1	1.8	1.8
2	4.16	3.95
3	3.41	2.57

Table A.8: The average peak interaction forces for all users and for the post user trial test.

To validate this finding, User 1 was asked to repeat the test only for the 3rd insertion. When the test setup was the same as in the user trial, the peak forces were around 2.3 N in the case of haptic feedback. However, when the distance is kept the same but the insertion point is changed, the forces went up to around 4.1 N. This validates that the qualities of phantom 3 had changed and therefore the tests for some users can not be included.

Moreover, a clear outlier was found in the first insertion for 4 users. This can be seen visually in Figure A.22. This is found to be due to a difference in manufacturing of the phantoms. Each phantom was made by pouring the material/s in a cup and waiting for it to cure. However, for phantom 1 and 2, the resulting phantoms were too large to use for one insertion. Therefore, they were cut to the desired sizes. Phantom 3 is the only phantom that was not cut and therefore had a small wall on the Dragonskin side, where the needle exits the phantom. It was noticed that for some insertions, this wall would not break easily for the first insertion, but extend for a while before breaking. This causes a large increase in puncturing forces that are not seen for other insertions. Therefore, the first insertion for each user is removed for phantom 3 to make sure all insertions are the same.

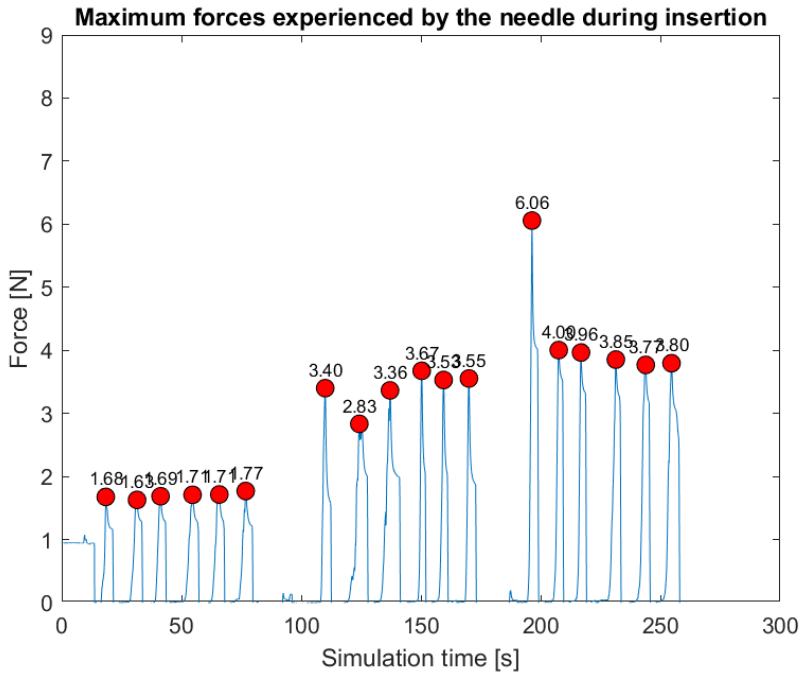

Figure A.22: The peak forces of User 2 when insertion into Phantom 3. Each 6 insertions correlate to each phantom. Phantom 3 shows a clear outlier in the first insertion. One second in simulation time is equal to about 2.3 seconds.

Bibliography

[1] K. H. Fuchs, "Minimally Invasive Surgery," *Endoscopy*, vol. 34, no. 2, pp. 154–159, Mar. 2002, publisher: © Georg Thieme Verlag Stuttgart · New York. [Online]. Available: http://www.thieme-connect.de/DOI/DOI?10.1055/s-2002-19857

[2] K. T. Foley, L. T. Holly, and J. D. Schwender, "Minimally Invasive Lumbar Fusion," *Spine*, vol. 28, no. 15S, p. S26, Aug. 2003. [Online]. Available: https://journals.lww.com/spinejournal/Fulltext/2003/08011/Minimally_Invasive_Lumbar_Fusion.6.aspx

[3] R. Bittner, M. A. Montgomery, E. Arregui, V. Bansal, J. Bingener, T. Bisgaard, H. Buhck, M. Dudai, G. S. Ferzli, R. J. Fitzgibbons, R. H. Fortelny, K. L. Grimes, U. Klinge, F. Koeckerling, S. Kumar, J. Kukleta, D. Lomanto, M. C. Misra, S. Morales-Conde, W. Reinpold, J. Rosenberg, K. Singh, M. Timoney, D. Weyhe, and P. Chowbey, "Update of guidelines on laparoscopic (TAPP) and endoscopic (TEP) treatment of inguinal hernia (International Endohernia Society)," *Surgical Endoscopy*, vol. 29, no. 2, pp. 289–321, Feb. 2015. [Online]. Available: https://doi.org/10.1007/s00464-014-3917-8

[4] A. Hatzipanayioti, S. Bodenstedt, F. von Bechtolsheim, I. Funke, F. Oehme, M. Distler, J. Weitz, S. Speidel, and S.-C. Li, "Associations Between Binocular Depth Perception and Performance Gains in Laparoscopic Skill Acquisition," *Frontiers in Human Neuroscience*, vol. 15, 2021. [Online]. Available: https://www.frontiersin.org/articles/10.3389/fnhum.2021.675700

[5] A. Hamed, S. C. Tang, H. Ren, A. Squires, C. Payne, K. Masamune, G. Tang, J. Mohammadpour, and Z. T. H. Tse, "Advances in Haptics, Tactile Sensing, and Manipulation for Robot-Assisted Minimally Invasive Surgery, Noninvasive Surgery, and Diagnosis," *Journal of Robotics*, vol. 2012, p. e412816, Dec. 2012, publisher: Hindawi. [Online]. Available: https://www.hindawi.com/journals/jr/2012/412816/

[6] C. Wagner, N. Stylopoulos, and R. Howe, "The role of force feedback in surgery: analysis of blunt dissection," in *Proceedings 10th Symposium on Haptic Interfaces for Virtual Environment and Teleoperator Systems. HAPTICS 2002.* Orlando, FL, USA: IEEE Comput. Soc, 2002, pp. 68–74. [Online]. Available: http://ieeexplore.ieee.org/document/998943/

[7] A. M. Okamura, "Haptic Feedback in Robot-Assisted Minimally Invasive Surgery," *Current opinion in urology*, vol. 19, no. 1, pp. 102–107, Jan. 2009. [Online]. Available: https://www.ncbi.nlm.nih.gov/pmc/articles/PMC2701448/

[8] H. Xin, J. S. Zelek, and H. Carnahan, "Laparoscopic surgery, perceptual limitations and force: A review," in *First Canadian student conference on biomedical computing*, vol. 144. Queen's University Kingston, ON, Canada, 2006. [Online]. Available: https://www.researchgate.net/profile/John-Zelek-2/publication/237774967_Laparoscopic_surgery_perceptual_limitations_and_force_A_review/links/0f31752dd5bf019665000000/Laparoscopic-surgery-perceptual-limitations-and-force-A-review.pdf

[9] E. P. Westebring–van der Putten, R. H. Goossens, J. J. Jakimowicz, and J. Dankelman, "Haptics in minimally invasive surgery–a review," *Minimally Invasive Therapy & Allied Technologies*, vol. 17, no. 1, pp. 3–16, 2008, publisher: Taylor & Francis.

[10] G. Tholey, J. P. Desai, and A. E. Castellanos, "Force Feedback Plays a Significant Role in Minimally Invasive Surgery: Results and Analysis," *Annals of Surgery*, vol. 241, no. 1, p. 102, Jan. 2005. [Online]. Available: https://journals.lww.com/annalsofsurgery/Fulltext/2005/01000/Force_Feedback_Plays_a_Significant_Role_in.14.aspx

[11] J. Miller, M. Braun, J. Bilz, S. Matich, C. Neupert, W. Kunert, and A. Kirschniak, "Impact of haptic feedback on applied intracorporeal forces using a novel surgical

robotic system—a randomized cross-over study with novices in an experimental setup," *Surgical Endoscopy*, vol. 35, no. 7, pp. 3554–3563, Jul. 2021. [Online]. Available: https://doi.org/10.1007/s00464-020-07818-8

[12] M. Gannon, "What are pneumatic actuators?" Oct. 2022. [Online]. Available: https://www.pneumatictips.com/what-are-pneumatic-actuators/

[13] M. Runciman, A. Darzi, and G. P. Mylonas, "Soft Robotics in Minimally Invasive Surgery," *Soft Robotics*, vol. 6, no. 4, pp. 423–443, Aug. 2019. [Online]. Available: https://www.ncbi.nlm.nih.gov/pmc/articles/PMC6690729/

[14] H. M. Le, T. N. Do, and S. J. Phee, "A survey on actuators-driven surgical robots," *Sensors and Actuators A: Physical*, vol. 247, pp. 323–354, Aug. 2016. [Online]. Available: https://linkinghub.elsevier.com/retrieve/pii/S0924424716302953

[15] M. W. Gifari, H. Naghibi, S. Stramigioli, and M. Abayazid, "A review on recent advances in soft surgical robots for endoscopic applications," *The International Journal of Medical Robotics and Computer Assisted Surgery*, vol. 15, no. 5, p. e2010, 2019, _eprint: https://onlinelibrary.wiley.com/doi/pdf/10.1002/rcs.2010. [Online]. Available: https://onlinelibrary.wiley.com/doi/abs/10.1002/rcs.2010

[16] N. Agharese, T. Cloyd, L. H. Blumenschein, M. Raitor, E. W. Hawkes, H. Culbertson, and A. M. Okamura, "HapWRAP: Soft growing wearable haptic device," in *2018 IEEE International Conference on Robotics and Automation (ICRA)*. IEEE, 2018, pp. 5466–5472.

[17] K. T. Yoshida, C. M. Nunez, S. R. Williams, A. M. Okamura, and M. Luo, "3-dof wearable, pneumatic haptic device to deliver normal, shear, vibration, and torsion feedback," in *2019 IEEE World Haptics Conference (WHC)*. IEEE, 2019, pp. 97–102.

[18] W. Wu and H. Culbertson, "Wearable haptic pneumatic device for creating the illusion of lateral motion on the arm," in *2019 IEEE World Haptics Conference (WHC)*. IEEE, 2019, pp. 193–198.

[19] G. Andrikopoulos, G. Nikolakopoulos, and S. Manesis, "A Survey on applications of Pneumatic Artificial Muscles," in *2011 19th Mediterranean Conference on Control & Automation (MED)*, Jun. 2011, pp. 1439–1446.

[20] B. Tondu and P. Lopez, "The McKibben muscle and its use in actuating robot-arms showing similarities with human arm behaviour," *Industrial Robot: An International Journal*, vol. 24, no. 6, pp. 432–439, Jan. 1997, publisher: MCB UP Ltd. [Online]. Available: https://doi.org/10.1108/01439919710192563

[21] C.-P. Chou and B. Hannaford, "Measurement and modeling of McKibben pneumatic artificial muscles," *IEEE Transactions on Robotics and Automation*, vol. 12, no. 1, pp. 90–102, Feb. 1996, conference Name: IEEE Transactions on Robotics and Automation. [Online]. Available: https://ieeexplore.ieee.org/abstract/document/481753

[22] K. C. Wickramatunge and T. Leephakpreeda, "Study on mechanical behaviors of pneumatic artificial muscle," *International Journal of Engineering Science*, vol. 48, no. 2, pp. 188–198, Feb. 2010. [Online]. Available: https://www.sciencedirect.com/science/article/pii/S0020722509001268

[23] T. Nakamura and H. Shinohara, "Position and Force Control Based on Mathematical Models of Pneumatic Artificial Muscles Reinforced by Straight Glass Fibers," in *Proceedings 2007 IEEE International Conference on Robotics and Automation*, Apr. 2007, pp. 4361–4366, iSSN: 1050-4729.

[24] E. H. Skorina, M. Luo, W. Y. Oo, W. Tao, F. Chen, S. Youssefian, N. Rahbar, and C. D. Onal, "Reverse pneumatic artificial muscles (rPAMs): Modeling, integration, and control," *PLOS ONE*, vol. 13, no. 10, p. e0204637, Oct. 2018, publisher: Public Library of Science. [Online]. Available: https://journals.plos.org/plosone/article?id=10.1371/journal.pone.0204637

[25] E. H. Skorina and C. D. Onal, "Soft Pneumatic Actuators: Modeling, Control, and Application," in *Smart Materials: Considerations on Earth and in Space*, L. Rasmussen, Ed. Cham: Springer International Publishing, 2022, pp. 129–219. [Online]. Available: https://doi.org/10.1007/978-3-030-70514-5_6

[26] T. McKechnie, J. Khamar, R. Daniel, Y. Lee, L. Park, A. G. Doumouras, D. Hong, M. Bhandari, and C. Eskicioglu, "The Senhance Surgical System in Colorectal Surgery: A Systematic Review," *Journal of Robotic Surgery*, vol. 17, no. 2, pp. 325–334, Apr. 2023. [Online]. Available: https://doi.org/10.1007/s11701-022-01455-0

[27] P. J. Schuler, U. Duvvuri, D. T. Friedrich, N. Rotter, M. O. Scheithauer, and T. K. Hoffmann, "First use of a computer-assisted operator-controlled flexible endoscope for transoral surgery," *The Laryngoscope*, vol. 125, no. 3, pp. 645–648, 2015, _eprint: https://onlinelibrary.wiley.com/doi/pdf/10.1002/lary.24957. [Online]. Available: https://onlinelibrary.wiley.com/doi/abs/10.1002/lary.24957

[28] G. S. Fischer, A. Krieger, I. Iordachita, C. Csoma, L. L. Whitcomb, and G. Fichtinger, "MRI Compatibility of Robot Actuation Techniques – A Comparative Study," in *Medical Image Computing and Computer-Assisted Intervention – MICCAI 2008*, ser. Lecture Notes in Computer Science, D. Metaxas, L. Axel, G. Fichtinger, and G. Székely, Eds. Berlin, Heidelberg: Springer, 2008, pp. 509–517.

[29] K. Y. Choi, J. Lee, N. ElHaouij, R. Picard, and H. Ishii, "Aspire: clippable, mobile pneumatic-haptic device for breathing rate regulation via personalizable tactile feedback," in *Extended Abstracts of the 2021 CHI Conference on Human Factors in Computing Systems*, 2021, pp. 1–8.

[30] D. Pamungkas and K. Ward, "Electro-tactile feedback system to enhance virtual reality experience," *Faculty of Engineering and Information Sciences - Papers: Part A*, pp. 465–470, Jan. 2016. [Online]. Available: https://ro.uow.edu.au/eispapers/5067

[31] I. Zubrycki and G. Granosik, "Novel Haptic Device Using Jamming Principle for Providing Kinaesthetic Feedback in Glove-Based Control Interface," *Journal of Intelligent & Robotic Systems*, vol. 85, no. 3, pp. 413–429, Mar. 2017. [Online]. Available: https://doi.org/10.1007/s10846-016-0392-6

[32] J. Artigas, R. Balachandran, C. Riecke, M. Stelzer, B. Weber, J.-H. Ryu, and A. Albu-Schaeffer, "KONTUR-2: Force-feedback teleoperation from the international space station," in *2016 IEEE International Conference on Robotics and Automation (ICRA)*, May 2016, pp. 1166–1173.

[33] J. P. Switkes, E. J. Rossetter, I. A. Coe, and J. C. Gerdes, "Handwheel Force Feedback for Lanekeeping Assistance: Combined Dynamics and Stability," *Journal of Dynamic Systems, Measurement, and Control*, vol. 128, no. 3, pp. 532–542, Nov. 2005. [Online]. Available: https://doi.org/10.1115/1.2229256

[34] H. Su, W. Shang, G. Li, N. Patel, and G. S. Fischer, "An MRI-Guided Telesurgery System Using a Fabry-Perot Interferometry Force Sensor and a Pneumatic Haptic Device," *Annals of Biomedical Engineering*, vol. 45, no. 8, pp. 1917–1928, Aug. 2017. [Online]. Available: https://doi.org/10.1007/s10439-017-1839-z

[35] I. El Rassi and J.-M. El Rassi, "A review of haptic feedback in tele-operated robotic surgery," *Journal of medical engineering & technology*, vol. 44, no. 5, pp. 247–254, 2020, publisher: Taylor & Francis.

[36] J. Douissard, M. E. Hagen, and P. Morel, "The da Vinci Surgical System," in *Bariatric Robotic Surgery: A Comprehensive Guide*, C. E. Domene, K. C. Kim, R. Vilallonga Puy, and P. Volpe, Eds. Cham: Springer International Publishing, 2019, pp. 13–27. [Online]. Available: https://doi.org/10.1007/978-3-030-17223-7_3

[37] R. Farinha, S. Puliatti, E. Mazzone, M. Amato, G. Rosiello, S. Yadav, R. De Groote, P. Piazza, C. A. Bravi, P. Koukourikis, K. H. Rha, G. Cacciamani, S. Micali, P. Wiklund, B. Rocco, and A. Mottrie, "Potential Contenders for the Leadership in Robotic Surgery," *Journal of Endourology*, vol. 36, no. 3, pp. 317–326, Mar. 2022.

[38] S. Alip, P. Koukourikis, W. K. Han, K. H. Rha, and J. C. Na, "Comparing Revo-i and da Vinci in Retzius-Sparing Robot-Assisted Radical Prostatectomy: A Preliminary Propensity Score Analysis of Outcomes," *Journal of Endourology*, vol. 36, no. 1, pp. 104–110, Jan. 2022, publisher: Mary Ann Liebert, Inc., publishers. [Online]. Available: https://www.liebertpub.com/doi/full/10.1089/end.2021.0421

[39] P. Koukourikis and K. H. Rha, "Robotic surgical systems in urology: What is currently available?" *Investigative and Clinical Urology*, vol. 62, no. 1, pp. 14–22, Jan. 2021. [Online]. Available: https://www.ncbi.nlm.nih.gov/pmc/articles/PMC7801159/

[40] C. Hatzfeld, C. Neupert, S. Matich, M. Braun, J. Bilz, J. Johannink, J. Miller, P. P. Pott, H. F. Schlaak, M. Kupnik, R. Werthschützky, and A. Kirschniak, "A teleoperated platform for transanal single-port surgery: Ergonomics and workspace aspects," in *2017 IEEE World Haptics Conference (WHC)*, Jun. 2017, pp. 1–6.

[41] X. Li, S. Guo, P. Shi, X. Jin, and M. Kawanishi, "An Endovascular Catheterization Robotic System Using Collaborative Operation with Magnetically Controlled Haptic Force Feedback," *Micromachines*, vol. 13, no. 4, p. 505, 2022, publisher: MDPI.

[42] W. Shang, H. Su, G. Li, and G. S. Fischer, "Teleoperation system with hybrid pneumatic-piezoelectric actuation for MRI-guided needle insertion with haptic feedback," in *2013 IEEE/RSJ International Conference on Intelligent Robots and Systems*, Nov. 2013, pp. 4092–4098, iSSN: 2153-0866.

[43] R. Miyazaki, T. Terata, T. Kanno, T. Tsuji, G. Endo, and K. Kawashima, "Compact haptic device using a pneumatic bellows for teleoperation of a surgical robot," in *2015 IEEE/RSJ International Conference on Intelligent Robots and Systems (IROS)*. IEEE, 2015, pp. 2018–2023.

[44] P. Shi, S. Guo, L. Zhang, X. Jin, H. Hirata, T. Tamiya, and M. Kawanishi, "Design and evaluation of a haptic robot-assisted catheter operating system with collision protection function," *IEEE Sensors Journal*, vol. 21, no. 18, pp. 20 807–20 816, 2021, publisher: IEEE.

[45] A. Okamura, C. Simone, and M. O'Leary, "Force modeling for needle insertion into soft tissue," *IEEE Transactions on Biomedical Engineering*, vol. 51, no. 10, pp. 1707–1716, Oct. 2004, conference Name: IEEE Transactions on Biomedical Engineering.

[46] T. L. de Jong, L. H. Pluymen, D. J. van Gerwen, G.-J. Kleinrensink, J. Dankelman, and J. J. van den Dobbelsteen, "PVA matches human liver in needle-tissue interaction," *Journal of the Mechanical Behavior of Biomedical Materials*, vol. 69, pp. 223–228, May 2017. [Online]. Available: https://www.sciencedirect.com/science/article/pii/S1751616117300218

[47] S. Payandeh and T. Li, "Toward new designs of haptic devices for minimally invasive surgery," *International Congress Series*, vol. 1256, pp. 775–781, Jun. 2003. [Online]. Available: https://www.sciencedirect.com/science/article/pii/S0531513103004187

[48] M. Tavakoli, R. PateI, and M. Moallem, "Design issues in a haptics-based master-slave system for minimally invasive surgery," in *IEEE International Conference on Robotics and Automation, 2004. Proceedings. ICRA '04. 2004*, vol. 1, Apr. 2004, pp. 371–376 Vol.1, iSSN: 1050-4729. [Online]. Available: https://ieeexplore.ieee.org/abstract/document/1307178?casa_token=Ht7KIAuX8foAAAAA:B9vdN3Tc_ZKF92p9PAbGBLP-9v7ehZ-WbvVwokIr6LAAa7D13LG79KoiuSKDtMHLh-0wRGORsQ

[49] M. Vicentini, S. Galvan, D. Botturi, and P. Fiorini, "Evaluation of force and torque magnitude discrimination thresholds on the human hand-arm system," *ACM Transactions on Applied Perception*, vol. 8, no. 1, pp. 1:1–1:16, Nov. 2010. [Online]. Available:

https://dl.acm.org/doi/10.1145/1857893.1857894

[50] B. Kalita, A. Leonessa, and S. K. Dwivedy, "A Review on the Development of Pneumatic Artificial Muscle Actuators: Force Model and Application," *Actuators*, vol. 11, no. 10, p. 288, Oct. 2022, number: 10 Publisher: Multidisciplinary Digital Publishing Institute. [Online]. Available: https://www.mdpi.com/2076-0825/11/10/288

[51] F. Daerden and D. Lefeber, "Pneumatic artificial muscles: actuators for robotics and automation," *European journal of mechanical and environmental engineering*, vol. 47, no. 1, pp. 11–21, 2002, publisher: Citeseer.

[52] S. Krishna, T. Nagarajan, and A.-M. Abdul-Rani, "Review of Current Development of Pneumatic Artificial Muscle," *Journal of Applied Sciences*, vol. 11, Oct. 2011.

[53] B. K. Woods, M. F. Gentry, C. S. Kothera, and N. M. Wereley, "Fatigue life testing of swaged pneumatic artificial muscles as actuators for aerospace applications," *Journal of Intelligent Material Systems and Structures*, vol. 23, no. 3, pp. 327–343, Feb. 2012, publisher: SAGE Publications Ltd STM. [Online]. Available: https://doi.org/10.1177/1045389X11433495

[54] J. Garbulinski, S. C. Balasankula, and N. M. Wereley, "Characterization and Analysis of Extensile Fluidic Artificial Muscles," *Actuators*, vol. 10, no. 2, p. 26, Feb. 2021, number: 2 Publisher: Multidisciplinary Digital Publishing Institute. [Online]. Available: https://www.mdpi.com/2076-0825/10/2/26

[55] F. Daerden, "Conception and realization of pleated pneumatic artificial muscles and their use as compliant actuation elements," *Vrije Universiteit Brussel*, p. 176, 1999.

[56] F. Daerden, D. Lefeber, B. Verrelst, and R. Van Ham, "Pleated pneumatic artificial muscles: actuators for automation and robotics," in *2001 IEEE/ASME International Conference on Advanced Intelligent Mechatronics. Proceedings (Cat. No.01TH8556)*, vol. 2, Jul. 2001, pp. 738–743 vol.2.

[57] Q. Guan, J. Sun, Y. Liu, N. M. Wereley, and J. Leng, "Characterization and nonlinear models of bending extensile/contractile pneumatic artificial muscles," *Smart Materials and Structures*, vol. 30, no. 2, p. 025024, Jan. 2021, publisher: IOP Publishing. [Online]. Available: https://dx.doi.org/10.1088/1361-665X/abd4b0

[58] T. E. Pillsbury, N. M. Wereley, and Q. Guan, "Comparison of contractile and extensile pneumatic artificial muscles," *Smart Materials and Structures*, vol. 26, no. 9, p. 095034, Aug. 2017, publisher: IOP Publishing. [Online]. Available: https://dx.doi.org/10.1088/1361-665X/aa7257

[59] S. Joe, M. Totaro, H. Wang, and L. Beccai, "Development of the Ultralight Hybrid Pneumatic Artificial Muscle: Modelling and optimization," *PLOS ONE*, vol. 16, no. 4, p. e0250325, Apr. 2021, publisher: Public Library of Science. [Online]. Available: https://journals.plos.org/plosone/article?id=10.1371/journal.pone.0250325

[60] E. H. Skorina, M. Luo, and C. D. Onal, "A Soft Robotic Wearable Wrist Device for Kinesthetic Haptic Feedback," *Frontiers in Robotics and AI*, vol. 5, 2018. [Online]. Available: https://www.frontiersin.org/articles/10.3389/frobt.2018.00083

[61] H. Li, K. Tadano, and K. Kawashima, "Achieving force perception in master-slave manipulators using pneumatic artificial muscles," in *2012 Proceedings of SICE Annual Conference (SICE)*, Aug. 2012, pp. 1342–1345.

[62] H. Li, K. Kawashima, K. Tadano, S. Ganguly, and S. Nakano, "Achieving Haptic Perception in Forceps' Manipulator Using Pneumatic Artificial Muscle," *IEEE/ASME Transactions on Mechatronics*, vol. 18, no. 1, pp. 74–85, Feb. 2013, conference Name: IEEE/ASME Transactions on Mechatronics.

[63] K. P. Ashwin and A. Ghosal, "A Soft-Robotic End-Effector for Independently Actuating Endoscopic Catheters," *Journal of Mechanisms and Robotics*, vol. 11, no. 061004, Oct. 2019. [Online]. Available: https://doi.org/10.1115/1.4044539

[64] E. Kelasidi, G. Andrikopoulos, G. Nikolakopoulos, and S. Manesis, "A survey on pneumatic muscle actuators modeling," in *2011 IEEE International Symposium on Industrial Electronics*. Gdansk, Poland: IEEE, Jun. 2011, pp. 1263–1269. [Online]. Available: http://ieeexplore.ieee.org/document/5984340/

[65] K. C. Wickramatunge and T. Leephakpreeda, "Empirical modeling of dynamic behaviors of pneumatic artificial muscle actuators," *ISA Transactions*, vol. 52, no. 6, pp. 825–834, Nov. 2013. [Online]. Available: https://linkinghub.elsevier.com/retrieve/pii/S001905781300092X

[66] T.-C. Tsai and M.-H. Chiang, "Design and Control of a 1-DOF Robotic Lower-Limb System Driven by Novel Single Pneumatic Artificial Muscle," *Applied Sciences*, vol. 10, no. 1, p. 43, Jan. 2020, number: 1 Publisher: Multidisciplinary Digital Publishing Institute. [Online]. Available: https://www.mdpi.com/2076-3417/10/1/43

[67] S. Chakravarthy, K. Aditya, and A. Ghosal, "Experimental Characterization and Control of Miniaturized Pneumatic Artificial Muscle," *Journal of Medical Devices*, vol. 8, no. 041011, Oct. 2014. [Online]. Available: https://doi.org/10.1115/1.4028420

[68] B. Ugurlu, P. Forni, C. Doppmann, E. Sariyildiz, and J. Morimoto, "Stable Control of Force, Position, and Stiffness for Robot Joints Powered via Pneumatic Muscles," *IEEE Transactions on Industrial Informatics*, vol. 15, no. 12, pp. 6270–6279, Dec. 2019, conference Name: IEEE Transactions on Industrial Informatics.

[69] P. Puangmali, K. Althoefer, L. D. Seneviratne, D. Murphy, and P. Dasgupta, "State-of-the-Art in Force and Tactile Sensing for Minimally Invasive Surgery," *IEEE Sensors Journal*, vol. 8, no. 4, pp. 371–381, Apr. 2008, conference Name: IEEE Sensors Journal.

[70] H. Su, I. I. Iordachita, J. Tokuda, N. Hata, X. Liu, R. Seifabadi, S. Xu, B. Wood, and G. S. Fischer, "Fiber-Optic Force Sensors for MRI-Guided Interventions and Rehabilitation: A Review," *IEEE Sensors Journal*, vol. 17, no. 7, pp. 1952–1963, Apr. 2017, conference Name: IEEE Sensors Journal.

[71] E. Franco and M. Ristic, "Adaptive control of a master-slave system for teleoperated needle insertion under MRI-guidance," in *2015 23rd Mediterranean Conference on Control and Automation (MED)*, Jun. 2015, pp. 61–67.

[72] N. Kumar, O. Piccin, L. Meylheuc, L. Barbé, and B. Bayle, "Design and Modeling of a Polymer Force Sensor," *IEEE/ASME Transactions on Mechatronics*, vol. 21, no. 1, pp. 555–564, Feb. 2016, conference Name: IEEE/ASME Transactions on Mechatronics. [Online]. Available: https://ieeexplore.ieee.org/abstract/document/7131564?casa_token=xMFEysnZpJcAAAAA:qYWDqPyny_D_yUUuEjAAtRdtPIFEGJrckMqVwLM4S1MPK5n5LH3TIEQPYnuU1fUL2W6WaqRp6A

[73] A. Verhoef, Anne, "The design of a pneumatic haptic device for teleoperated minimally invasive medical applications," Master's thesis, University of Twente, Enschede, Jul. 2022.

[74] E. H. Skorina, W. Tao, F. Chen, M. Luo, and C. D. Onal, "Motion control of a soft-actuated modular manipulator," in *2016 IEEE International Conference on Robotics and Automation (ICRA)*, May 2016, pp. 4997–5002.

[75] "Hardness Comparison Chart." [Online]. Available: https://hapcoincorporated.com/resources/hardness-comparison-chart/

[76] "Durometer Shore Hardness Scale." [Online]. Available: https://www.smooth-on.com/page/durometer-shore-hardness-scale/

[77] "GD-10." [Online]. Available: https://www.digikey.nl/en/products/detail/uneo-inc/GD-10/15657160

[78] "Bambu Lab X1-Carbon Combo 3D Printer." [Online]. Available: https://eu.store.bambulab.com/en-nl/products/x1-carbon-combo

[79] "iglide® J260-PF, filament for 3D printing." [Online]. Available: https://www.igus.com/product/716?artNr=J260-PF-0175-0750

[80] "Onyx - Composite 3D Printing Material." [Online]. Available: https://markforged.com/materials/plastics/onyx

[81] "Carbon Fiber Composite 3D Printer: Markforged Mark Two." [Online]. Available: https://markforged.com/3d-printers/mark-two

[82] "BD7281YG-CTR - Operational Amplifier, Rail to Rail I/O, 1 Amplifier, 7 MHz, 10 V/µs." [Online]. Available: https://ie.farnell.com/rohm/bd7281yg-ctr/op-amp-7mhz-ssop-5-125deg-c/dp/4137642

[83] Y. Fernando and M. Parnichkun, "Development and Control of a Flexible Actuation-Based Delta Robot," in *IECON 2022 – 48th Annual Conference of the IEEE Industrial Electronics Society*, Oct. 2022, pp. 1–6, iSSN: 2577-1647.

[84] S. Xie, H. Liu, and Y. Wang, "A method for the length-pressure hysteresis modeling of pneumatic artificial muscles," *Science China Technological Sciences*, vol. 63, no. 5, pp. 829–837, May 2020. [Online]. Available: https://doi.org/10.1007/s11431-019-9554-y

[85] T. J. Yeh, M.-J. Wu, T.-J. Lu, F.-K. Wu, and C.-R. Huang, "Control of McKibben pneumatic muscles for a power-assist, lower-limb orthosis," *Mechatronics*, vol. 20, no. 6, pp. 686–697, Sep. 2010. [Online]. Available: https://www.sciencedirect.com/science/article/pii/S0957415810001285

[86] S. Xie, G. Ren, and B. Wang, "A modified asymmetric generalized Prandtl–Ishlinskii model for characterizing the irregular asymmetric hysteresis of self-made pneumatic muscle actuators," *Mechanism and Machine Theory*, vol. 149, p. 103836, Jul. 2020. [Online]. Available: https://www.sciencedirect.com/science/article/pii/S0094114X20300574

[87] M. Motheram, "Force-based measurement of tissue stiffness in 1-DoF needle insertion robotic device for liver interventions." Master's thesis, University of Twente, Enschede, Oct. 2023.

[88] S.-J. Estermann, D. H. Pahr, and A. Reisinger, "Quantifying tactile properties of liver tissue, silicone elastomers, and a 3D printed polymer for manufacturing realistic organ models," *Journal of the Mechanical Behavior of Biomedical Materials*, vol. 104, p. 103630, Apr. 2020. [Online]. Available: https://www.sciencedirect.com/science/article/pii/S1751616119312949

[89] S. McKinley, A. Garg, S. Sen, D. V. Gealy, J. P. McKinley, Y. Jen, M. Guo, D. Boyd, and K. Goldberg, "An interchangeable surgical instrument system with application to supervised automation of multilateral tumor resection," in *2016 IEEE International Conference on Automation Science and Engineering (CASE)*, Aug. 2016, pp. 821–826, iSSN: 2161-8089. [Online]. Available: https://ieeexplore.ieee.org/abstract/document/7743487

[90] D. J. van Gerwen, J. Dankelman, and J. J. van den Dobbelsteen, "Needle–tissue interaction forces – A survey of experimental data," *Medical Engineering & Physics*, vol. 34, no. 6, pp. 665–680, Jul. 2012. [Online]. Available: https://www.sciencedirect.com/science/article/pii/S1350453312000938

[91] "ATI Industrial Automation: F/T Sensor mini40." [Online]. Available: https://www.ati-ia.com/products/ft/ft_models.aspx?id=mini40

[92] "MPA0505S-1W - Isolated Through Hole DC/DC Converter, ITE, 1:1, 1 W, 2 Output, 5 V, 100 mA." [Online]. Available: https://ie.farnell.com/multicomp-pro/mpa0505s-1w/dc-

dc-converter-2-o-p-1w/dp/3652553

[93] "LM7905CT - IC, V REG, -5V." [Online]. Available: https://ie.farnell.com/onsemi/lm7905ct/ic-v-reg-5v/dp/4196729

[94] "FSA Series Force Sensors | Honeywell." [Online]. Available: https://sps.honeywell.com/us/en/products/advanced-sensing-technologies/healthcare-sensing/force-sensors/fsa-series